TEMPERATURE DEPENDENCE OF TUNNELING IN INTRINSIC JOSEPHSON JUNCTIONS OF HIGH TEMPERATURE SUPERCONDUCTORS

A Thesis submitted to
The Graduate School of Engineering and Science of
İzmir Institute of Technology
in Partial Fulfillment of the Requirements for the Degree of

MASTER OF SCIENCE

in Physics

by
Yılmaz ŞİMŞEK

March 2008
İZMİR

We approve the thesis of **Yılmaz ŞİMŞEK**

_____

Assoc. Prof. Lütfi ÖZYÜZER
Supervisor

_____

Prof. Doğan ABUKAY
Committee Member

_____

Prof. Mustafa Erol
Committee Member

_____

Assoc. Prof. Salih OKUR
Committee Member

_____

Assoc. Prof. Yusuf SELAMET
Committee Member

19 March 2008
Date

_____

Assoc. Prof. Lütfi ÖZYÜZER
Head of the Physics Department

_____

Prof. Hasan BÖKE
Dean of the Graduate School of Engineering and Science

ACKNOWLEDGEMENTS

I would like to express my gratitude to all those who gave me the possibility to complete this thesis. Firstly, I would like to thank to my supervisor, Lütfi Özyüzer for his instructive guidance, stimulating suggestions and encouragement helped me during my master thesis education. I want to thank Dr. Kenneth E Gray, Dr Dave G. Hinks and Dr Ulrich Welp for their supports and providing high quality BSCCO single crystal. I am indebted to the staff of Center for Material Research of IYTE for their patients at my detailed characterizations. This research was supported by TUBITAK.

I also extend my thanks to all former colleagues from Izmir Institute of Technology for their supporting, discussing and comments. Especially I am obliged to Cihan Kurter, Savaş Ulucan, Kaan Oğuz, Mehtap Özdemir, Kadir Vahaplar, Hatun Çinkaya and Hasan Köseoğlu. Also I am greatly indebted to my friends who are Beyhan Puliçe, Eylem Durgun and Önder Aslan to sincerely support me in all the time.

And my family. I can't find any better words to explain their love and express my thanks for their helps.

ABSTRACT

TEMPERATURE DEPENDENCE OF TUNNELING IN INTRINSIC JOSEPHSON JUNCTIONS OF HIGH TEMPERATURE SUPERCONDUCTORS

The lack of coherent, continuous and tunable compact solid-state sources of electromagnetic radiations at terahertz (THz) frequency range (0.3-30 THz) can be solved by high temperature superconductors (HTS) which are better candidates for generation of THz radiation. THz sources have potential application areas in materials characterization, biology, communication, medicine and security. The HTSs have large energy gap intervals which are available for radiations at THz frequency range, so recently, they were used as better converters from DC-voltage to high frequency radiation in junction technologies. $Bi_2Sr_2CaCu_2O_{8+\delta}$ (Bi2212) HTS single crystals include natural superconductor-insulator-superconductor multi-junctions called intrinsic Josephson junctions. For generation of coherent continuous and powerful THz radiations, we have fabricated large and tall mesas on Ca rich Bi2212, although mesas with small planar and lateral dimensions were preferred in recent studies because of the heating effect. We have used under-doped Bi2212 to control the heating problem. The mesas with size of 100x300 μm^2 have been fabricated by vacuum evaporation, photo-lithography and ion beam etching techniques. Their heights and lateral dimensions were analyzed by Atomic Force Microscopy. We have investigated temperature dependence of c-axis resistivity and current-voltage (I-V) tunneling characteristics of under-doped Bi2212 which exhibit exponentially increases in resistivity from 300 K to T_c. The influences of heating effect were analyzed at temperature evolution of I-V measurements. Finally, bolometric detections of emission from long edges of mesas were done.

ÖZET

YÜKSEK SICAKLIK ÜSTÜN İLETKENLERİNDEKİ ÖZGÜN JOSEPHSON EKLEMLERİNİN TÜNELLEMESİNİN SICAKLIĞA BAĞIMLILIĞI

Terahertz frekans aralığında (0.3-30 THz) koherent aralıksız ve ayarlanabilir bir şekilde elektromanyetik ışıma yapacak kompakt katı-hal kaynaklarının eksikliği, bu ışınlarını elde etmede daha iyi bir aday olan yüksek sıcaklık üstüniletkenlerle çözülebilir. THz kaynakları; materyal karakterize etmede, biyolojide, iletişimde, tıpta ve güvenlik alanlarında geniş uygulama potansiyeline sahiptir. Yüksek sıcaklık üstüniletkenleri ise THz frekans aralığına ışıma yapmak için uygun olan büyük enerji aralıklarına sahiptir. Bu yüzden bu üstüniletkenler eklemli yapı teknolojilerinde, DC voltajı yüksek frekanslı ışımaya çeviren iyi bir dönüştürücü olarak kullanılmaktadırlar. Bir üstüniletken olan $Bi_2Sr_2CaCu_2O_{8+d}$ (Bi2212) tek kristalleri özgün Josephson eklemleri şeklinde anılan doğal üstüniletken yalıtkan üstüniletken gibi üst üste çoklu eklemli yapılar içerir. Isınma olaylarından ötürü küçük düzlemsel ve yanalsal boyutlu mesalar tercih edilmesine rağmen, koherent aralıksız ve güçlü bir şekilde THz ışımalarını elde etmek için, Ca ile zenginleştirilmiş Bi2212 üzerine geniş ve uzun boyutlarda mesalar ürettik. Isınma problemini kontrol edebilmek için normal düzeyin altında O_2 katkılandırılmış Bi2212 kullandık. 100x300 μm^2 boyutlu mesalar vakumlu buharlaştırma, fotolitografi ve iyon demeti aşındırma metotlarıyla üretildi. Mesaların yükseklikleri ve yanal boyutları Atomik Kuvvet Mikroskobuyla analiz edildi. Bi2212'nin sıcaklığa bağlı c-ekseni özdirencini ve akım-voltaj (I-V) tünelleme niteliklerini inceledik. Bu incelemelerde 300 K ten T_c'ye üssel olarak artan bir özdirenç normal düzeyin altında O_2 katkılandırılmış bir Bi2212 üstüniletkeni ile çalışıldığını göstermektedir. Sıcaklıkla değişen I-V ölçümlerinde ısınma olayının etkileri analiz edildi. Son olarak mesaların uzun kenarlarından bolometrik ışıma algılama ölçümleri yapıldı.

TABLE AND CONTENTS

LIST OF FIGURES

LIST OF TABLES

CHAPTER 1

INTRODUCTION

1.1. Superconductivity

After the development of helium liquefaction techniques in the laboratory of Heike Kammerlingh Onnes in 1908, scientists have been able to investigate the electrical behaviors of materials at low temperatures. Before the discovery of superconducting materials, it was already known that cooling a metal increases its conductivity due to decreased electron-phonon interactions. After an unexpected discovery revealed by Kammerlingh Onnes in 1911, superconductivity was regarded as a major scientific mystery with their most remarkable properties that are zero resistance and perfect diamagnetism for a large part of last century. In the following years, superconductivity was observed in many metals, alloys and compounds. Increasing the research on superconductivity with discovering new superconductor materials enabled to reveal the second outstanding feature of it that is perfect diamagnetism discovered by W. Meissner and R. Ochsenfeld in 1933. They found that when material is at superconductor phase, external magnetic field is removed from interior of a field-cooled superconductor. However, there was no theoretical explaining on superconductors in spite of experimental discoveries, so many outstanding scientists such as Einstein, Landau, and Heisenberg tried to find an explaining on the superconducting phenomenon. In 1957 the microscopic theory of superconductivity was formulated by Bardeen, Cooper and Schrieffer, which is known as the BCS theory (Bardeen, et al. 1957). This theory tries to explain conductance of conventional superconductor without electrical resistance and views superconductivity as a macroscopic quantum mechanical effect. The main conceptual element of the theory is based on the pairing of electrons close to the Fermi level into pairs through interaction with the crystal lattice. Whereas it is well known that two electrons in a vacuum repel each other by Coulomb force, there is net attraction between two electrons that form the so-called Cooper pair in a superconductor material below the critical temperature. The pairs of electrons having different behavior from single electrons act more like boson which can condense into

the same energy level with opposite momenta and spins. In superconductors, this pairing result from an attractive interaction between the electrons and lattice vibrations; the coupling to the lattice is called a phonon interaction. Bardeen, Cooper, and Schrieffer received the Nobel Prize in 1972 for the development of the theory of superconductivity.

After discovery of number of new superconducting materials with their novel properties, it was demonstrated by some experimental studies that they exhibited different behaviors, so they were classified such as conventional and unconventional superconductors. Conventional superconductors usually have low critical temperatures ranging from less than 1 K to around 20 K and have the property of excluding magnetic fields completely from the interior of the superconductor, that is known Meissner effect. The superconductivity exists only below their critical temperatures and below a critical magnetic field strength. Type-II superconductors including all known high-temperature superconductors (HTSs) have much higher critical fields and therefore could carry much higher current densities while remaining in the superconducting state. Although the macroscopic causes of superconductivity in conventional superconductors can be well described, it is not completely clear that this theory can explain superconductivity in the high temperature superconductors (Wesche 1998). In the conventional superconductors, electrons have spherical wave function and interact with each other via the vibrations of the crystal lattice. The two electrons of a Cooper pair form a state in which the total angular momentum L and the total spin S are zero. Therefore a cooper pair has an equal change of traveling in any direction and it can be said that a pairing shows s-wave symmetry. In this case, the superconducting state in the material essentially exhibits the same properties at each direction except for the case in which a barrier layer is inserted into material (Josephson Junction). On the other hand, when we investigate reasons making some superconductor unconventional, the values of S and L for a cooper pair should be considered. It is almost well known that superconductor prefer a spin singlet state (S=0). For the state with S=0, the angular momentum have an even multiple of ħ (L=0, 2ħ, 4ħ, etc). Although for most superconductor, the state with L=0 and S=0 is energetically favored, the state with L=2ħ is realized at HTSs whose superconducting order parameter likely has d-wave symmetry while some studies show evidence of s-wave or mixed symmetries. This is the first version of an unconventional superconductor. However, such an interaction of the electrons with the crystal structure at pairing mechanism in conventional

superconductor is not likely defined in unconventional superconductors because they have the anisotropic superconducting state in k-space. On the other hand, it is not known whether the electron-phonon interaction always leads to conventional superconductivity or different interaction always cause unconventional superconductivity because there are no experimental indications for opposite of this. In this point, it is considered that unconventional superconductors have layered structure (Buckel and Kleiner 2004).

Since spin of the Cooper pairs is zero, Pauli's exclusive principle is not available any longer in the superconductors. Thus they can occupy the same quantum state and the occupation of energy state is described by Bose-Einstein distribution law. All Cooper pairs have same momentum, but it is not possible when energy resulting from applied electric field exceeds the energy gap of the Cooper pair. The expressing of energy gap (Δ) in a superconductor and a semiconductor is quite different from each other. In superconductor, the energy 2Δ can be defined as a binding energy of the Cooper pair and it is enough energy to break a cooper pair in a superconductor. After breaking of pairs, the single electrons occur and they are called quasi-particles. Experimentally, the energy gap varies with temperature that is also predicted by BCS theory. At T=0, the ratio $2\Delta_{(0)} /k_BT_c$ variation with superconductor elements are typically between 3.2 and 4.6 but this radio predicted by BCS theory is equal to 3.5 (Wesche 1998).

1.2. High Temperature Superconductors

Usage of the liquid helium discovered by H. K. Onnes in 1911 in order to reach the very low temperatures led to find new superconducting materials with increasing their critical temperature (T_c) values in subsequent decades. Until 1986, physicists had believed that BCS theory forbade superconductivity at temperatures between 30 K and 40 K due to thermal vibrations. However, a interesting research renewed superconductivity was published by Bednorz and Müller in that year and they discovered superconductivity in a ceramic compound material, lanthanum barium copper oxide ($La_{2-x}Ba_xCuO_4$), with transition temperature of 35 K (Bednorz and Müller 1986). Making this ceramic compound important discover in superconductivity was that it has not only high critical temperature but also was first cuprate in new class

superconducting materials known as copper oxide superconductors. After a year, replacing the lanthanum with yttrium at LBCO materials, yttrium barium copper oxide compound, $YBa_2Cu_3O_{7-x}$ (YBCO), was found with T_c around 90 K (Wu, et al. 1987). It was important commercially because liquid nitrogen produced cheaply could then be used as a refrigerant (at atmospheric pressure, the boiling point of nitrogen is 77 K). In the same year another superconducting compound including bismuth, strontium, calcium and copper (BSCCO) was discovered. Two superconducting phases were characterized as $Bi_2Sr_2CaCu_2O_{8+\delta}$ (Bi2212) and $Bi_2Sr_2Ca_2Cu_3O_{10+\delta}$ (Bi2223) with their T_c 95 K and 110 K respectively (Chu, et al. 1998). After a very short time, thallium barium calcium copper oxide compound, $Tl_2Ba_2Ca_2Cu_3O_\delta$ (Tl2223) which has around T_c 125 K was found in 1988 (Hazen, et al. 1988). The last superconductor compound $HgBa_2Ca_2Cu_3O_{8+\delta}$ (Hg1223) with maximum transition temperature T_c around 135 K was found in 1993 (Schilling, et al. 1993).

All of the HTSs have a layered crystal structure and include copper oxide layers providing superconductivity separated by non-superconductor layers. They are base on oxygen defect modification of a perovskite structure which is adopted by many oxides that have the chemical formula ABO_2. Its structure is a primitive cube, with the A-cation in the middle of the cube, the B-cation in the corner and the anion, commonly oxygen, in the centre of the face edges. Because of these layered structures of HTSs, they have anisotropic behaviors at critical field, London penetration dept, coherence length and resistivity. They are extremely type II superconductors and only these superconductors can be used for magnet and energy applications which can be well defined by the Gindzburg-Landau theory (Ginzburg and Landau 1950). In 1959, it has been showed that this theory can be derived from the BCS theory (Gor'kov 1959). Type I and type II superconductors are different with respect to critical fields, London penetration dept λ and coherence length ξ. While $\xi>\lambda$ shows the characteristic of type I superconductors, the situation of $\xi<\lambda$ is found in type II superconductors. If the ratio λ/ξ called the Ginzburg-Landau parameter (κ) is greater than $1/\sqrt{2}$, superconductor must be type II (Wesche 1998). Although the coherence length values ξ of HTSs are short, they have large critical magnetic field. Besides these different parameters, Shubnikov firstly found an unusual behavior of some superconductor in external magnetic field. After 20 years in order to explain the Shubnikov's experiment, Abrikosov using the Gindzburg-Landau theory theoretically showed that there are two types of superconducting materials which are categorized as type-I and type-II superconductor.

For example, while type I superconductor materials expel magnetic flux completely from their interior until a critical magnetic field values, at the high presence of an applied external magnetic field, a mixed state in the type-II superconductor material is characterized by the properties of the vortex that is formed at point where the magnetic field penetrates the superconductor in a flux tube through the sample. Due to penetration of magnetic flux, the region in which is near the core of the vortex acts as a normal metal. Type-II superconductors have two critical magnetic fields which are the lower critical magnetic field B_{c1} and the upper critical magnetic field B_{c2}. If applied field is less than B_{c1}, the superconductor completely expel the magnetic field as a type-I superconductor. Superconductor in magnetic field between B_{c1} and B_{c2} mixed state is formed and at B_{c2} material become normal state (Bourdillons 1993).

1.3. Josephson Effect

Tunneling phenomena in superconductor provides valuable information about superconducting materials such as energy gap and other superconducting features. Josephson junctions include two superconducting layers separated by very thin insulating layer. Josephson theoretically predicted cooper pair tunneling across the insulating layers, apart from single electron tunneling, so they are called as Josephson junction (Josephson 1962). The insulating layer in SIS junctions can be such as cracks, grain boundaries and point contacts. The single electron tunneling is a well known phenomena and based on classical mechanics but his theoretical prediction on pair tunneling presented new important conception to superconductive theories. He predicted that the cooper pair tunneling current through the barrier is depended on the difference of phases of the effective wave functions on the two sides of the junction and the phase difference is both temporally and spatially variable. Apart from single electron tunneling, there are no excitation and bias across the junction. Cooper pair tunneling occurs the Josephson current flowing without resistance until the critical current value I_c of the SIS junction is exceeded. After the critical current value I_c, voltage and current jump to values exhibiting single electron (quasi-particle) tunneling characteristic on the I-V (Duzer and Turner 1999).

There are two principle phenomena in Josephson effect which are DC and AC Josephson effects. When Josephson current flows at absence of any electrical and

magnetic field, DC Josephson effect occurs. The current resulting from cooper pair tunneling across the thin insulating layer at zero voltage is dependent on phase differences between two superconductors on either side of the junction. If a constant nonzero voltage is applied across the insulating barrier, an alternating Josephson current occurs. This oscillating current is explained by AC Josephson effect. This oscillating current generates emission. Because of the radiation frequency proportional to the voltage, Josephson junctions are used such a voltage-frequency converter (Bourdillon and Bourdillon 1993).

1.4. Tunneling in High Temperature Superconductors

It is known there are two types of tunneling in SIS junctions, which include single electron and cooper pair tunneling across the insulating barrier. Tunneling spectroscopy of superconductors leads to get information about superconducting state, energy gap feature, critical current, and their temperature evolutions. However these superconducting features in HTSs exhibit differences from conventional superconductors. There are theoretical difficulties in explaining these differences. For example, energy gap in HTSs is dependent on the direction of flowing current. Therefore they exhibit anisotropic electrical behaviors because of unconventional pairing state. In HTSs, it is mentioned the presence of d wave pairing symmetry leading to anisotropic energy gap on Fermi surface while pairing mechanism in conventional superconductor is s wave symmetry. However some studies on experimental evidence of their pairing mechanism continue (Buckel and Kleiner 2004).

All of the HTSs have layered structures. For example $Bi_2Sr_2CaCu_2O_{8+\delta}$ (Bi2212) high temperature superconductor includes natural SIS layered multi-junction stacks called intrinsic Josephson junction (IJJ). Since the IJJs are naturally stacked along the c-axis of Bi2212 single crystal, they exhibit anisotropic electrical behaviors and their electrical measurements provide to get better information about HTSs than artificially stacked Josephson junctions because the influences of junction interfaces on measurements are reduced to minimum in perfect and thin IJJs. In tunneling spectroscopy of Bi2212 along the c-axis, it is possible to see combined tunneling behaviors of all IJJ. Because of their layered structure, they are widely used in superconducting junction devices. Recently tunneling behaviors of their perfect layered

junctions have been promising in superconducting device technologies. The most important development is their capabilities on generation of THz radiation.

1.5. THz Radiation

Radiations at terahertz (THz) frequency range (0.3-30 10^{12} Hz) are considered to have many important application areas in physics, biology, chemistry, astronomy and medicine. The rich THz frequency interval for molecular spectroscopy is caused by rotational and vibrational absorption modes of the most molecules in THz frequency range. In addition to this, their non-ionising properties make the characterizations safer than x-rays and they can easily pass through the some materials such as clothing, paper, cardboard, wood, masonry, plastic and ceramics. Since the properties of THz radiations are very important for wide application areas, it is entailed to produce the sources generating these radiations (Ferguson and Zhang 2002). However, there are still lacks of THz sources and difficulties in their generations. The radiations at above and below THz frequency range are provided by semiconductors. Although there are many studies on THz radiation in semiconducting technology, some limiting problems makes them underdevelopment for sources emitting coherent continuous and tunable THz radiation with high power (Bae and Lee 2006).

It is well known from ac Josephson effect that radiation frequency proportional to the voltage, so a Josephson junction play a role in device technologies such as converter from dc voltage to high frequency radiations. Since HTSs have large energy gap interval, they are better candidate to generate significant THz radiation spectrum. Recently in order to obtain radiation with more power and higher frequency, the studies on generation of THz from HTS superconductor devices increase and it was demonstrated that device lateral and planar dimensions affect the radiation power and frequency. On the other hand, there are still lacks of compact solid-state THz radiation sources in spite of many attempts in both semiconducting and superconducting technology.

CHAPTER 2

IJJs TUNNELING IN HTS

Single crystal of high temperature superconductors (HTSs) e.g. $Bi_2Sr_2CaCu_2O_{8+\delta}$ (Bi2212), forms layered structure and these natural stacks of superconductor-insulator-superconductor (SIS) multi-junctions called intrinsic Josephson Junctions (IJJs). Recent experiments, including tunneling measurements along the c-axis in Bi2212 have been performed in order to justify that the superconducting CuO_2 layers are coupled by the Josephson effect through the block layers (Tachiki, et al. 1995). After the intrinsic tunneling of Cooper pairs in Bi2212 with perfect layered crystal structure was experimentally confirmed by (Kleiner, et al. 1992), the studies on tunneling in Bi2212 became very important for physicists to understand the intrinsic Josephson effect. Moreover they are also power tools for vortex physics and many applications in superconducting electronics (Yurgens 2000). One of their preferred application areas in recent research is that they serve the purpose for generating of THz radiation (T-rays). It is very important because there are lacks of compact, solid-state sources for generating this versatile radiation. IJJ effect has important role on generating of T-rays, so research on layered HTSs was updated for generating T-rays.

Making the T-rays so important is their frequency range which is suitable for molecular spectroscopy because the most molecules have rotational and vibrational absorption modes in that range. To excite electromagnetic waves in layered structures, many instructive ideas have been proposed and tried, among which the method making use of moving Josephson vortices in magnetic field application is a quite popular one. Especially, the coherent, continuous and frequency-tunable characters of generated waves expected from HTSs, the researchers were extensively interested in generation of powerful T-rays based on characteristics of IJJ tunneling (Batov, et al. 2006). Powerful T-rays requires mesas with large lateral areas. In that study, the dimensions of mesa on crystal are intended to generate THz emission with coherent, continues and sizable. The important of both sizes of high mesa and properties of Bi2212 crystal in generation of THz emission was emphasized in a paper published by (Ozyuzer, et al. 2007). In this study, they succeeded to generate THz emission with required properties using the

excitation of electromagnetic cavity resonance inside superconducting Bi2212 single crystal and the effect of mesa area and height on emission power and frequency was demonstrated. The exciting development for compact source of THz radiation leads my thesis study and reveals possibilities of generation of THz radiation from superconductor. As the indication of study in the paper, the mesas with large area including large number of IJJs were fabricated and it is planned to generate THz emission from superconducting Bi2212. On the other hand, due to strong coupling between CuO_2 layers, large Bi2212 mesas suffer from heating at high bias which we will address in this study.

2.1. Crystal Structure and Physical Properties of BSCCO

The bismuth-based family of HTSCs studied in the last 20 years has several phases which are generally formulated by $Bi_2Sr_2Ca_{n-1}Cu_nO_{2n+4+\delta}$ (BSCCO). It is well known that the BSCCO consists of three phases which are (n=1) $Bi_2Sr_2CuO_{6+\delta}$ (Bi2201) with $T_c \leq 20$ (Akimitsu, et al. 1987), $Bi_2Sr_2CaCu_2O_{8+\delta}$ (n=2, Bi2212 phase) with $T_c \approx 90$ K and $Bi_2Sr_2Ca_2Cu_3O_{10+\delta}$ (Bi2223 phase) with $T_c = 110$ K (Maeda, et al. 1988). BSCCO has a crystal structure in which superconducting CuO_2 layers are alternately stacked with insulator blocking Bi-O and Sr-O layers along to c axis. Here superconductivity is restricted only to the CuO_2 layers with about 0.3 nm thickness. Bi-O and Sr-O layers which behave as passive spacer or charge reservoirs are intermediate planes with thickness of 12 Å. This model defining superconductor and insulator layers in BSCCO single crystal is known as multilayer model. The natural stacks of superconductor-insulator-superconductor (SIS) multi-junction called intrinsic Josephson Junction (IJJ), where each junction has a thickness of only 1.5 nm (Figure 2.1.a). The parameter n also corresponds to the number of superconducting layers in the structure. For example, structure of Bi2212 phase includes two CuO_2 layers separated by Ca layer. The unit cell of Bi2212 has a pseudo-tetragonal symmetry with lattice parameter; a = b = 5.4 and c = 31 Å (Matsui, et al. 1988). Sequence of its stacking atomic layers is like that,
$(BiO)_2$ / SrO / CuO_2 / Ca / CuO_2 / SrO / $(BiO)_2$ / SrO / CuO_2 / Ca / CuO_2 / SrO / $(BiO)_2$.

There are two kinds of layers in crystal structure of Bi2212 according to structure types. One consisting SrO / CuO_2 / Ca / CuO_2 / SrO has a structure of perovskite type, while another consisiting SrO / $(BiO)_2$ / SrO has a structure of NaCl

type. The layered structure of Bi2212 HTSs including IJJs makes the crystal anisotropic material. Thus Josephson tunneling along to c axis occurs between superconducting (Cu-O) layers separated by insulating layers unlike electrical behaviors of the crystal at a-b planes. Besides, layered HTSs have different coherence lengths and penetration depths at different directions. At a-b planes coherence length ξ_{ab} (between 20 and 40 Å) is larger than coherence length ξ_c (≈1 Å) along to c axis. In spite of small coherence lengths of Bi2212, penetration depth λ_{ab} is equal to 2000 Å. It means Bi2212 with the Ginzburg-Landau parameter κ larger than 100 exhibits behaviors of type II superconductors (Ting Wei 1995).

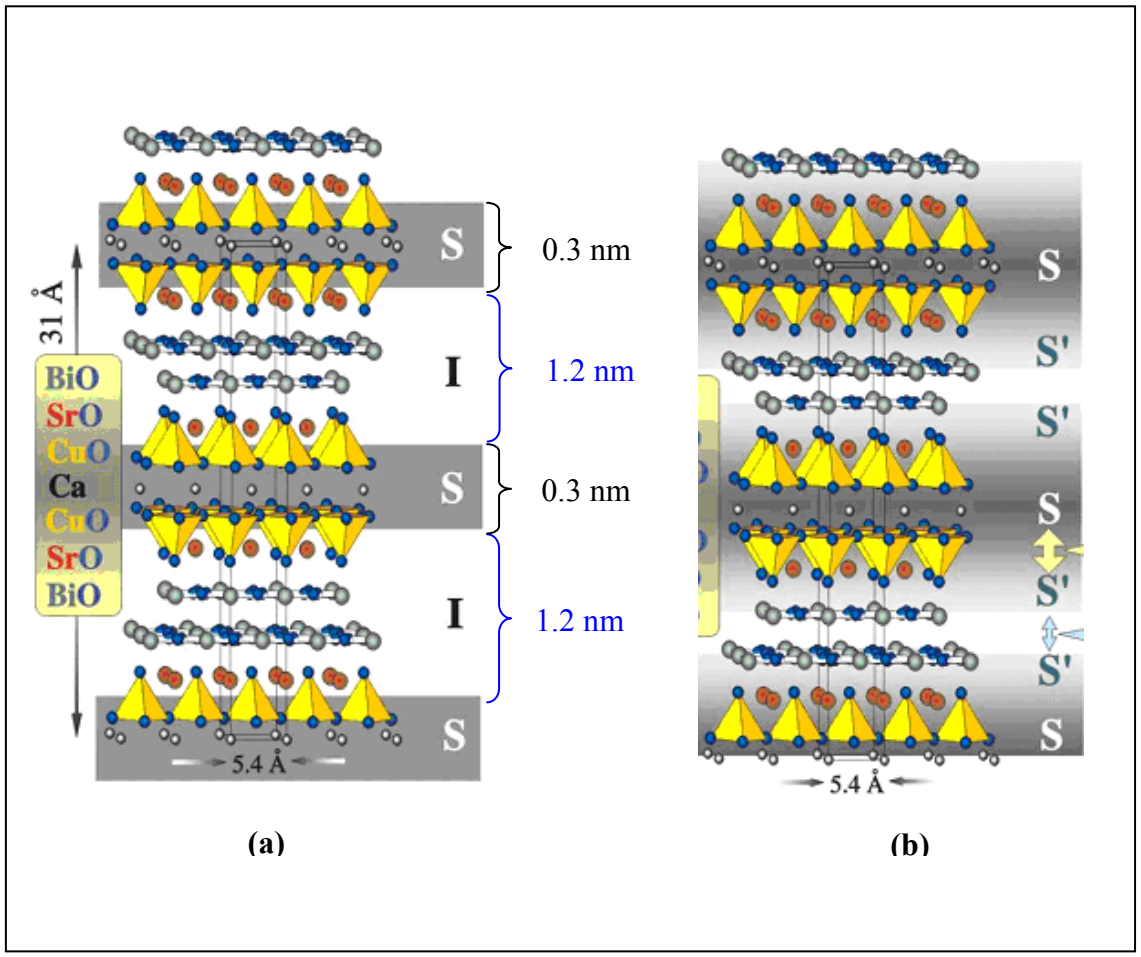

Figure 2.1. BSCCO crystal structures belong to Bi2212 phase. a) The layer structures according to multilayer model (only superconductivity with Cu-O planes) b) According to proximity model, it shows the possible variation of the superconductor energy gap from the darkened region to lighted region (Source: Yurgens 2000)

On the other hand, small coherence length ξ_c under 1 Å makes Josephson tunneling difficult across the long distance between Cu-O layers. In spite of the difficulty in Josephson tunneling at multilayer model, it is necessary to mention about another model defining superconductivity in structure of Bi2212. It is the proximity model that the Bi-O layers together Cu-O layers contribute together to superconductivity. The figure 2.1b shows the assumption of proximity model at structure of Bi2212 with schematic of IJJ becoming as SS′-I- SS′. The Josephson tunneling occurs between adjacent Bi-O layers with small order parameters and strong proximity coupling. It explains why the strong temperature dependence and small value of energy gap parameter at IJJ tunneling occur. Thus the Josephson tunneling shows a smaller energy gap corresponding to a weaker superconductivity (S′) of the Bi-O layers. (Yurgens, et al. 1996).

2.2. Tunneling Spectroscopy

Because of the layered structure of Bi2212 single crystal such as natural stacks of SIS multi-junctions called intrinsic Josephson Junctions, large anisotropic electrical behaviors of the HTSs are considered to be a rich source for superconductivity. The large hysteresis and multiple branches of current flow at the current-voltage (I-V) characteristics along to c axis is not only interesting subject for researches, but also comprehensively a starting point of the limitations on possible theories of HTSs. The results from I-V measurements provide evidences for these theories and require reassessment of many works. For example, tunneling spectroscopy of layered HTSs provide us wealth of important information on superconducting energy gap value with temperature dependence, number of IJJs, pseudo-gap pairing mechanism and coupling through the block layers. Moreover, at magnetic field application, tunneling spectroscopy is primarily important to derive properties of the vortex system in HTSs. Therefore researchers are focused on experiments including the tunneling spectroscopy which directly address the issue of unconventionality (Zasadzinski 2002). Before adding more detail to tunneling results of HTSs mentioned above, it is beneficial to remember basic tunneling phenomenology briefly.

2.2.1. Basic Tunneling Phenomenology

Tunneling known quantum mechanical effect is based on the transition of a particle through a classically-forbidden energy state or potential barrier. Normally, it can be thought to pass through the barrier, only if a particle has the kinetic energy E larger than the height of the barrier. Unlike the prudence of classical mechanics, quantum mechanics accepts the objects different from classical objects such as ball and makes tunneling possible. The objects in quantum mechanics are emphasized to exhibit wavelike behavior. For example, an electron moving with momentum (p = mv) also has a wave-length λ= h/p (fundamental of de Broglie relationship). Thus it is possible that the wave function describing the particle can extend to the other side of the barrier. However, it is well known that at normal metal-insulator- normal metal junction (NIN), empty target energy states of other metal are available since tunneling can occur (Pauli principle). In this manner, tunnel current is dependent on not only the number of incident electron but also the number of the empty target states (Wesche 1998).

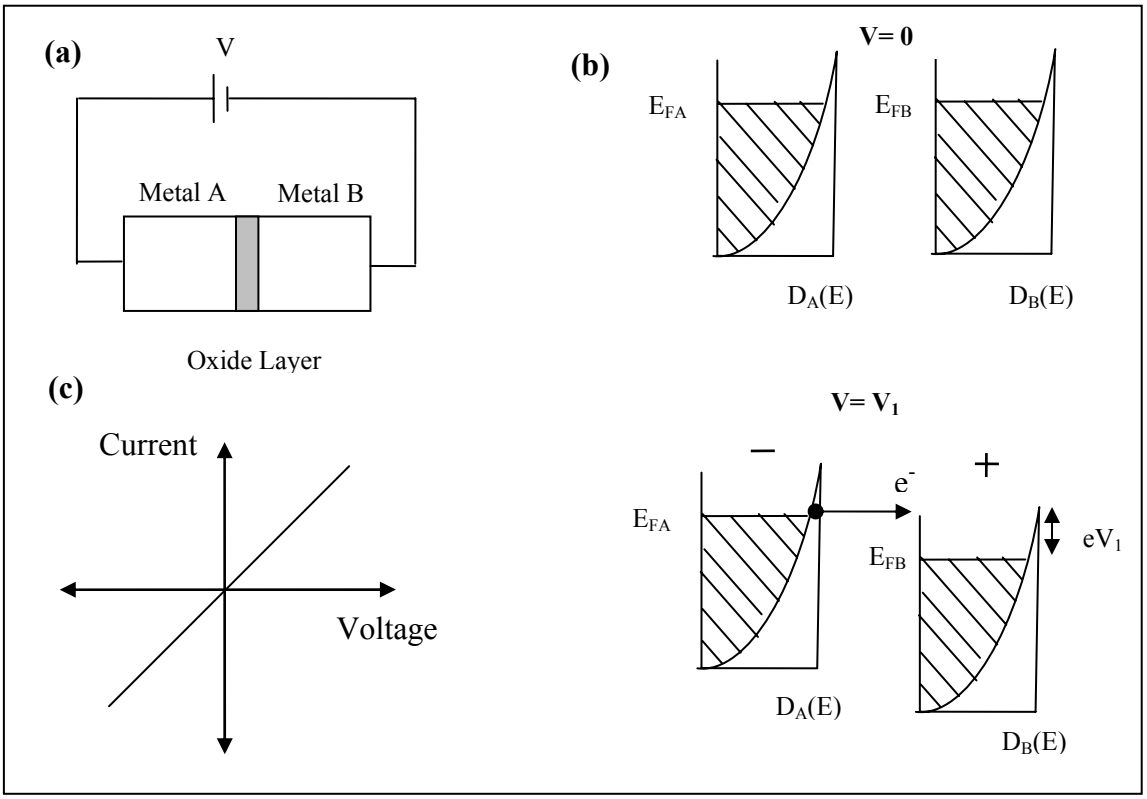

Figure 2.2. Tunneling in NIN junction a) Schematic of NIN junction with thin insulating layer b) Variation of Fermi energies with applied voltage at metals c) I-V characteristic of NIN junction (Source: Wesche 1998)

Experimental set-up for the tunneling current measurement, density of states for the metals and I-V tunneling characteristic of NIN junction are shown in (Figure 2.2) The tunneling probability is exponentially depended on the width of potential barrier. In order to increase the number of allowed transitions in the one direction, a voltage V is applied because tunneling will only occur from a filled state to empty state. The figure 2.2.b shows a differences eV_1 of the Fermi energies of the two metals at applied voltage and the states in the hatched areas are occupied at T= 0. Figure 2.2.c shows variation of tunneling current proportional to applied voltage.

2.2.2. Tunneling in SIN Junction

Unlike current proportional to applied voltage at NIN junction, tunneling characteristic at Superconductor-Insulator-Normal Junction (SIN) reveals different behavior with characteristic of current-voltage (I-V) deviating from straight line due to existence of energy gap (Δ) of superconductor. No tunneling current flows until voltage reaches the value of Δ/e since there are no states available for electrons tunnel into. Therefore I-V measurements are mainly used to determine the superconducting energy gap. It was first time that the I-V measurement at SIN junctions has been used by Giaver to determine the energy gap (Giaver 1960). Since cooper pairs have zero spin, they are represented by Bose-condensation. Thus it is not wrong to say that they populate the same quantum state at the Fermi energy E_F.

To explain SIN tunneling there are two different representations of energy levels that are semiconductor and Bose condensation representations. According to Bose condensation representation, the SIN tunneling processes are shown in (Figure 2.3) and at absolute zero; the Cooper pairs having behavior of boson are condensed into a level located at a distance Δ below the bottom of the conduction band of the superconductor. When an applied voltage reaches the value of Δ/e, the Fermi energy of the superconductor connected to the positive pole of a battery is shifted to lower value in which the empty energy states of the superconductor and Fermi energy of the normal conductor are at the same level. It makes electron tunneling possible from the Fermi energy of normal conductor to the empty energy states of the superconductor. When superconductor at SIN junction is connected to the negative pole, at voltage $V= -\Delta/e$ the Fermi energy of the superconductor is shifted up as much as value of the energy gap Δ.

Thus it is possible to break the cooper pairs whose one of the electrons tunnels into normal conductor. The other electrons have enough energy Δ for excitation to empty state of superconductor (Wesche 1998).

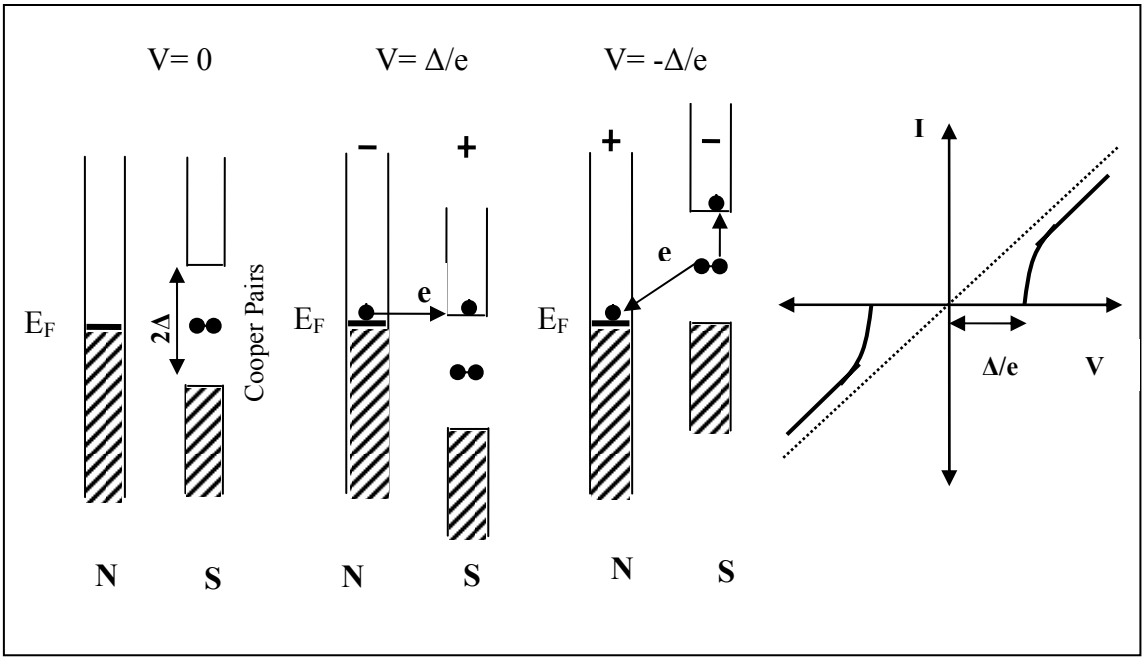

Figure 2.3. The SIN tunneling process with representation of Bose condensation and its current-voltage (I-V) characteristic at T= 0 K (Source: Wesche 1998)

The particles occurred by breaking the cooper pairs are called quasi- particles. In order to calculate the tunneling current, the one dimensional density of state in normal state $N_n(E)$ and the density of states of quasi-particle excitations in superconductor state $N_s(E)$ must be known. It is given by (Equation 2.1) at T= 0 K.

$$I_{sn}(T=0) = \frac{2\pi e}{\hbar} \int_{-\infty}^{\infty} \left|T^2\right| \; N_n(E'-eV) \; N_s(E') \left[f(E'-eV) - f(E') \right] dE' \tag{2.1}$$

$$For \; \Delta < E' \leq eV$$

In this equation, $[T^2]$ is the tunneling matrix element and $f(E,T)= [1+\exp(E/ k_BT)]^{-1}$ is the Fermi-Dirac function. According to BCS theory, the rate of the density of states on both sides of the insulating barrier given by (Equation 2.2) provides us to make an assumption between I-V characteristic and the density of states of quasi-particle in superconductor, $N_s(E)$.

$$\frac{N_s}{N_n} = \begin{cases} 0 & |E| < \Delta \\ \dfrac{E}{\sqrt{E^2 - \Delta^2}} & |E| \geq \Delta \end{cases} \tag{2.2}$$

Since $N_n(E)$ is essentially constant near the Fermi level, the tunneling characteristic corresponds directly to the density of states of quasi-particle excitations $N_s(E)$. The deviation of (Equation 2.1) to the voltage, tunneling conductance dI/dV is proportional to the density of states of the superconductor. Using (Equations 2.1 and Equation 2.2) and calculating the integral, the expression of dI/dV can be written as (Equation 2.3) where G_n is the normal tunneling conductance.

$$\left(\frac{dI_{sn}}{dV}\right)_{T=0} = \begin{Bmatrix} G_n |V| / \left[V^2 - (\Delta/e)^2\right] & |eV| \geq \Delta \\ 0 & |eV| < \Delta \end{Bmatrix} \tag{2.3}$$

Besides it is well known that energy gap is dependent on temperature, there is an important result from above equations that is variation of tunneling current with temperature. Figure 2.4 shows the density of near the Fermi level E_F in SIN junction and tunneling current variation with thermal excitation. While in conventional superconductor, the gap completely vanished after the critical temperature T_c, at I-V spectrum in HTSs this sharp transition from the curve to the straight line during the phase transitions because of the existence of the pseudo-gap (Duzer and Turner 1999).

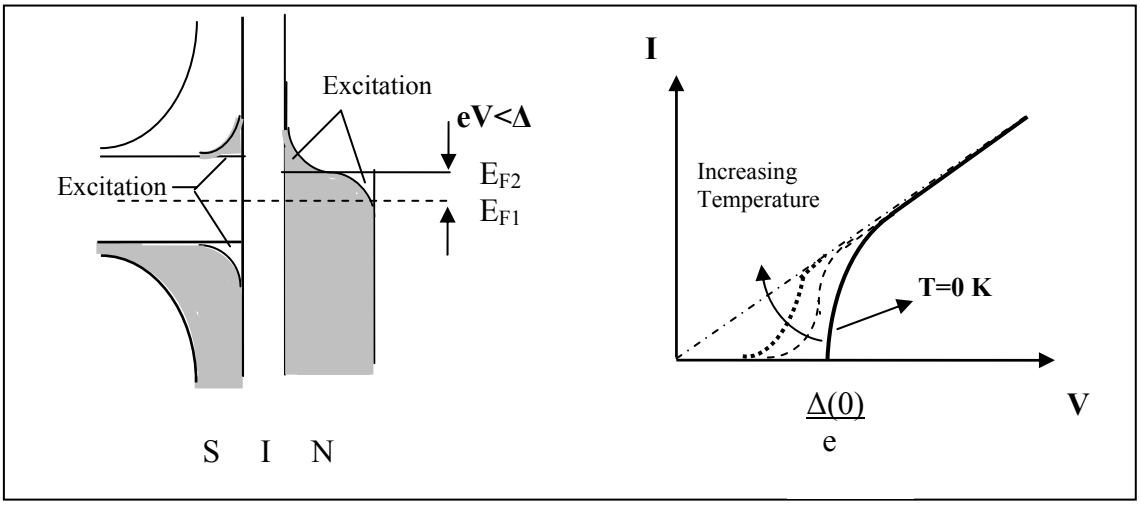

Figure 2.4. The DOS near the Fermi level in SIN junction at $T<T_c$ (left) and variation of tunneling current with temperature (Source: Duzer and Turner 1999)

2.2.3. Tunneling in SIS Junction

In Superconductor insulator superconductor (SIS) tunneling spectroscopy, the focus of the experiments is on single electron (quasi-particle) tunneling which directly addresses the issue of unconventionality including temperature dependence of the gap size, gap symmetry, pseudo-gap and pairing mechanism. Therefore tunneling in HTSs with their large anisotropic properties and thermal fluctuation represents a large research field including the observation of many new effects experimentally.

One of two representations of single tunneling between two identical superconductors, Bose condensation representation is shown in (Figure 2.5). In order to start electron tunneling, applied voltage that causes shifting the Fermi level of the second superconductor connected to the positive pole of a battery to lower value is increased until the value of 2Δ/e. Thus Cooper pair breaking become possible in first superconductor and one of electron belong to pair can tunnel to the empty (quasi-particle) energy state of second superconductor. Since releasing energy from pair breaking is equal and greater than the energy gap value of first superconductor, the second electron of broken pair is excited to the quasi-particle energy state of first superconductor. At voltage V= -2Δ/e direction of tunneling reversely changes (Schmidt 1997).

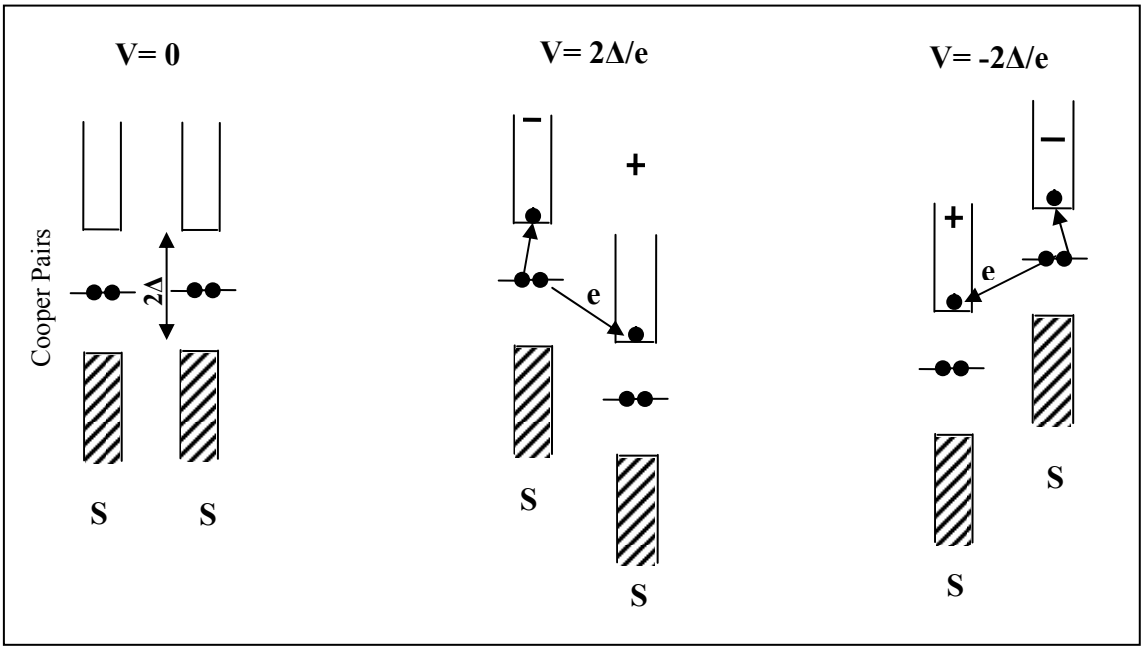

Figure 2.5. Bose condensation representation of single electron tunneling between two identical superconductors (Source: Wesche 1998)

In SIS tunneling spectroscopy, apart from single electron tunneling, Cooper pair tunneling through a very thin insulating layer is possible when applied voltage is zero. In 1962 B. D. Josephson predicted that the pair tunneling current is depended on the difference of phases of the effective wave functions on the two sides of the junction and the phase difference is both temporally and spatially variable (Josephson 1962). Although Cooper pairs tunneling through the barrier as particles with a spatial extension ξ_c is seen to be difficult, it can be well understood as the tunneling of the wave function describing the collective of the Cooper pairs. When the energy associated with coupling exceeds the thermal fluctuation energy, Cooper pairs can tunnel through the barrier without energy loss. Apart from single electron tunneling, there are no excitation and bias across the junction. The Josephson current is carried by Cooper pair and flows without resistance until the critical current value I_c of the SIS junction. After the critical current value I_c is exceeded, voltage and current jump to values on the I-V quasi-particle tunneling characteristic (Duzer and Turner 1999). I-V characteristic of the SIS junction is shown in (Figure 2.6).

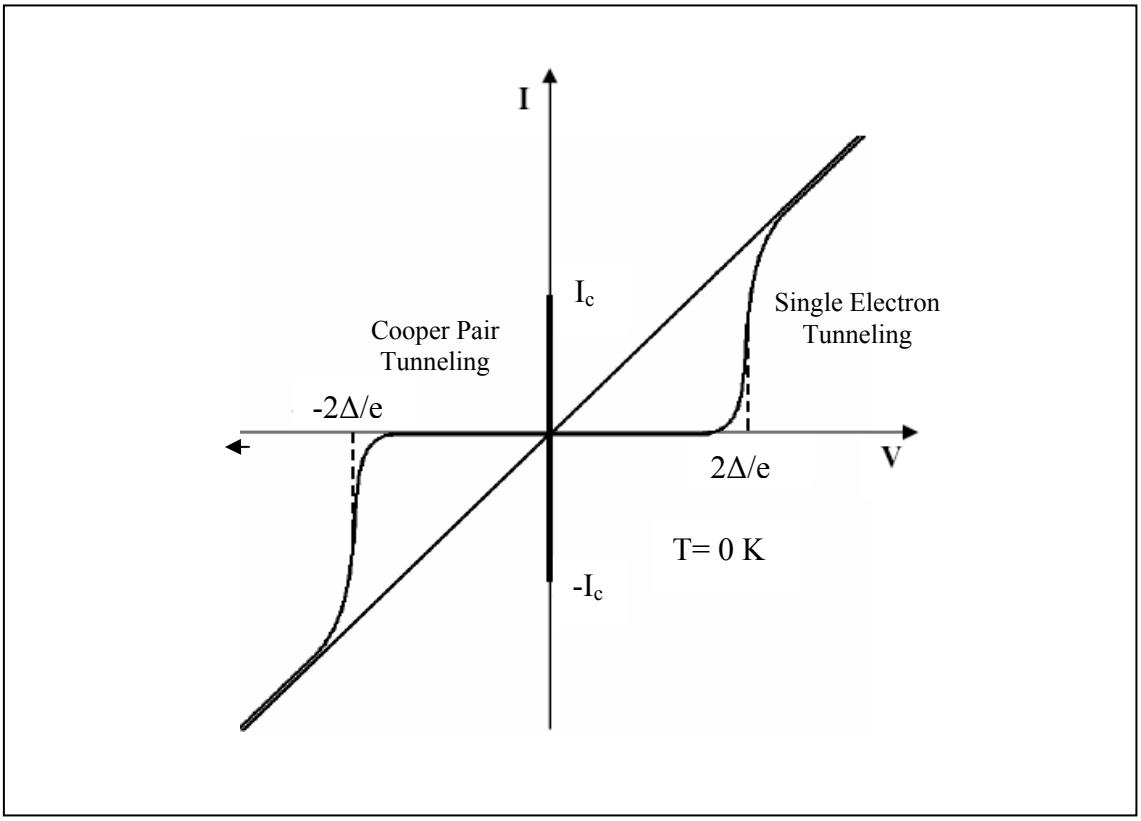

Figure 2.6. I-V characteristic of SIS junction with quasi-particle and Cooper pair tunneling at T= 0 K (Source: Wesche 1998)

In SIS junction, the tunneling conductance and the convolution of the density of states function of superconductor are proportional each other. The SIS tunneling current I_{ss} at T=0 is given by (Equation 2.4).

$$I_{SS} = \frac{G_n}{e} \int_{-\infty}^{\infty} \frac{|E' - eV|}{\sqrt{\left[(eV - E')^2 - \Delta^2\right]}} \frac{|E'|}{\sqrt{(E'^2 - \Delta^2}} \left[f(E' - eV) - f(E') \right] dE \qquad (2.4)$$

where G_n is normal tunneling conductance when tunneling occurs between two identical superconductors. Tunneling current, I_{ss} at voltage V= 2Δ/e is

$$I_c = \frac{1}{2} \pi \left(\frac{G_n}{e} \right) \Delta_{(0)} \qquad (2.5)$$

which is known as Josephson current. However, I-V characteristic seen in (Figure 2.6) will change due to thermal excitation when temperature starts to rise from absolute zero. Thus both DOS and energy gap decrease with temperature (Duzer and Turner 1999).

Superconductor energy gap structure in HTS cuprates is depended on not only temperature but also direction. While the energy gap in conventional superconductors is a constant in k space (s wave symmetry), HTSs with d wave pairing symmetry have anisotropic energy gap on the Fermi surface. Simple d-wave DOS defined by BCS type interaction of a two dimensional superconductor is given by

$$N_s(E,k) = \mathrm{Re}\left\{ \frac{E - i\Gamma}{\sqrt{(E - i\Gamma)^2 - \Delta(k)^2}} \right\} \qquad (2.6)$$

where Γ is a smearing parameter to account for quasi-particle lifetime and the k dependent energy gap, Δ(k)=Δ cos(2φ) with maximum value of gap, Δ and polar angle in k-space φ (Won and Maki 1994). Temperature dependent of energy gap is given by below equation where k_B is the Boltzmann constant (Bardeen, et al. 1957).

$$\Delta(T) = 3.2\ k_B T_c\ (1 - T/T_c)^{1/2} \qquad (2.7)$$

In SIS junction tunneling spectroscopy, c-axis tunneling of highly anisotropic layered HTSs such as Bi2212 is the most important in the limitations on their possible theories because of their natural stacks of SIS multi-junction (Intrinsic Josephson Junction, IJJ) with thickness of 1.5 nm. Therefore IJJ is not only an interesting subject for research by itself, but also is a powerful tool to understand the nature of HTSs including physics of vortices in superconducting electronic applications. The I-V characteristic of layered HTSs along the natural IJJ stacks includes several branches due to individual switching of each junction from Josephson state to quasi-particle state when the bias current exceeds the individual critical current of each junction (Yurgens 2000). Thus each of the junctions acts as one of the single branch in large gap voltage of all junctions and the branches are almost vertical these voltages. In order to well understand the c-axis electrical behaviors of Bi2212, it will be beneficial to explain them on graphs including experimental I-V data. Figure 2.7 shows I-V along to c-axis of Bi2212 and dI/dV-V graphs at 4.2 K published by (Ozyuzer, et al. 2005). In this study including comparison of I-V characteristics of both IJJ and SIS junctions observed from the same crystal, differences in their energy gap values and I-V characteristic features are first realized. Seven quasi-particle branches at the I-V graph corresponding to seven individual IJJs and dI/dV belong to same data are seen in (Figure 2.7.a and Figure 2.7.b) respectively. Since it has seven branches, tunneling conductance peak, is divided into seven in order to obtain the value of $2\Delta/e$. If comparison in (Figure 2.7.c) between the value of Δ obtained from IJJ I-V data and energy gap Δ of SIS junction is considered, underestimate value of Δ in IJJ tunneling measurement is observed. The reason of lower energy gap value is excessive temperature than the bath temperature occurring at local heating area in IJJ stacks. Also the heating effect causes the absence of dip and hump feature in IJJ, while they are observed SIS and SIN junction I-V measurements. Influences of the heating effect and non-equilibrium on tunneling measurement are unwanted negative characteristic of IJJ in Bi2212 because they cause the lost of the superconductivity at local areas on Bi2212. Beside the absence of dip and hump feature, sharp conductance peaks in IJJ tunneling characteristic rather than peak in SIS junction are seen. Moreover in the study, the temperature dependence of the energy gap has been investigated and it was observed that the values of Δ obtained from both SIS junction and IJJ decreasing with increasing temperature. Thus it is expected from temperature dependence of energy gap and also (Equation 2.7) that energy gap disappears above the critical temperature but it is not so

that. The gap feature above T_c continues with expression of a pseudo-gap as a characteristic property of HTSs (Ozyuzer, et al. 2005). The strong temperature dependence of energy gap and pseudo-gap feature of Bi2212 superconductor were observed in many studies.

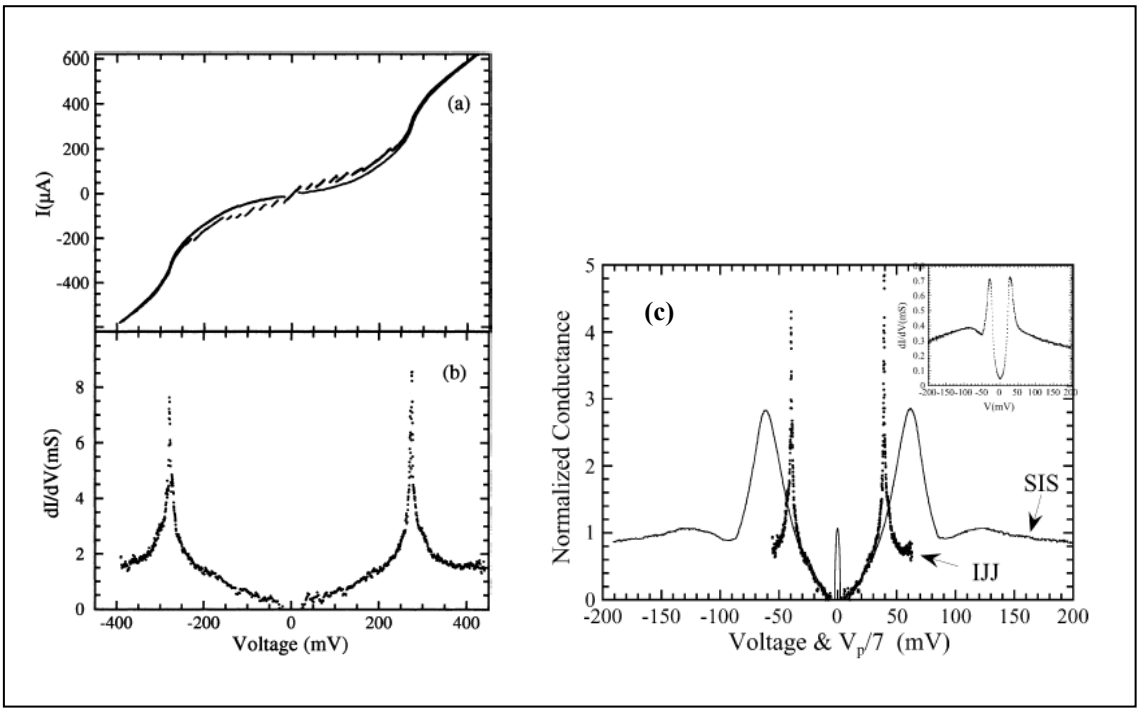

Figure 2.7. Tunneling characteristics of Bi2212 at 4.2 K with quasi-particle branches (a) I-V (b) dI/dV (c) Comparison of normalized conductance of SIS and IJJ (Source: Ozyuzer, et al. 2005)

The poor thermal conductivity of all HTSs causes a local overheating in superconductor structure. As increasing the number of IJJs in the quasi-particle state, the overheating increases and causes smaller voltage jump (conductance peak) in I-V curves. Moreover Non-equilibrium effect that is easy quasi-particle self injection through the high transmissive IJJ tunneling barrier (about 3 Å thickness in Bi2212) increases the heating effect in the structure. This effect also leads to back-bending of the I-V curve in the sub-gap region. In order to reduce the heating effects in stacks, one of the various attempts is that decreasing the lateral area of the mesa leads to improve heat conduction. However, since the same current per unit area through the junctions flows, the non-equilibrium effect still occurs and causes the Joule heating (Zasadzinski 2002). Therefore this method is partly successful in observing the energy gap in I-V curves. The other way is to use the short current pulse tunneling measurements which provides

free I-V characteristic different from gap suppression because of joule heating in IJJ (Suziki, et al. 1999). One effective method is that use the intercalation process expanding layered superconductor material along the c axis in order to increase the junction resistance. In this way the number of quasi-particles tunneling through barrier is decreased. On the other hand, it causes the decreasing at coupling between superconducting layers and critical temperature, T_c. Intercalation reaction is carried out by vapor transport reaction and in this reaction, the materials such a guest molecules of HgX_2 (X= Br, I) are used (Ohhashi, et al. 2004). Figure 2.8 shows how the molecule of $HgBr_2$ intercalates into adjacent Bi-O layer in Bi2212 structure and expansion along to c-axis of Bi2212 occur. There is difficulty in obtaining homogeneous expansion with intercalation along to c-axis of the crystal. It is analyzed with respect to X ray diffraction (XRD) results.

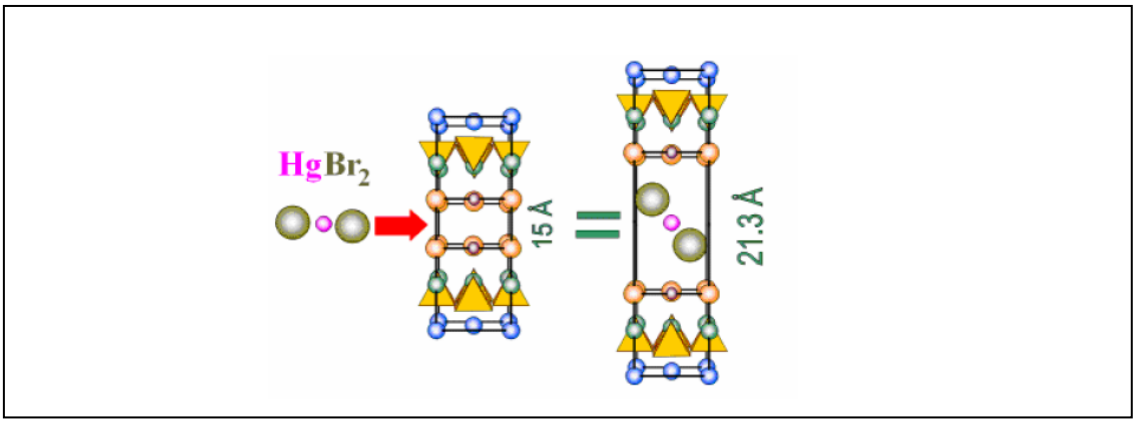

Figure 2.8. The $HgBr_2$ intercalation representation in Bi2212 structure (Source: Yurgens 2002)

2.3. Pseudo-Gap Feature in HTSs

Since superconductor materials are exactly normal phase above T_c, it is expected that tunneling measurements along to c-axis exhibits normal state properties with linear dependence. However, at these measurements, obtaining the non-linear behaviors in I-V measurements above T_c has attracted much attention in recent years. This effect results from the presence of a partial energy gap called pseudo-gap and points the unusual pairing mechanism above T_c in HTSs. The pseudo-gap known as precursor of superconductivity has been characterized in various experiment such as in-plane resistivity, angle-resolved photoemission spectroscopy (ARPES), NMR, specific heat

and optical measurements (Yurgens 2000). It is also known as a property of the under-doped phase and the magnitude of pseudo-gap is inversely dependent on doping level, p, although the pseudo-gap has been observed to exist at all doping concentrations due to mistaken determination on the local doping level of material in some works. In order not to obtain such conflicting observations, it is needed to benefit from a clear relationship between the energy gap and doping concentration (Miyakava, et al. 1999). Thus, the absence of the pseudo-gap in heavily over-doped Bi2212 whose doping level determined by the energy gap value has been verified from tunneling spectroscopy of break junction (Ozyuzer, et al. 2002).

The characteristic temperatures of an under-doped HTSs at the observation of the presence of pseudo-gap are T_c and T^*. They are shown in (Figure 2.9) on scale of temperature. While temperature is decreasing at the temperature, T^*, the pseudo-gap starts to appear then the Cooper pairs start to form. Below the temperature, T_c. there is a dominance of superconducting gap. The characteristic temperature can be detected by some experimental techniques. For example the starting point of the non-linear behavior in the resistivity measurements along to c-axis is known as pseudo-gap temperature, T^* (Yurgens 2002).

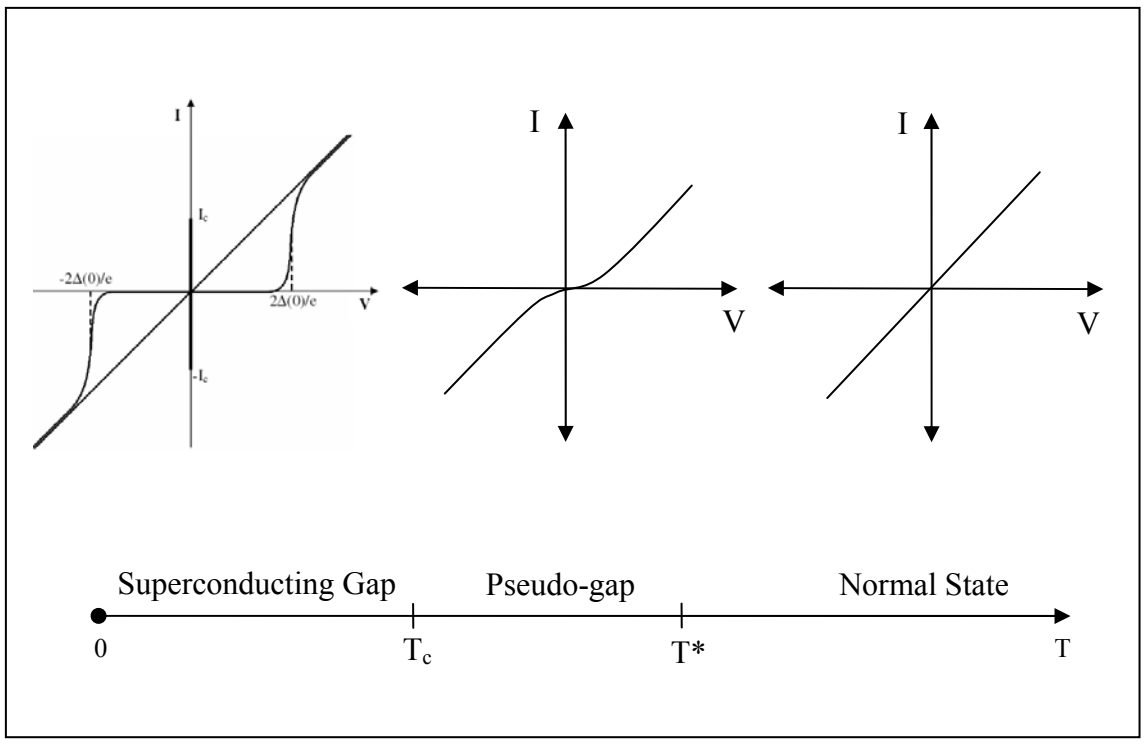

Figure 2.9. Temperature evolution of c-axis I-V characteristics of Bi2212 in under-doped region (Source: Wesche 1998)

2.4. Charge Doping

Generally, the number of electrons or holes at Fermi level in materials is increased by doping which has also the most profound influences on superconductivity. In the superconductor it not only provides the phase transitions but also changes the critical temperature and energy gap value of superconductors. To change charge carriers in superconductor, there are two methods which are substitution of metallic atoms in charge reservoirs by higher valence atoms and changing of the number of the oxygen atoms. According to doping levels, variations at Tc and phase transitions are shown in (Figure 2.10).

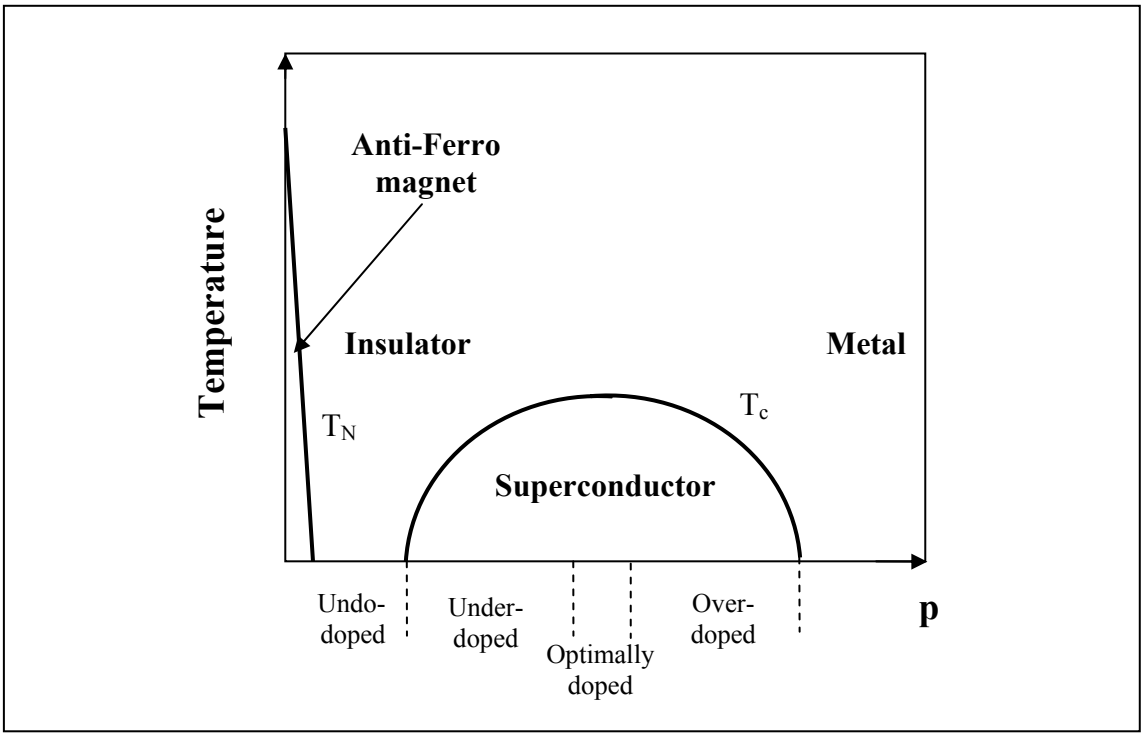

Figure 2.10. The variation of the cuprate superconducting properties with increasing hole concentration (Source: Ozyuzer, et al. 2002)

Apart from conventional superconductor, HTS cuprates have been justified to exhibit non-monotonically doping dependence of T_c that is represented empirical relation

$$\frac{T_c(p)}{T_c(\max)} \cong 1 - 82.6\,(p - 0.16)^2 \tag{2.8}$$

where T_c(max) is maximum critical temperature for given cuprate superconductor and p is the doping level. Thus increasing doping levels from undo-doped to over-doped critical temperature, T_c and energy gap, Δ have the same non-monotonic variations. For example, unlike the expected prescience a superconductor in over-doped region has small values of T_c and Δ (Miyakawa, et al. 1998).

The temperature dependence of resistivity of Bi2212 superconductor changes with doping level in Cu-O planes. In (Figure 2.11), along to c-axis of Bi2212 the variations at resistivities versus temperature with respect to doping level are approximately shown. They were collected from some studies (Silva, et al. 2003, Kendziora, et al. 1993 and Kleiner and Muller 1994) on oxygen doping level dependence of resistivity changing with temperature. As can be seen in (Figure 2.11), while the R-T behavior of a material in the un-doped region is same to semiconductor, phase transition of an under-doped superconductor is seen with variation of resistivity that firstly falls through the minimum values then raises the maximum values until critical temperature value. At variation of oxygen level from the optimally-doped to over-doped, superconductors' out of plane resistivities gradually start to exhibit metallic behavior.

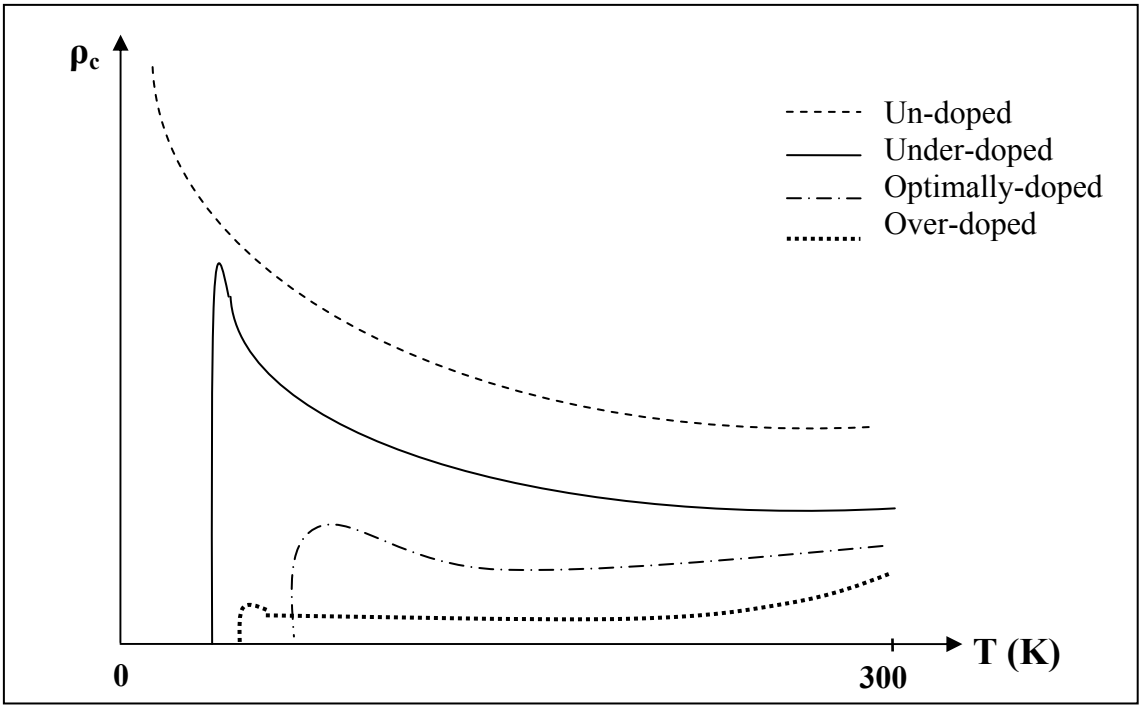

Figure 2.11. Representation of the variation of c-axis resistivity versus temperature at different doping levels (Source: collected by Silva, et al. 2003, Kendziora, et al. 1993 Kleiner and Muller 1994)

2.5. Terahertz Emission from Bi2212

Recently many people at science and technology are interested in the electromagnetic waves in terahertz (THz = 10^{12} Hz) frequency range (0.3-30 THz) because of their important application areas including physics, biology, chemistry, astronomy and medicine. The frequency interval of THz emission at electromagnetic spectrum is between microwaves and far infrared radiation and this region is a rich area for molecular spectroscopy because the most molecules have rotational and vibrational absorption modes in the THz frequency range. For example, it is predicted that the collective vibrational modes of many proteins and DNA molecules are in THz range and it makes them important in biomedical applications from cancer detection to genetic analysis. Besides they are thought to use material diagnostics like x-ray, in application areas of biology and medicine they have important advantage which their non-ionising properties make the characterizations safer than x-rays. Moreover their easy passing through the some materials such as clothing, paper, cardboard, wood, masonry, plastic and ceramics enable them to become important in security because these materials are relatively non-absorbing in THz frequency range (Ferguson and Zhang 2002).

Electromagnetic waves with frequency below and above the THz frequency range (0.3-30 THz) are widely generated by semiconducting electronics based on high-speed transistors and the photonics based on the semiconducting laser respectively. However, in this frequency range there are still lacks of THz sources and difficulties in its generation although their functional advantages in many application areas entail the evolution of the THz sources in science (Bae and Lee 2006). Recently, the research on THz radiations sources with high power, low cost and portable has been increasing. A part of the investigations of THz sources includes semiconductor technology (Ferguson and Zhang 2002), like THz quantum-cascade technique (Köhler, et al. 2002) etc. THz generation using the semiconductors are based on sinusoidal current oscillation (electronic) and transition electronic states between quantum levels (photonic) but in both of them there are some disadvantages making them under-development in technology. One of them is that generation of THz by the transit of charge carriers in electronics takes long while the other disadvantages is that in THz frequency range photon energy much lower than thermal energy at the room temperature (Bae, et al. 2007). Since they are planned to use in technological areas, they should be continuous,

coherent and frequency tunable as well. Therefore the research has gone towards the novel THz sources which include technology of HTSs layered structure. One of the several reasons making HTSs suitable candidate for the generation of THz radiation is their layered structure which enables the propagation of electromagnetic wave by unique excitation called Josephson plasma oscillations and frequency of the Josephson plasma is between THz ranges (Tachiki, et al. 1994).

After consequent studies in spite of some problems in demonstrating a good performance of radiation emitted from superconductors, the research on THz emission in superconducting technology has alternately increased. For that reason, the conventional superconductor and HTSs were used but recently IJJs in layered HTSs were preferred in order to solve the limitation problem on both emission power and frequency. In such versatile studies on IJJs, we can classify theoretical models with their experimental configurations on generation of THz emission from layered superconductors into several categories. In the all models, the important of versatile IJJs tunneling behavior at THz technology has been considered and demonstrated to enable the emission of THz radiation in last years. Moreover, the common point of emission principles from layered superconductors is based on excitation of cavity modes in IJJs like laser technology and ac Josephson effect. In order to excite cavity mode, two instructive ideas have been considered in the last decade. One of them includes fluxon dynamics in IJJ of stacked Bi2212 and this model has been proposed by (Tachiki, et al. 1994) and demonstrated by some experimental studies with magnetic field application. The other study includes the excitation cavity mode in stacks of IJJs without external magnetic field. In these experimental studies, to generate THz emission in IJJs researchers used mesa with different heights and dimensions on layered HTS (Kleiner 2007). The last development in THz research done by (Ozyuzer, et al. 2007) has demonstrated to generate coherent continuous THz electromagnetic wave emitted from long edges of large mesa whose height is about 1 μm. Although their mesa dimensions were not latterly used due to presence of heating effect, they have succeeded to excite cavity mode in multi junction stacks similar to laser technology. For both superconducting and semiconducting technologies it is required to make compact solid-state sources emitting continuous and coherent THz radiation. The meaning of coherent radiation is oscillation of all IJJs in same phase. Beside these THz sources, there are some the studies on detection of THz emission by using same ac Josephson effect in IJJs (Batov, et al. 2006).

Tachiki et al have been studying a model and defining experimental set up for THz emission by layered HTSs since 1994. Their present simulation based on the fluxon dynamic for THz radiation in IJJs of Bi2212 is shown in (Figure 2.12). In the simulation, one of the excitation way called Josephson plasma is defined and it is explained that decaying excited plasma creates electromagnetic waves with THz frequency range. This experimental set up includes magnetic field application along the axis parallel to layered structure of Bi2212 superconductors, while external DC current is being applied along c-axis perpendicular to layers. This external magnetic field (~ 1 T) parallel to layers induces fluxons whose centers are in the insulating layers. The fluxons having non-periodic configuration in layers flow in negative direction of b with velocity of v shown in (Figure 2.12) and this dense flowing of fluxons induces a voltage differences in each IJJ layers of superconductor. The voltage difference causes an oscillating Josephson current in the direction of c axis of Bi2212. Intense and coherent THz emission along to negative direction of b is based on interaction between the oscillating current and Josephson plasma. Thus they are emitted from IJJ to dielectric through interface.

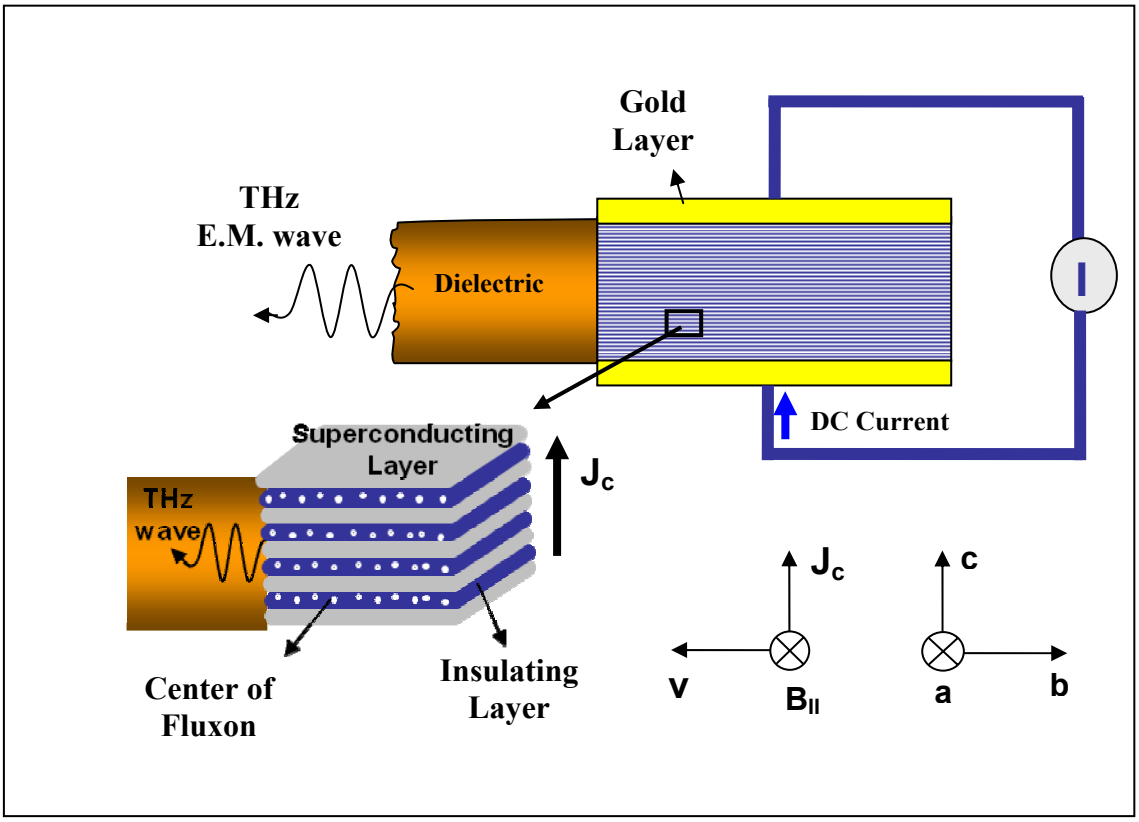

Figure 2.12. Schematic diagram for THz emission

(Source: Tachiki, et al. 2005)

Although the plasma waves have transverse and longitudinal which are c-axis and a-axis respectively, only the transverse component converts into electromagnetic wave at the interface between IJJ and dielectric. The frequency tunability of the THz emission from layered structures is defined by changing applied current, so tunable frequency range is limited by critical current of the superconductors since it is emphasized that there are no any THz emissions when the external current is larger than critical current value (Tachiki, et al. 2005).

In my thesis, I have studied on generation of THz emission that is one of main properties of IJJs in Bi2212 superconductor. In my study, I have fabricated large mesa (100x300 μm^2) including many IJJs. The lateral and planar dimensions of fabricated mesas are selected according to a study done by (Ozyuzer, et al. 2007). They could generate coherent THz emission from long side of large mesa whose height was approximately 1 µm. The mesa on Bi2212 single crystal includes of about 670 IJJs. The emission of radiation from long side of mesa by cavity mode like laser works was obtained during I-V characteristic measurements. When DC voltage is applied along to c-axis of Bi2212 superconducting single crystal, the current is oscillated in synchronized all of IJJs by standing electromagnetic wave. While the electromagnetic wave in Bi2212 single crystal propagates like Josephson plasma, it converts the noticeable emission from long side faces of mesa into cavity. That is seen in (Figure 2.13).

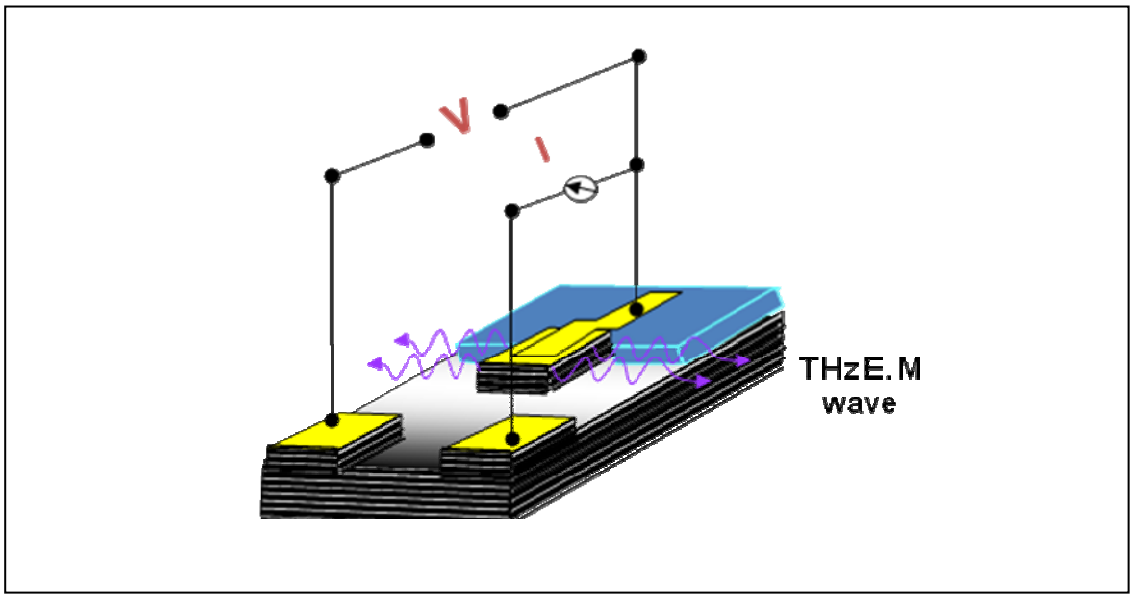

Figure 2.13. Our schematic of mesa and electrical contacts on Bi2212 for emission of THz radiation

The bolometric measurements were obtained while simultaneously recording I-V measurements through c-axis of Bi2212. When bias voltage decrease, radiation power is detected by bolometer. In order to distinguish electromagnetic wave from thermal radiation, they used polarize property of THz emission. On the other hand thermal radiation peaks were detected by bolometer because of heating of mesa at the highest currents. Moreover, if Bi2212 single crystal has high critical current value, heating effect at high current occurs and blocks the emission from mesa. Also large mesa area they used is a different reason to heat superconducting mesa. To solve this problem they used Bi2212 with low critical current value.

In the study, depending of emission frequency on mesa dimensions was demonstrated and obtained results are very agreement with frequency of fundamental cavity resonance. This frequency is given by,

$$f = \frac{c_0}{2nw} \tag{2.9}$$

where w is width of mesa and n is refractive index of Bi2212. The maximum frequency that is 0.85 THz was obtained from mesa whose width of 40 μm. Number of IJJs is corresponding to emission power of radiation because emission power from one individual IJJ is very low. It is emphasized that power is proportional with the square of the number of coherently oscillation of IJJ. Therefore mesas with high thickness were fabricated (Ozyuzer, et al. 2007).

While decreasing bias voltage on c-axis of mesa and phase transition of all IJJs from normal state to superconducting state, THz emission peaks have been detected at different DC voltage values. It can be resemble the operation principle of the quantum cascade laser in semiconductors. In (Figure 2.14), the non-equilibrium quasi-particle population in Josephson junction stacks during the presence of bias voltage is shown. A quasi-particle tunneling through the insulating barrier firstly relaxes to the bottom of empty state of superconductors and thus braking radiation is emitted. The quasi-particle recombines with the other quasi-particle at bottom of empty state and in this way, recombination radiation is emitted. Repeating of these processes creates to cascade amplification of radiation in SIS stacks. Since single junction can not be efficient to create cascade amplification, many of Josephson junctions are required. Also they should be identical with respect to critical current value. Recombination radiation is

dominant in cascade amplification of radiation (Krasnov 2006). The braking and recombination radiation are shown schematic energy diagram of Josephson junction in (Figure 2.14).

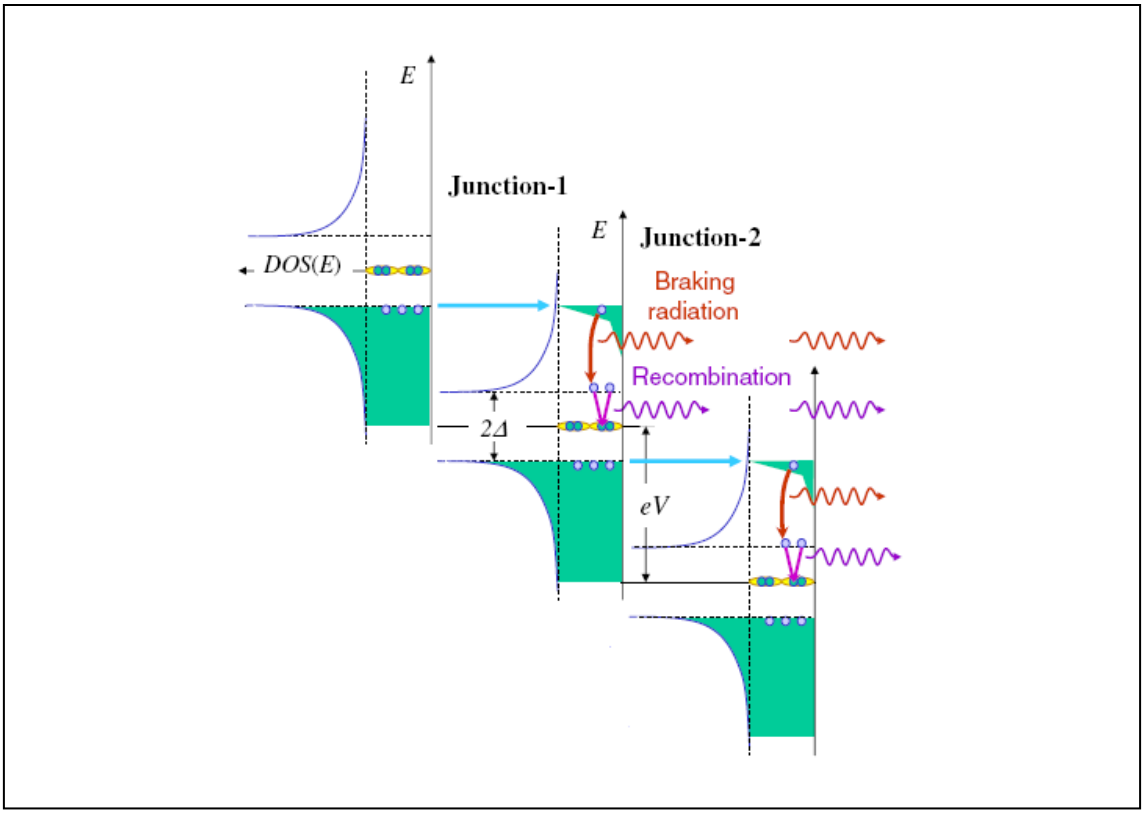

Figure 2.14. Schematic energy diagram of Josephson junction indicating non-equilibrium quasi-particle population (Source: Krasnov 2006)

CHAPTER 3

EXPERIMENT

3.1. Purpose

The main purpose of our work is fabrication of mesas with large area on Bi2212 single crystal for generation of terahertz (THz) radiation. In this purpose, mesas fabricated by various experimental processes are anticipated to have smooth rectangular prism shape with large area and high thickness which are related to capability of emitting THz rays. In addition, the surface and electrical characterizations of the mesas are important for our study. Atomic Force Microscope (AFM) was used to analyze mesa height, the lateral angle of the mesa and thickness of the gold layer. In electrical characterizations including R-T and I-V measurements along the c-axis of Bi2212 crystal, the electrical behaviors proper to layered structure of HTSs were investigated. In this chapter, the all of experimental processes including from the mesa fabrication to all electrical measurements will be described step by step.

3.2. Growth of Bi2212 Single Crystals

The high quality single crystals of Ca-rich Bi2212 which are used in our studies have been prepared by D.G. Hinks at Argonne National Laboratory. They were grown by the floating zone method and in order to obtain under-doped Bi2212 superconductors the single crystals can be annealed in argon gas flow (Ozyuzer, et al. 2003).

There are many processes in production of the Bi2212 superconductor which include such as sintering and melting the superconductor compounds. Although the fabrication of HTSs by sintering process is easy, this method is only preferred for the bulk HTSs and these superconducting materials have porous structure and random arrangement of superconducting grains. Therefore it is difficult to obtain a smooth structure including the uniform orientation of the superconducting crystal completely on the bulk HTSs (Michishita, et al. 1996). In order to produce the layered HTSs with the high quality and c-axis aligned structure, the researchers use the melting processes

including the melt-textured growth method (Jin, et al. 1988) and the laser-heated pedestal growth method (Feigelson, et al. 1988).

The floating zone method (FZM) which is one of the melt processes is used to obtain such a high quality uniform single crystal of HTS. Since it is a crucible-free technique and compounds are heated by IR radiation in optical system, the layered superconducting structures with high purity are fabricated without contamination during the process. The wide range of temperature adjusted by IR radiation power provides fabrication of many superconducting materials by FZM. The most important property of the fabricated materials by the FZM is better crystals with large size dimensions and uniform aligned structure than the bulk structure of this materials. For anisotropic electrical measurements, it is very important to fabricate a smooth uniform structure (mesa) with required sizes on the growth materials, so the perfect crystals are preferred. It makes FZM very important in superconducting devices (Michishita, et al. 1996).

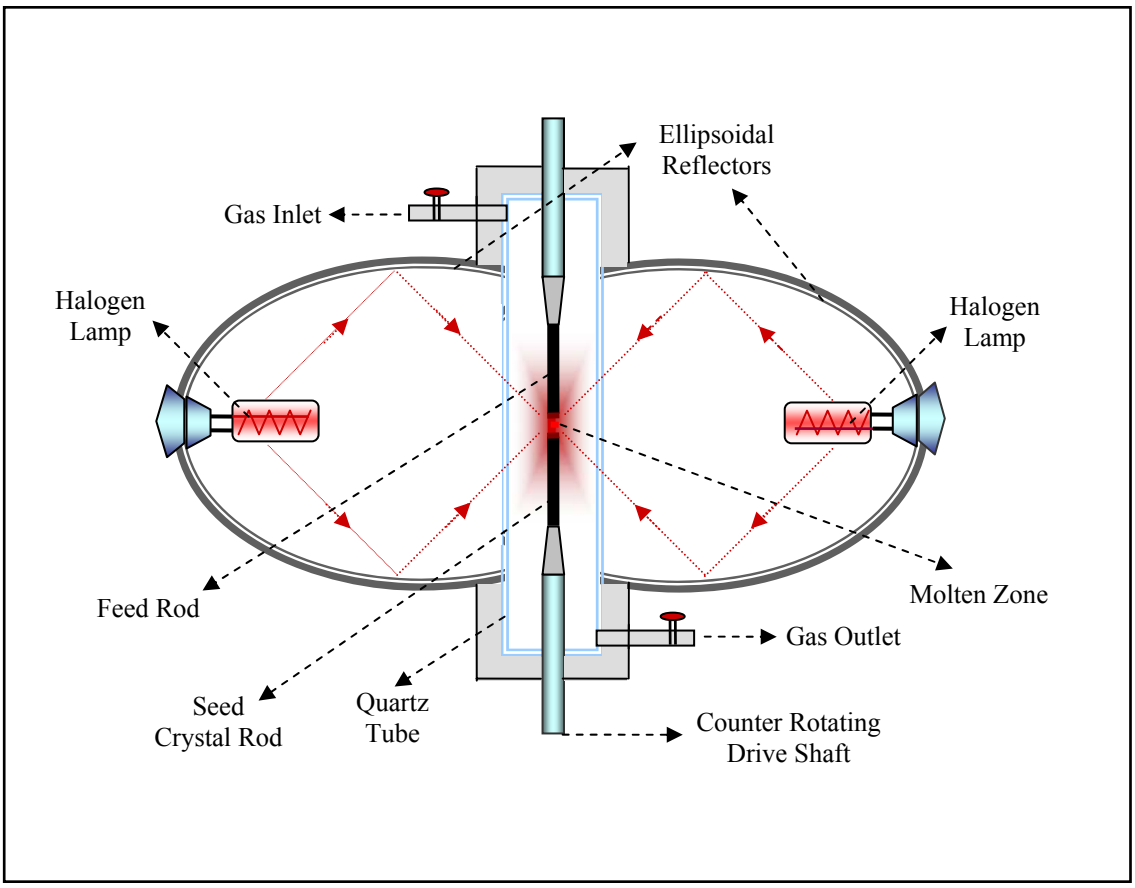

Figure 3.1. Double ellipsoid image furnaces for crystal growth with floating zone method (Source: Revcolevschi and Jogoudez 1997)

This technique generally includes an optical system focusing the light emitted by halogen lamp to the melting zone in the image furnace. Since the superconducting compounds are only heated by focusing light, there is no other material used near the melting zone in order to conduct the heating to compounds. Therefore the fabrication doesn't include contamination during the process. There are several experimental setups for FZM. In terms of the energy output, generally an experimental configuration including two ellipsoidal reflectors and halogen lamps are preferred. This setup seen in (Figure 3.1) has been shown at a review published by (Revcolevschi and Jogoude 1997). Two halogen lamps located at one of the two focal points of the each ellipsoid chamber emit radiations that are focused by ellipsoidal reflectors to the other common focal point of each ellipsoid in which is molten zone. The geometric shape of the ellipsoidal reflector covering inside the chamber enables focusing the radiation from a focus point to other focus point as the motions of the ball on the ellipsoidal billiard table. Before the floating zone process, superconducting bulk material formed as a rod is prepared by using calcine and sintering processes. The superconducting rod is divided into two pieces which are used as the feed and seed crystal rods in ellipsoidal furnace. Then they are coaxially mounted inside the quartz tube and their junction is in the center of the common focus point of each ellipsoid. The junction of two rods which is in molten zone is heated by halogen lamps so they begin to melt. By obtaining refractory oxide single crystals, the rods are moved downwards at fixed speed. Thus superconducting crystal is solidified with unidirectional growth. During the growth, feed rod and seed crystal rods are rotated to obtain the homogeneous aligned crystal structure. The superconducting layered single crystal rod with Bi2212 phase whose growth direction is parallel to [110] a-b plane is obtained at the end of the FZM. The crystals have not only a layered structure with a-b alignment along to growth direction but also c-axis alignment in the transverse section. The crystal growth in the quartz tube is performed in O_2 gas flow to supply oxygen to crystal. The pressure of O_2 is used as one of the growth parameters since it is affect the growth temperature and stabilization of the molten zone. Although there are many phases of BSCCO, Bi2212 is preferred because of its easy synthesis as a pure phase. (Revcolevschi and Jogoudez 1997).

In our studies, the critical temperature (T_c) of as grown single crystals Bi2212 with Ca rich is about 72-74 K with sharp phase transition (Ozyuzer, et al. 2003). The influences of Ca content in single crystal structure on unit cell of Bi2212 and critical temperature with respect to O_2 doping have been investigated at some studies. It has

been shown that Bi2212 enriched with Ca has poor oxygen content. Moreover it was claimed that the excess of Ca content as a resident in Sr site disorder Sr-O planes and random potential on Cu-O planes is induced due to disorder on Sr-O. Since this potential causes pair breaking, the critical temperature of the superconductor suppressed. In other words, T_c is decreasing as Ca content in Bi2212 is increasing. (Tokita, et al. 2001).

3.3. Mesa Fabrication

In order to form mesa structure on the smooth surface of Ca-rich Bi2212 single crystals which contain natural intrinsic Josephson junction (IJJ) stacks along the c-axis, there are many experimental processes which are needed to be attentiveness. The mesa on superconducting Bi2212 single crystal with size of 100x300 μm^2 has been obtained using photolithography and argon ion beam etching techniques. First of all, the single crystal from smooth a-b surface is glued onto a sapphire substrate by silver epoxy shown in (Figure 3.2.a). Since direction of the normal vector of substrate is same with c-axis of Bi2212 crystal, the height of mesas fabricated on Bi2212 surface as a matchbox is lied along to c-axis of the crystal and its electrical measurements reveal c-axis behaviors of Bi2212 with IJJ. Here the reason of using the silver epoxy and sapphire substrate is their perfect thermal conductors because differences between crystal temperature and measured temperature on cold-head by sensor affect electrical results on mesa. Moreover since crystal needs to cool during the electrical measurement, it is much important that materials between crystal and cooling head are good thermal conductor to measure crystal temperature correctly and decrease local heating on crystal. In addition there are difficulties in controlling of crystal temperature in the cooling system unless materials with the best thermal conductivity are chosen because heating due to electrical measurement occurs. In order to get a fresh and smooth surface on Bi2212, the crystal was mechanically cleaved with adhesive tape (Figure 3.2.b). The adhesive tape is completely spread out on crystal then pulled out carefully until we get smooth fresh surface on Bi2212. After the cleaving process, gold layer with thickness of 100 nm is immediately deposited by a thermal evaporation technique on fresh surface of the crystal in order not to lose clean fresh surface in the course of time (Figure 3.2.c).

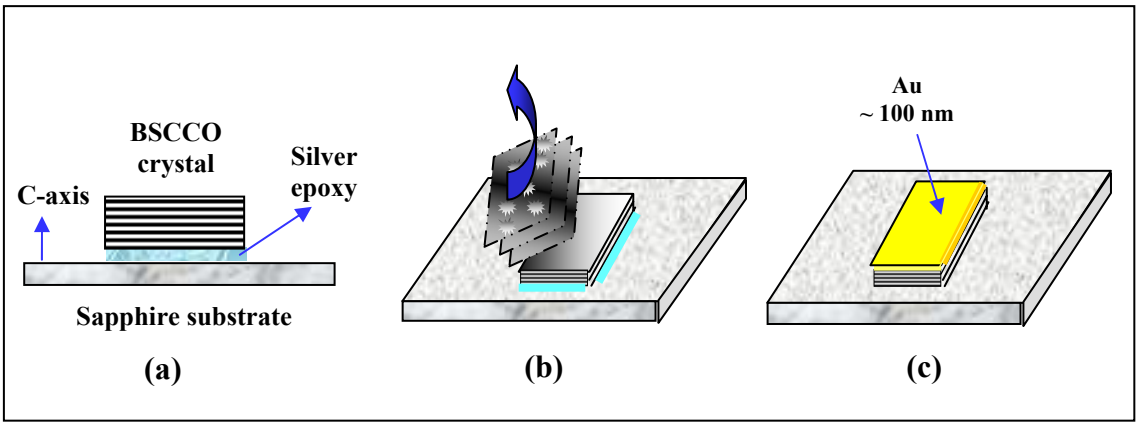

Figure 3.2. The steps in the beginning for the mesa fabrication a) Adhesion crystal on substrate b) Cleaving crystal c) After gold layer deposition on crystal

The gold material is not only good conductor but also protects the crystal surface from water and chemicals during the photolithography process. Moreover since it is non-reactive material, gold layer protect surface from oxidation. In order to measure gold thickness by atomic force microscope (AFM), clean glass is mounted near crystal in evaporator since the gold layer with same thickness on crystal is deposited on glass.

The vacuum thermal evaporation technique seen in (Figure 3.3) provides to obtain gold layer without damaging to Bi2212 surface. This technique includes evaporation of the material in filament boat heated by high current source and re-condensation of the material with vapor state onto cooler substrate. Generally it needs high temperatures to evaporate the material and in our system it is carried out by passing large current through the filament boat. The value of the current necessary for evaporation temperature changes with respect to filament boat resistance (its sizes). It is between 190 and 200 A for our filament boat. Deposition and thickness of film on the substrate are controlled by shutter and it also provides to get good quality thin films which have not contamination coming from other materials in the boat at the starting of evaporation.

Moreover, for the good quality film evaporation should be done in vacuum around 10^{-6} Torr. It is not only necessary to avoid reaction between the vapor and atmosphere but also to increase the mean free path of vapor atoms. Thus they do not undergo collisions with the surrounding gas molecules inside the evaporation chamber. In order to reach high vacuum, turbo molecular pump with back pumping is used in our system. Thickness of the deposition is measured by thickness monitor and shutter is closed when required thickness reaches.

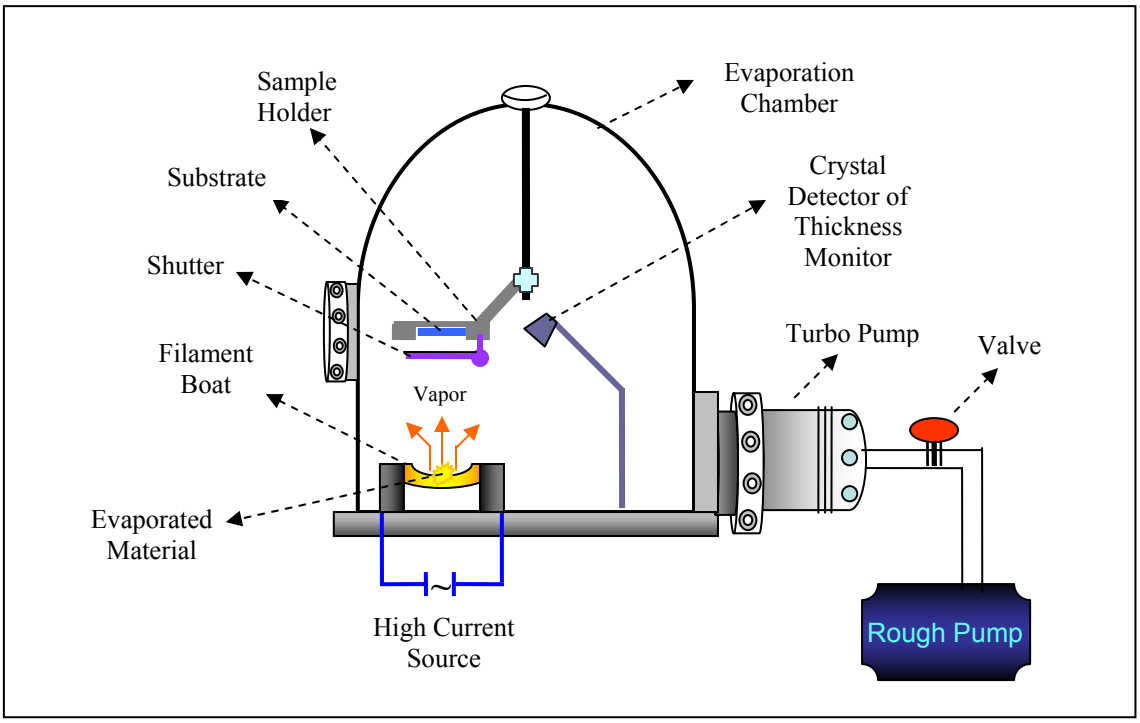

Figure 3.3. Schematic representation of our vacuum thermal evaporation system

The second step in processes of mesa fabrication involves photolithography which is used in micro fabrication to patterns photoresist (PR) layer on the gold layer of crystal. Thus selective areas without regions protected by PR layer are etched down by ion beam while PR patterns protect mesa areas from etching. Photolithography includes several steps in sequence (Figure 3.4).

Since PR is sensitive to light, these processes are done in dark room. The first step is that the crystal surface is covered with PR by spin coater (Figure 3.4.). It provides to obtain uniform smooth PR layer and also enables to adjust thickness of the layer by changing the velocity of the spin coater and coating time (Figure 3.4). In order to drive off the excess solvent in the PR, soft bake is done at temperature of 90^0C for 30 minutes. After soft bake, viscous PR layer is obtained on gold layer of Bi2212. We use positive PR that means when it is exposed to UV light under a mask, exposed area where UV light passes through the mask is removed by developer solution which is sodium hydroxide (NaOH) with concentration of 0.2 M. Thus we obtain PR patterns whose sizes are same with mask patterns in which are not allowed to passing of the UV light (Figure 3.4). Generally we have used masks whose mesa sizes of 100x300 μm and their patterns should be opaque while region without the patterns are completely transparent to UV light. The last process is the hard bake that solidifies the remaining

PR to make more durable layer for ion beam etching (In photolithographic processes I have benefited from previous thesis studies performed by (Kurter 2005, Ozdemir 2006).

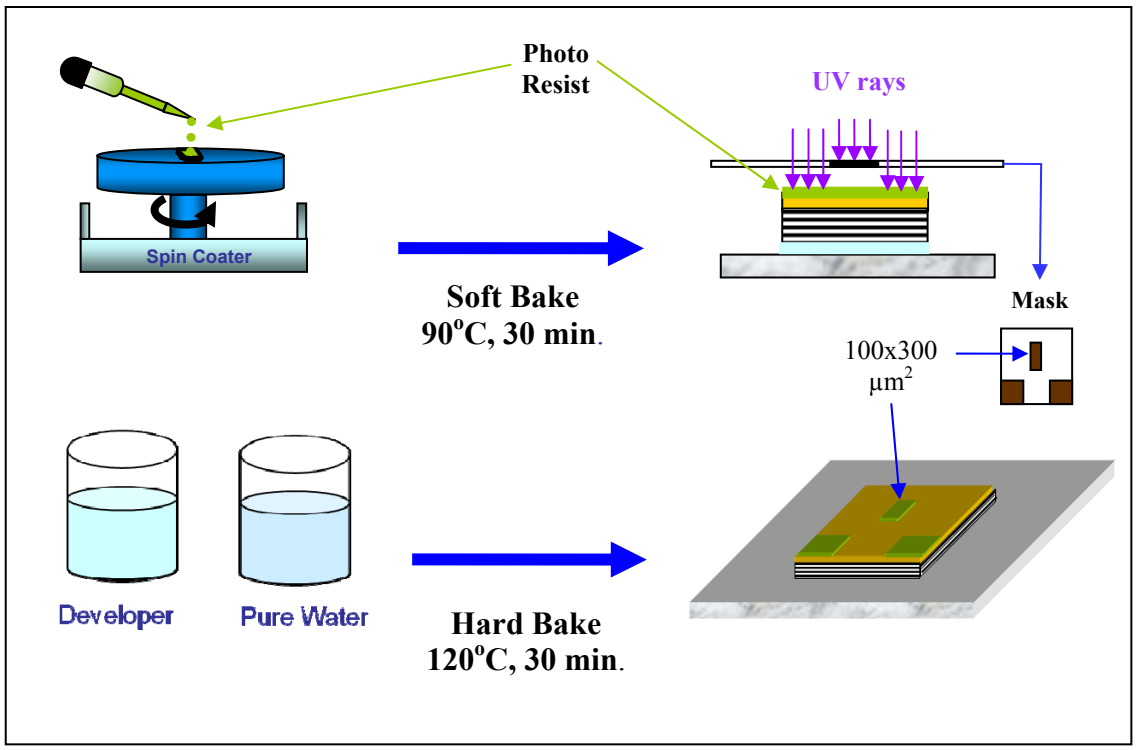

Figure 3.4. The schematic representation of photolithographic processes

After the preparation PR pattern on gold layer of Bi2212, sample is mounted in ion beam system that produces ion beam accelerated thought the surface of sample to etch down some area unprotected by PR layer on crystal. Since the regions protected by PR layer are not etched, the mesa structure with required sizes on Bi2212 single crystal is obtained after the etching.

In (Figure 3.5) ion beam source on the chamber ionizes the inert Argon gases whose quantity adjusted by gas flow controller and accelerates them towards the sample holder. High vacuum is necessary to increase mean free path of ion beam and it increases the possibility of etching on crystal without lost of their energies by colliding with each other and other atoms in the chamber. Therefore turbo molecular pump with back pump is used to reach the high vacuum that is 10^{-6} Torr for our system. The angle between incident ion beam and sample surface is 45^{o} and the crystal whose long size of the PR pattern is lied down on surface of the sample holder is mounted. Since the heating occurred on sample due to the long etching may affect the superconducting

properties of Bi2212 single crystal, sample holder should be cooled during the etching. Therefore in our system crystal is cooled by continuous flow water circulated through a pipe from the out of chamber to sample holder. Moreover since we did not measure the temperature on the superconducting crystal during the etching, we do not know how much the temperature on crystal rises in spite of cooling system. Therefore the crystal has been etched intermittently.

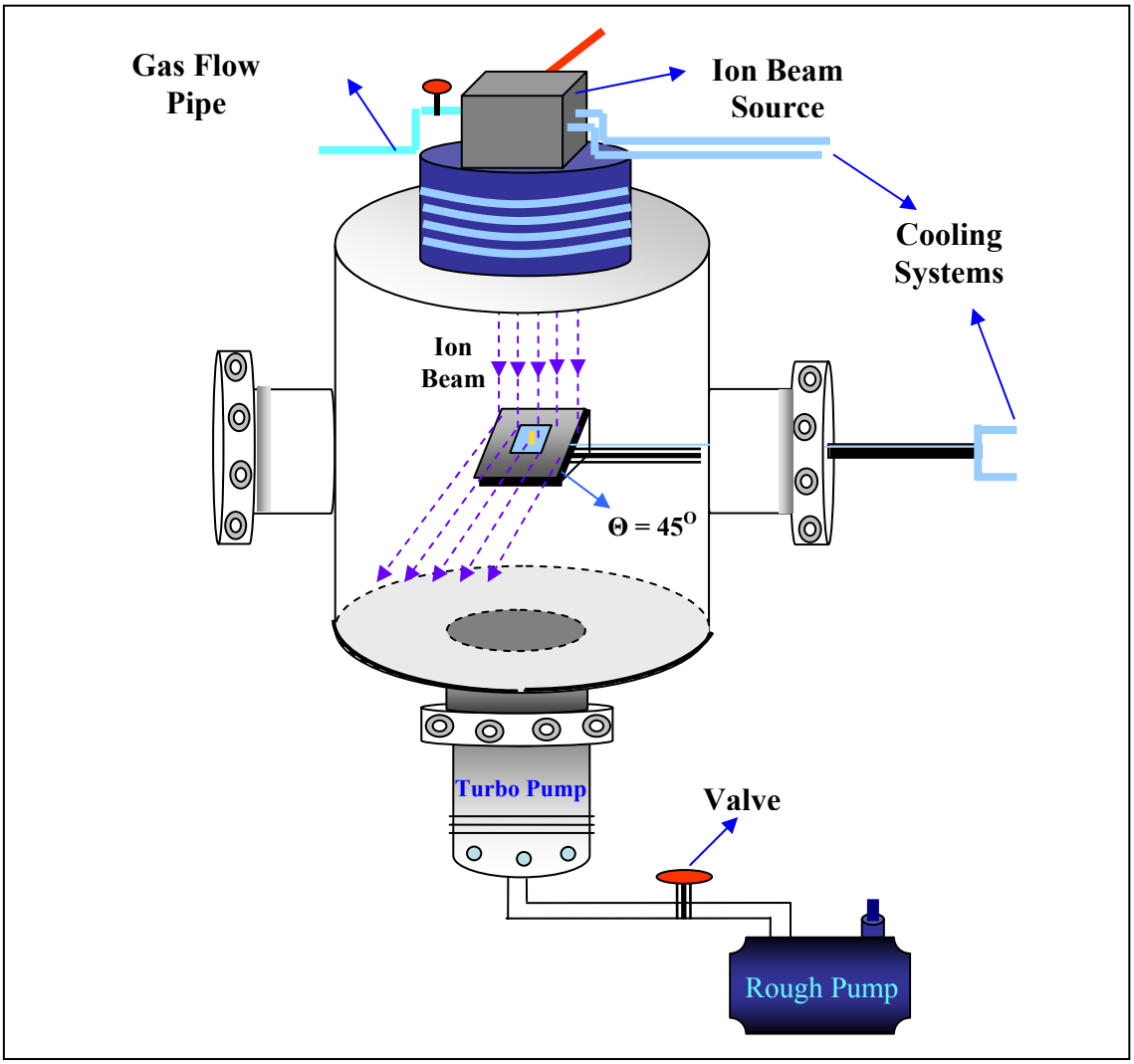

Figure 3.5. The schematic representation of our ion beam etching system

Because of the difficulties in making a contact on small area of the mesa, we use a different contact technique including several processes. Firstly CaF_2 insulating layer is deposited by evaporation onto crystal and small area of the mesa in which are not covered by a mask (Figure 3.6.a). Then a shadow mask whose split lying along the mesa and insulating layer is placed on substrate and a gold stripe with width of 50 μm is

deposited by evaporation on insulating layer and mesa (Figure 3.6.b). Finally three gold probe wires belong to I-V are connected by silver epoxy on two patterns and mesa. The contact on mesa is common probe for measurements of current and voltage (Figure 3.6.c).

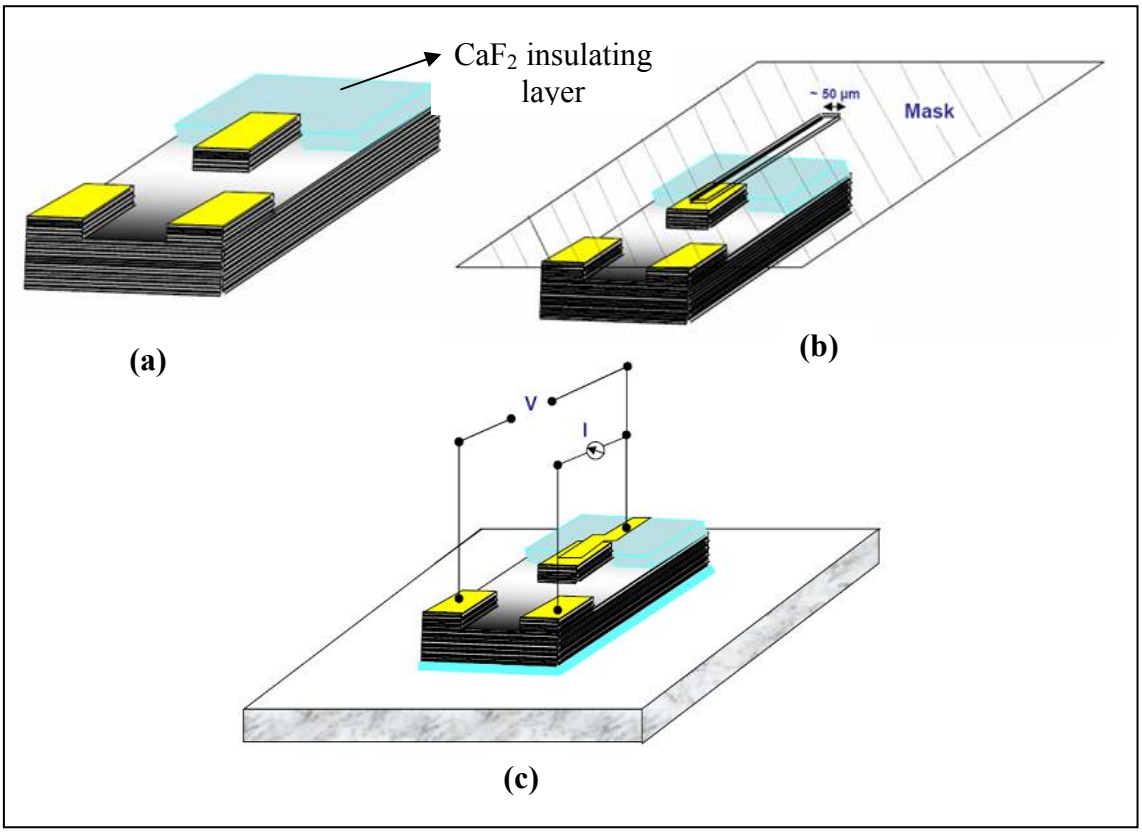

Figure 3.6. The three point contact technique on small area of the mesa a) CaF_2 deposition onto crystal and small part of mesa b) Gold stripe deposition on mesa and CaF_2 layer c) The three probe contact

3.4. R-T and I-V Measurements

The closed cycle cooler system seen in (Figure 3.7) is used in order to decrease temperature of the crystal below T_c and measure superconducting behaviors of the Bi2212 crystal. The system includes a vacuum loading cryostat built, a water cooled compressor and a temperature controller. The working principle of the system is based on expansion of He gas in cold head of the cryostat. Firstly He gas is compressed to 16.5 bar by the water cooled compressor then compressed gas is transferred by flexible line to cryostat. By expanding the He gas in cold head, cooling is produced and

controlled by the temperature controller. The region between sample holder and shield of the cryostat is pumped to create a thermal isolation with vacuum and keep the ambient thermal effects to cooling system at minimum. The vacuum should be 10^{-4} or 10^{-5} mbar to attain required low temperatures. Because of the low vacuum values (~10^{-2} mbar), the sample temperature is able to attain about the minimum value of 20 K. Moreover it makes both thermal equilibrium and temperature controller quite difficult during the measurements. On the other hand, there are several advantages of this cooling system, most of which it is very economic because it includes a closed cycle cooling without lost of the He gas. Also temperature is able to be fixed at required temperatures by temperature controller connecting to heater and compressor. The second cooling system, continuous flow He cryostat system was used for bolometric measurements.

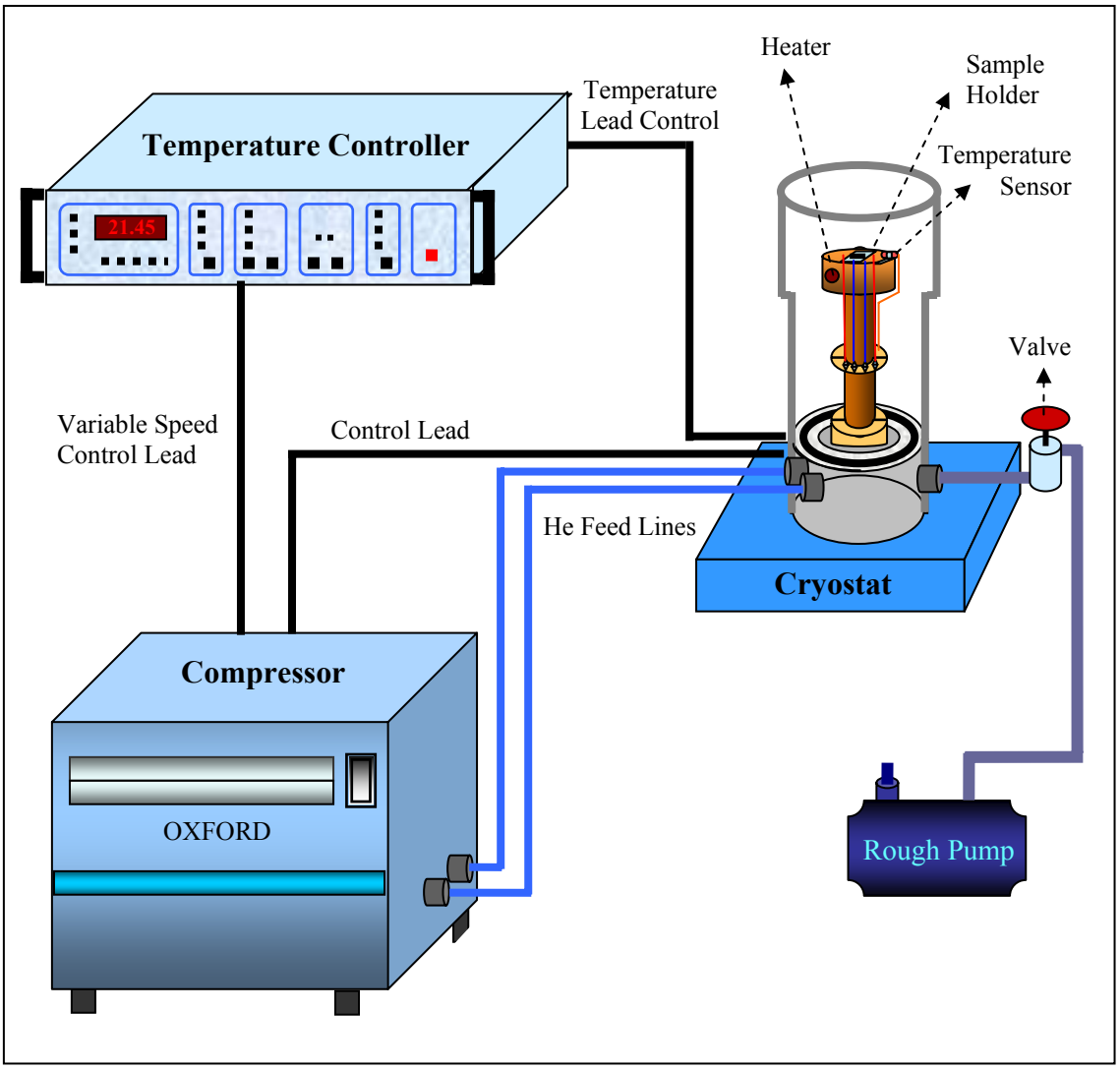

Figure 3.7. The schematic of our closed cycle cooling system

We have done resistance versus temperature (R-T) and current versus voltage (I-V) measurements on mesa and the schematic representation of our experimental setups for the measurements is shown in (Figure 3.8). The setups are interfaced with a computer and controlled by Lab-view program that contains serial instrument control, data analysis and data storage. In addition its graphical programming tool provides to see drift of the experimental result during the measurement and it has a block diagram form that allows creating program for the measurements. Thus required data acquisition with accurate measurement is obtained.

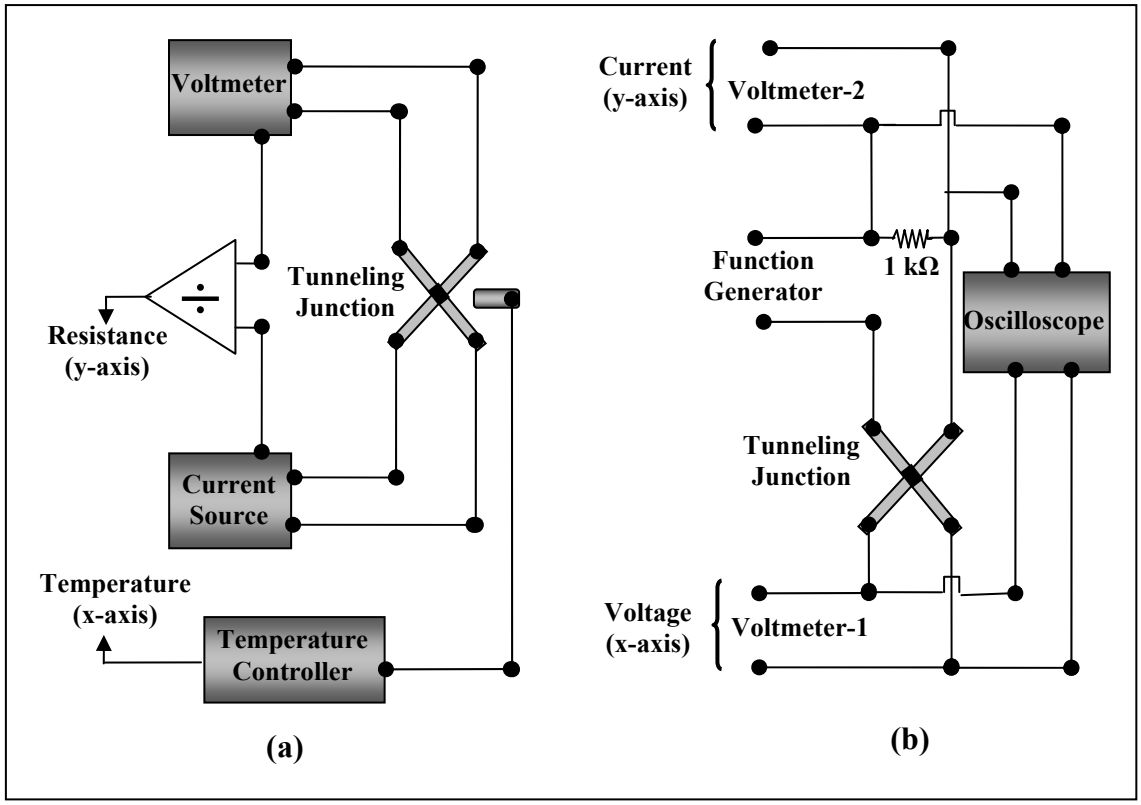

Figure 3.8. Schematic representations of our experimental setups (a) R-T (b) I-V measurements

During the variations of temperature between room temperature and 20 K, simultaneously changing mesa resistance values with temperature are measured using the experimental setup seen in (Figure 3.8.a) and it includes current source, voltmeter and temperature controller which are interfaced with a computer. The variations at voltage and temperature are measured by voltmeter and temperature controller respectively. Since applied current along to mesa height is constant during the measurement, experimental data is analyzed and stored such as R-T by Lab-view

program. In order to acquire accurate data, current with both positive and negative direction are rapidly applied by current source and at same temperature resistance is measured twice. Thus average resistance versus temperature is used. Since a good thermal isolation with vacuum between cold head and shield at cryostat can not be well created, there is a problem in thermal equilibrium between crystal and cooling head. Therefore for the accurate data, measurement during the increasing temperature is considered for R-T.

Figure 3.8.b shows I-V experimental setup interfaced with a computer. This setup includes two voltmeters to measure voltage of mesa including all junctions and applied current on resistance serially connected to circuit between function generator and mesa. Function generator is used to apply current with required frequencies and amplitudes. Sample temperature is kept constant by heater in cryostat and the amount of Helium gas flow which are controlled by temperature controller during the I-V measurement. In order to take a good I-V measurement with hysterical behavior and much quasi-particle branches, current with low frequency (5 mHz) is applied while its amplitude is gradually increasing until obtaining whole hysterical curve including normal state. Oscillator provides to see the voltage jump value and I-V drift before starting to measurement. Thus data including current versus voltage and constant temperature is obtained by Lab-view program. I-V measurements have been done at various temperatures.

3.5. Bolometric Detection of Emission from IJJs

The bolometric measurements were obtained while I-V measurements through c-axis of Bi2212 are simultaneously recording. When bias voltage decrease, the experiments of detection of emission from long side of mesa on Bi2212 by bolometer have been considered. A continuous flow cryostat system was used to perform the bolometric experiments in wide temperature range. For cooling the crystal, liquid He transfers from external reservoir to copper cold finger inside cryostat. The sample temperature on cold finger is controlled by heater and temperature sensor that are interfaced by a temperature controller. It is very important to not only investigate temperature dependence of I-V characteristic of IJJs but also detection of emission from mesa at different temperatures. The system also has optical cryostat to detect the

radiation emitted from samples. It has turbo molecular pumping system that pumps between cold finger and shield of the cryostat until ultra high vacuum. Because of good thermal isolation, temperature of sample can be decreased to about 4.5 K and also the influence of ambient temperature on measurement is reduced by ultra high vacuum thermal isolation.

The sapphire substrates were mounted on cold finger in cryostat as its long side of mesas was opposite the window of optical cryostat. Because our Si bolometer is able to detect the discontinuous radiation, chopper between cryostat window and bolometer was mounted to modulate emission of radiation to pulse. The chopping frequency for our measurements is 140 Hz. The Si Bolometer is cooled by liquid He for its operation temperature. Output signal from bolometer is amplified by lock-in amplifier and it refers to emission power of radiation emitted from mesa. Our first purpose is to observe emission peak from sample during I-V measurement, so the system is as enough as to give information us about whether crystal structure, tunneling characteristic of whole IJJs and mesa lateral dimensions are available for THz emission. Since our proposed method on synchronization of IJJs in mesa for obtaining THz emission needs DC voltage applied through the tall mesa (Ozyuzer, et al. 2007). This DC voltage values corresponding with emission peak of all IJJs were scanned by bolometric measurement during I-V measurements through the tall mesa. Therefore two measurements were simultaneously recorded. At the measurements, used devices which are function generator, voltmeter, temperature controller and lock-in amplifier are interfaced by a computer and controller by Lab-view program.

CHAPTER 4

RESULTS AND DISCUSSION

In this study, large and tall mesas on Ca rich Bi2212 single crystals have been fabricated using vacuum deposition, photolithography and ion beam etching technique. Since main purpose of our study is intended for generation of THz radiation, mesas with required sizes and heights have been fabricated according to our emission principle. The fabrication of good mesas is first step of our studies and many experiments were done for required mesa structure.

The c-axis of Bi2212 single crystal is laid along the mesa height, so number of IJJs along the mesa height is obtained after fabrication processes. Since it is known that thickness of an IJJ is 1.5 nm, the number of IJJs in mesa is calculated from mesa height. For example, mesa with height of 1μm contains approximately 670 IJJs. Therefore thickness measurements are very important for our study and they were analyzed by atomic force microscope (AFM).

Electrical characterizations of mesas were done by R-T and I-V measurements to get information on their superconducting and temperature dependence of tunneling behaviors in IJJs. Moreover their temperature dependences and influence of heating effect are analyzed in these electrical characterizations. In a study published by Kadowaki, et al. (2006), THz radiation power was investigated at various temperatures and it was found that emission power from IJJs in Bi2212 changes with temperature. It was also claimed in another study done by (Ozyuzer, et al. 2007). They have obtained that coherent THz emissions with some powers exists at different temperatures in superconducting state. Therefore I-V measurements of fabricated mesas at various temperatures were analyzed before bolometric detection of emission.

Temperature is one of the parameters in detection of THz radiation emitted from IJJs stacks, so bolometric measurements were repeated at different temperature for same mesa. These measurements on emission peak detection from long side of mesas were simultaneously recorded with I-V measurements. These measurements were allowed to be repeated severally at constant temperatures because bolometric output peaks should be reproducible for each scanning of bias voltage decreasing toward to zero. Thus it is clearly said that they are emissions from Bi2212 single crystals.

4.1. Results of Thickness Measurements on Mesas

Tapping mode was used at AFM measurements that were done in center for materials research of Izmir Institute of Technology. Some advantages of the tapping mode are that lateral resolution of this mode on sample with soft surface is the most improved in other modes of AFM and it also minimizes surface distortion (Martin, et al. 1987). At surface topographic images of AFM, color contrast such as variation from brightness to darkness is used to determine rough structure on surface. Beside 2-D surface topographic analyses of mesa, 3-D image, step height and lateral angle of fabricated mesa have been analyzed by using raw AFM data.

Heights of the fabricated mesas have been measured by AFM but this height includes also gold layer thickness. In order to learn only mesa height we need to subtract it from measured thickness of mesa with gold layer, so it is necessary to measure gold layer thickness on mesa. On the other hand, it is not possible to measure gold layer thickness on mesa, so before the starting evaporation we mount clean glass near the sample in evaporator. Since same gold layer thickness onto both crystal and glass are deposited at end of the evaporation, we measure gold layer thickness on ditch in which lightly scratching only gold layer by needle.

The reason of preference gold layer deposition on mesa is only to protect the fresh crystal surface during the mesa fabrication so thick gold layer is not necessary. Although we planned it about 100 nm, we have obtained different gold layer thicknesses because it could not completely be controlled during the evaporation. However there is no influence of gold thickness on electrical measurement since it is also a good thermal conductor.

The step-height analyses of some gold layer thicknesses on different mesas are shown in (Figure 4.1 and Figure 4.2) which are belong to iyte-mesa1 and HB26 respectively. According to this step height analysis, thicknesses of gold layers on mesas are approximately 139 nm and 75 nm respectively. These thickness values were used to find only mesa heights. Therefore they have been measured for each gold layer on mesa severally. The thickness values of gold layers on whole fabricated mesas are shown in (Table 4.2).

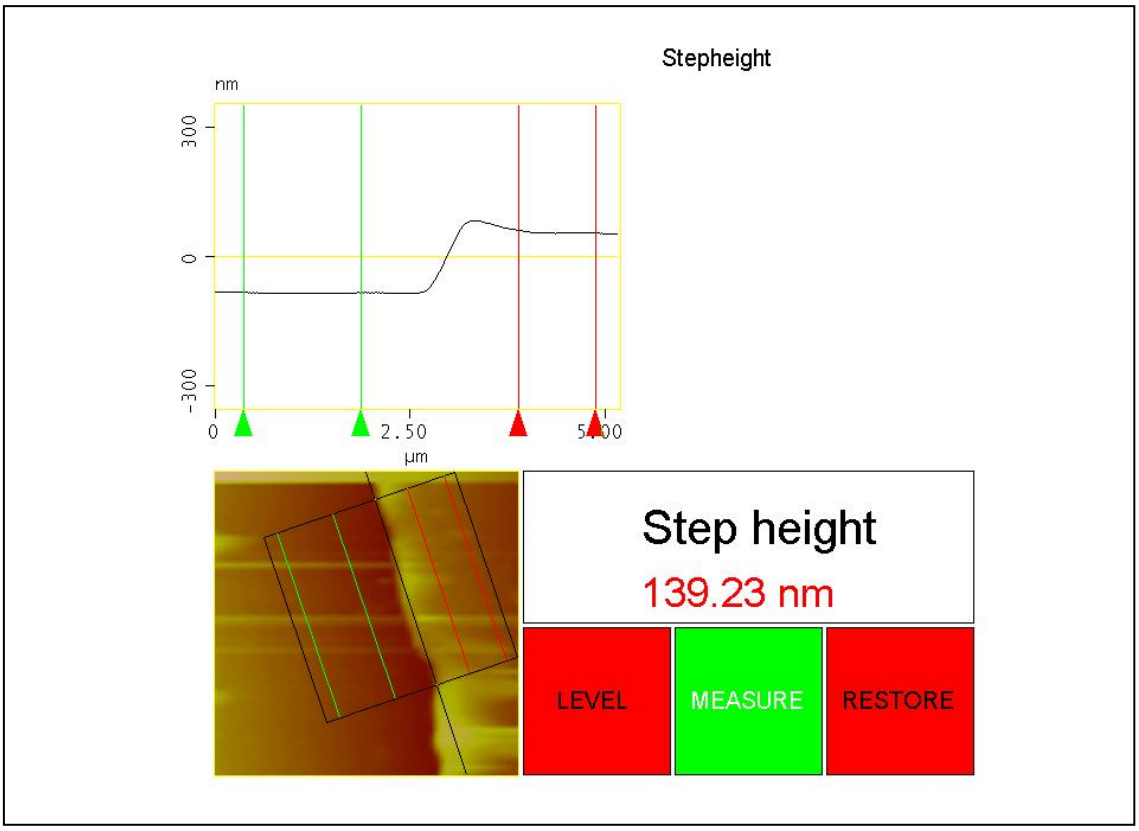

Figure 4.1. Step height analyses of gold layer onto iyte mesa1

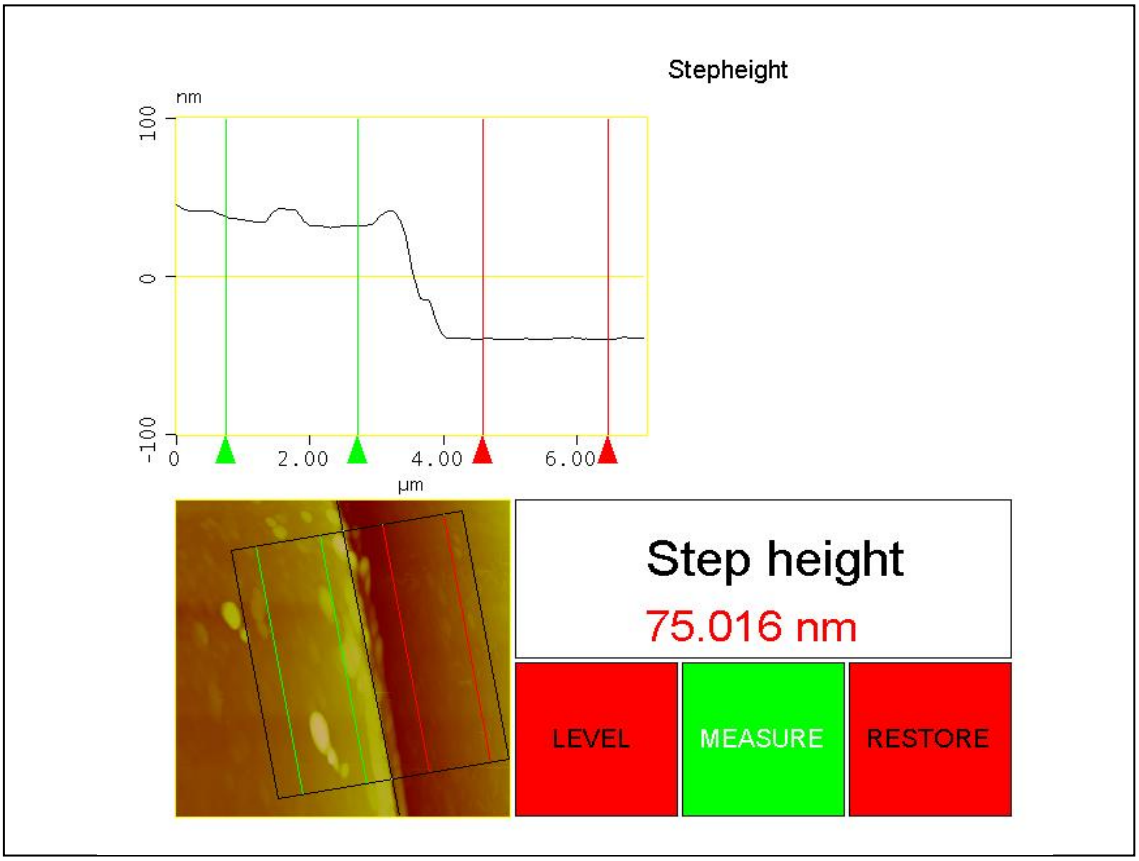

Figure 4.2. Step height analyses of gold layer onto mesa of HB26 sample

The results of AFM measurements on mesas provide us to get information about mesa heights and their lateral angles at the end of whole fabrication processes, so AFM analysis is a control mechanism of our mesa fabrication process that enables to not only both see retroactively errors of the experimental process but also deduce about our prudential results. In order to also investigate homogeneous distributions of mesa height and lateral angles for each edge of the mesa, these measurements have been done on different edges of mesa. Figure 4.3 and Figure 4.4 show step-height analyses and 3D images that are belong to two different mesas. Each of figures includes AFM images measured on different edges of mesa. It is seen for all measurements that mesas with height of 1 μm were roughly obtained at the end of etching with about 2-3 hours. For each sample, heights measured different edges of the mesa are roughly same. Although they are enough for study, lateral angles of fabricated mesas are very low. All of the lateral angles and thicknesses of mesas are shown in (Table 4.1). The edges of mesa are numbered as can be seen in (Figure 4.5.a) and the angles corresponding to these numbers are shown in the (Table 4.1). For all fabricated mesas, the lateral angles are below angle of 45 degrees. It seems such a main problem in generation of THz emission because low lateral angles means that mesas are trapezoid geometric shape. It is expected that if the all of junctions have same area, synchronization in mesa occurs.

There are several reasons why mesas with low lateral angle were obtained. Main reason is thicker photoresist layer about 2.5 times greater than fabricated mesa height and its thickness is about 2.3 μm. On the other hand it should be thick to protect mesa area during the ion beam etching with long time. However, thicker photo-resist layer cause low lateral angle because ions are accelerated through the mesa with angle of 45 degree and thick photoresist shades the region at the edge of the mesa against the ion beam etching. Thus while mesa height is increasing with etching time, mesa starts to spread out and mesa with low lateral angle is obtained (Figure 4.5.b). Therefore lower lateral angle at the bottom edge of mesa have been measured due to more shading and location of mesas on sample holder in ion beam chamber is important. It was mounted on holder like that its long edges of mesa lies parallel to this angle of sample holder. It enables to obtain high lateral angles of both long edges of mesa but, these angles are not still high enough after the ion beam etching. It also results from parameters at ion beam etching. At last studies of our group, mesa is rotated during etching and these parameters are changed. These results will occur in next thesis studies of our group members. In my thesis, ion beam etching parameters are shown in (Table 4.1).

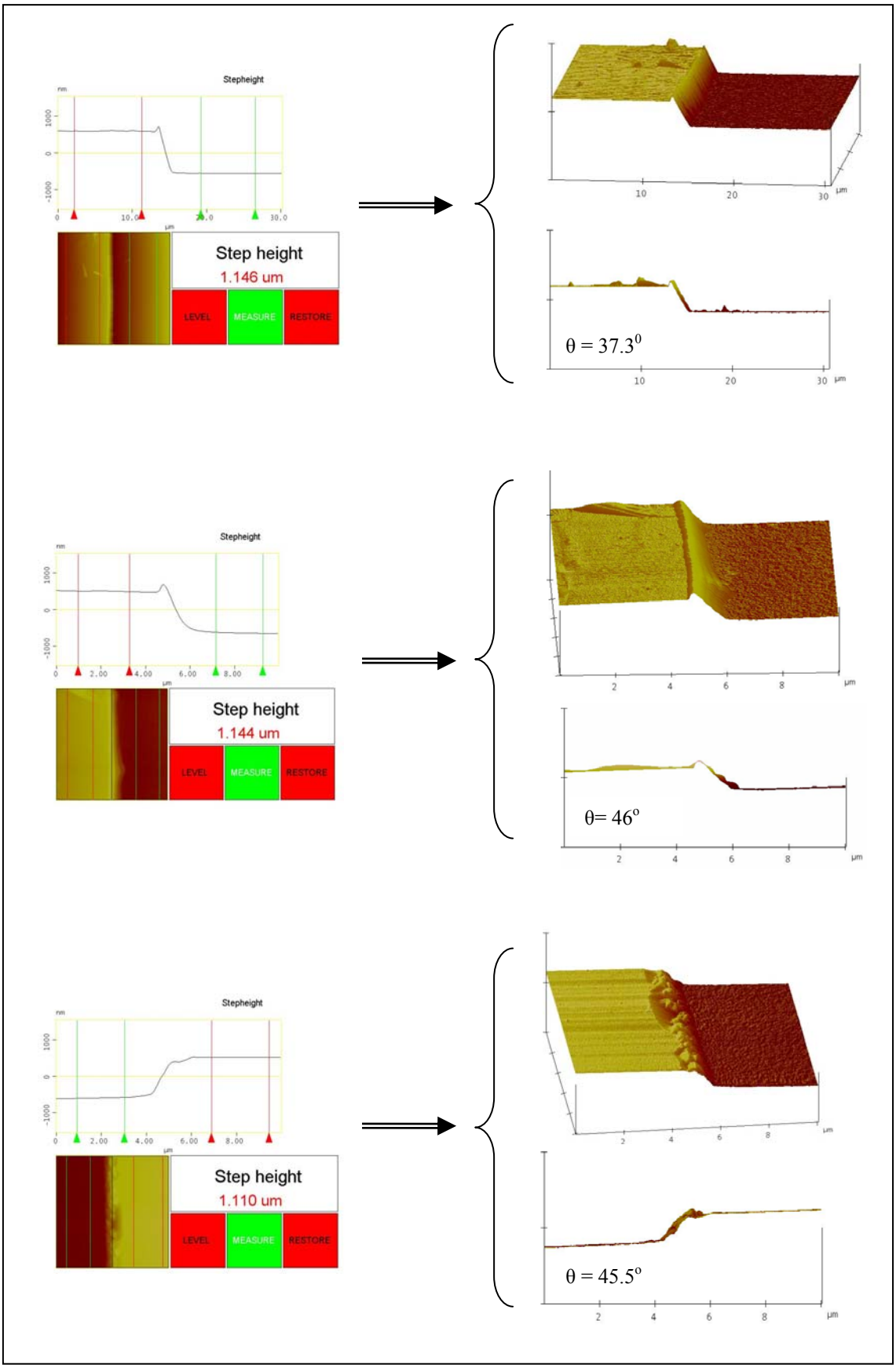

Figure 4.3. Step height and lateral angle analyses of HB26

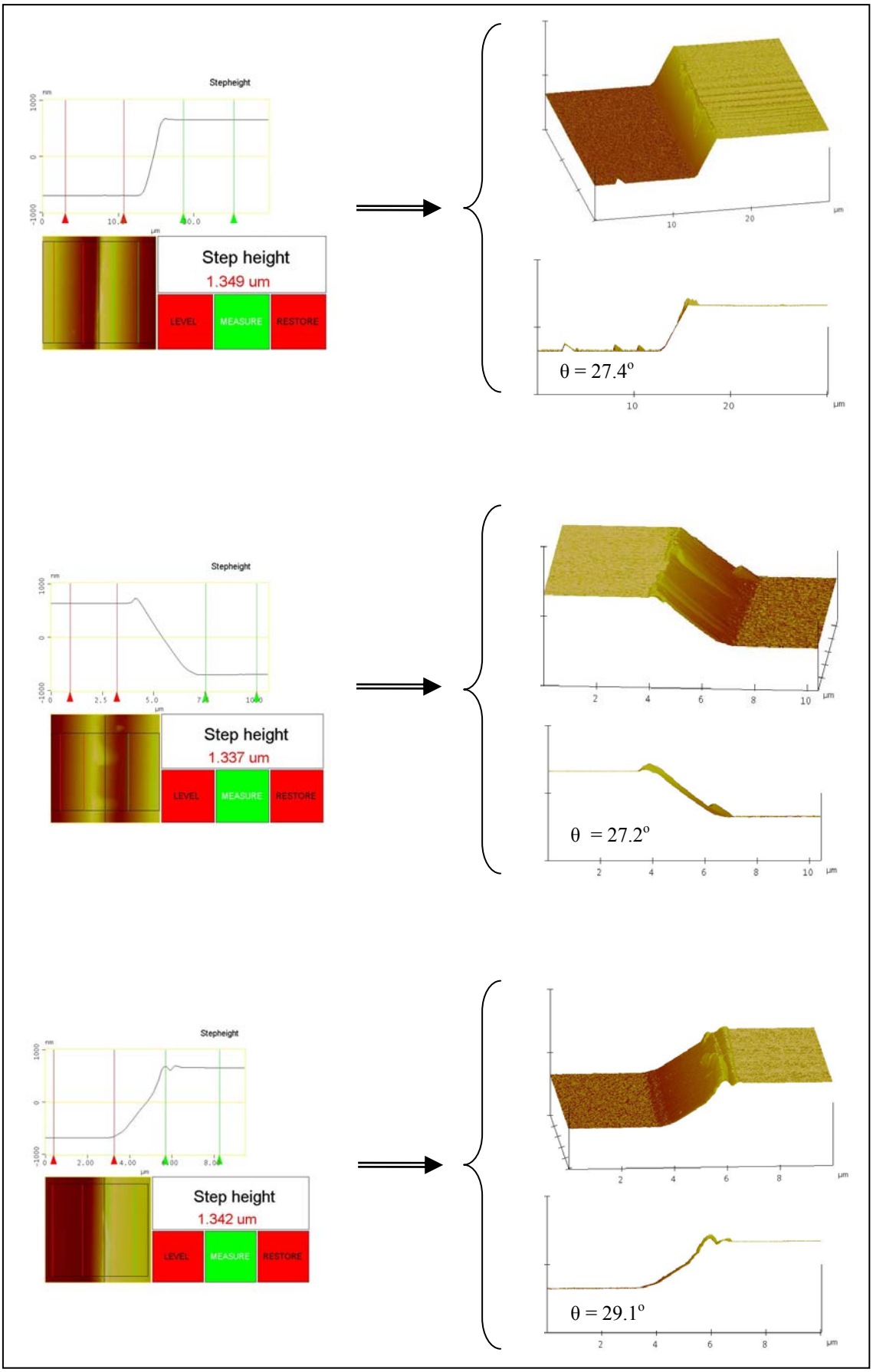

Figure 4.4. Step height and lateral angle analyses of HB28

Table 4.1. AFM results of mesas and their experimental parameters in mesa fabrication processes

Sample	PR Thick. (µm)	Ion Beam Etching				Mesa Height (µm)	Lateral Angles of mesa			
		Power (W)	Gas Flow (sccm)	Time (min.)	Cool. Sample		1	2	3	4
Iyte-mesa1	2.3	22 W 700 V	Ar 20	150	No	0.851	-	27	-	-
HB26	2.3	42 W 700 V	Ar 15	140	Circul. Water	1.058	41	-	45	-
HB28	2.3	42 W 700 V	Ar 15	140	Circul. Water	1.276	28	-	27	-
HB34	2.3	42 W 700 V	Ar 15	120	Circul. Water	1.36	33	-	34	-
HB35	2.3	46 W 700 V	Ar 15	120	Circul. Water	1.002	21	-	-	-

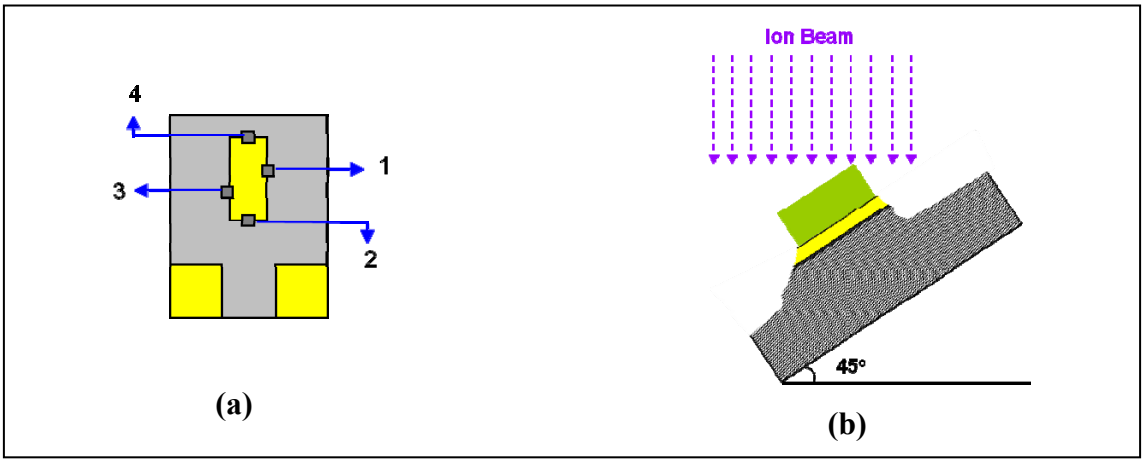

Figure 4.5. The lateral angles of regions on mesa a) Regions of AFM measurements on mesa b) Schematic representation of low lateral angle during the ion beam etching

Because of collisions between ions and crystal atoms, heating occurs during the ion beam etching. Therefore sample holder was cooled by continuous flow water to dissipate heating on sample generated during etching. We believe that good cooling system, continuous rotation of sample and adjustable tilt angle between sample normal and ion beam axis solve our etching problems in mesa lateral dimensions. Also thin and more resistant photoresist layer is required.

4.2. Electrical Results

4.2.1. Temperature Dependence of c-axis Resistance in Bi2212

We have measured resistance versus temperature through the height of mesas using closed cycle Helium cooling and continuous flow He cryostat systems. The temperature dependence of c-axis resistances of Bi2212 and phase transition from the normal conductor to superconductor are seen in (Figure 4.6, Figure 4.7, Figure 4.8 and Figure 4.9) that are belong to sample of the iyte-mesa1, HB26, HB28 and HB34 respectively.

Firstly the sharp phase transitions to superconducting state are seen in R-T figures. Transition temperatures and their transition width values (ΔT) are shown in (Table 4.2). Although all of Bi2212 superconducting single crystals used for mesa fabrication are in under-doped region, there are differences in their transition temperatures due to different cooling system. For example, vacuum in close cycle cooling system is not well enough to reduce influence of ambient temperature on crystal and makes cooling of sample difficult. In new cooling systems there is no such a problem, because it reaches better vacuum values (10^{-6} Torr). Moreover oxygen doping rate can be different inside each of the crystal or changed by some heating processes at mesa fabrication. The oxygen doping rate in Bi2212 crystal changes its transition temperature. In a previous study done on same crystal, the critical temperatures (T_c) of as grown crystals have been published to be about 72-74 K. In under-doped region, T_c of Ca rich Bi2212 single crystal was demonstrated to be about 62 K. If we examine our T_c values which change between temperatures of 64 K and 73 K (Table 4.2), it is seen from phase diagram of Bi2212 that they are in under-doped region. Beside the influence of doping rate on T_c, it was shown that Ca rich Bi2212 crystal has less transition width than stoichiometric Bi2212 in that phase diagram (Ozyuzer, et al. 2003).

From the 300 K to T_c, characteristic behaviors of temperature dependent resistance of as-grown Bi2212 single crystal along the c-axis are seen in these figures. That is, the exponential increasing resistance from room temperature to T_c was well observed and the variations at mesa resistances are shown in (Table 4.2). For all fabricated mesas, the ratios of R_{Tc}/ R_{300K} are between 3.5 and 5.

Table 4.2. Variation of resistance of mesa on Ca rich Bi2212 single crystal and their transition temperature

Sample Name	Mesa Size (μm)	Thickness Measurements		Resist. vs. Temp.			Critical Temperature	
		Au Layer (nm)	Mesa (nm)	$R_{300\,K}$ (Ω)	R_{Tc} (Ω)	$\frac{R_{300K}}{R_{T_C}}$	T_c (K)	ΔT (K)
Iyte mesa-1	100x300	139	851	5.40	18.61	3.45	73.5	6.81
HB26	100x300	75.06	1058.3	7.45	38.41	5.15	64.8	1.42
HB28	100x300	66.02	1276.6	8.62	38.71	4.5	64.1	3.75
HB34	100x300	131	1360	12.31	46.94	3.81	65.0	8.06
HB 35	100x300	145	1002	31.17	119.4	3.83	69.1	8.62

From the critical temperatures to low temperatures, increasing in resistance is unusually seen on all R-T graphs. This case is not a temperature dependent electrical behavior proper to superconducting crystal. It result from three probe contact method that is not generally preferred to four point contact method for accurate measurement because there is one contact probe on mesa which is used for both applying current and measuring voltage and it causes the resistance at superconducting state. However four point contact is very difficult to fabricate on mesa and it is required some experimental processes with technical equipments. It is also found in a paper published by (Yurgens, et al. in 1997).

In R-T graph of HB34, contact resistance is clearly seen below T_c. In order to minimize contact resistance, samples were annealed at 350 ^oC, but it was not generally preferred since oxygen doping level in Bi2212 does not change. There are several reasons of contact resistance. Firstly it may be caused by resistance of silver epoxy connected gold wire to patterns on Bi2212, because this conducting adhesion is obtained by mixing two equal composites. If they are not mixed well, its conductance will be low. The other reason is the interface between gold layer and surface of Bi2212. This kind of contact resistance increase at low temperature, because the interface behaves tunneling barriers and temperature dependence of barrier height is dominant in contact resistance. Therefore in R-T graphs, we see increasing in resistance from T_c to low temperatures.

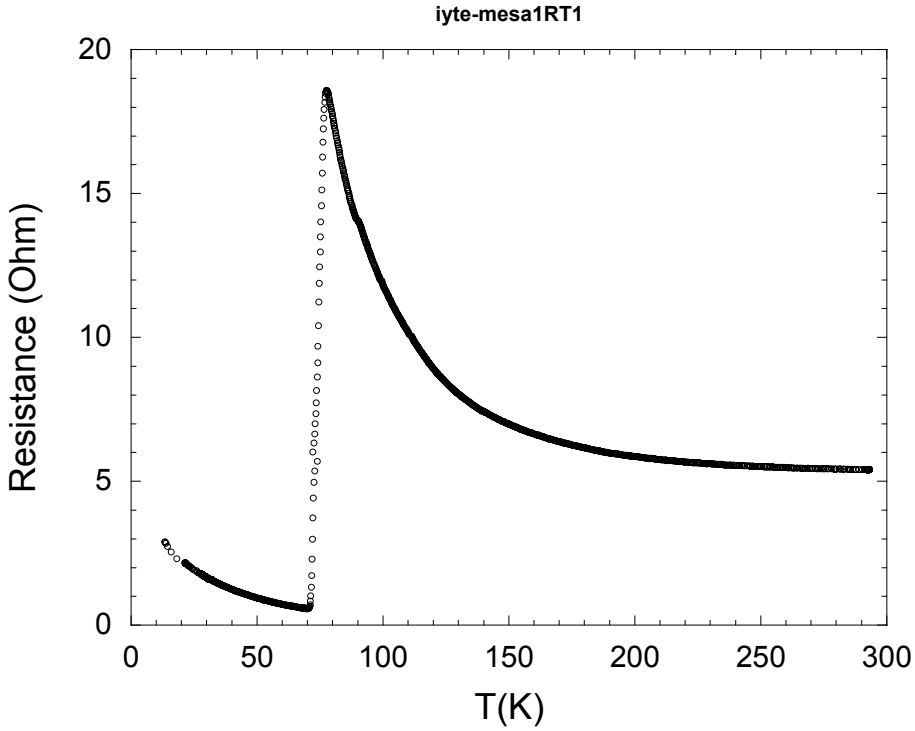

Figure 4.6. Variation of resistance versus temperature of iyte-mesa1

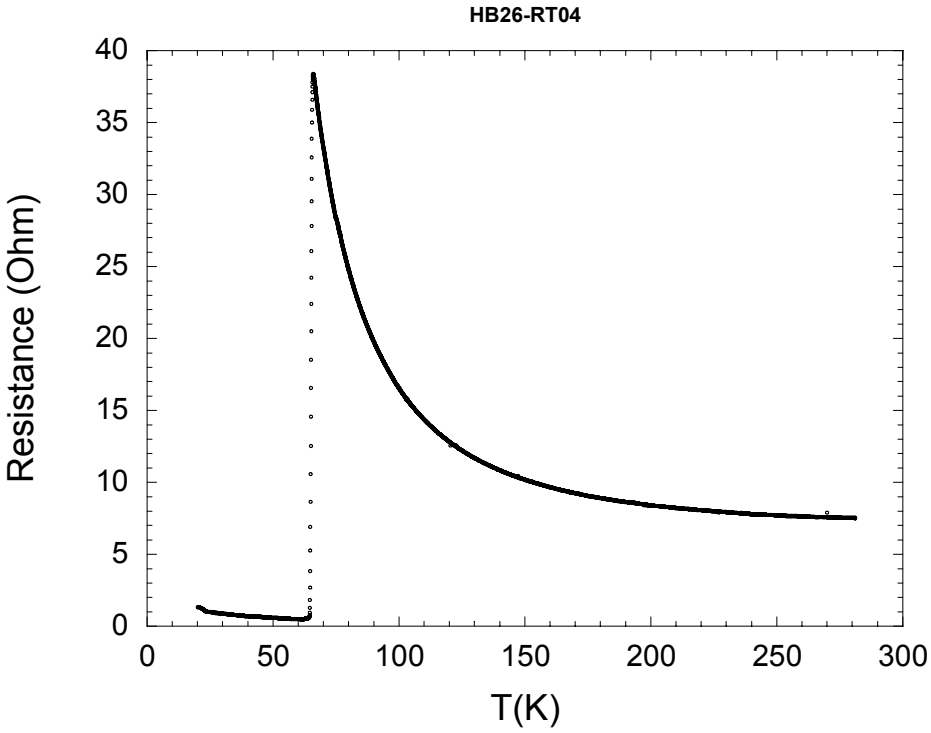

Figure 4.7. Variation of resistance versus temperature of HB26

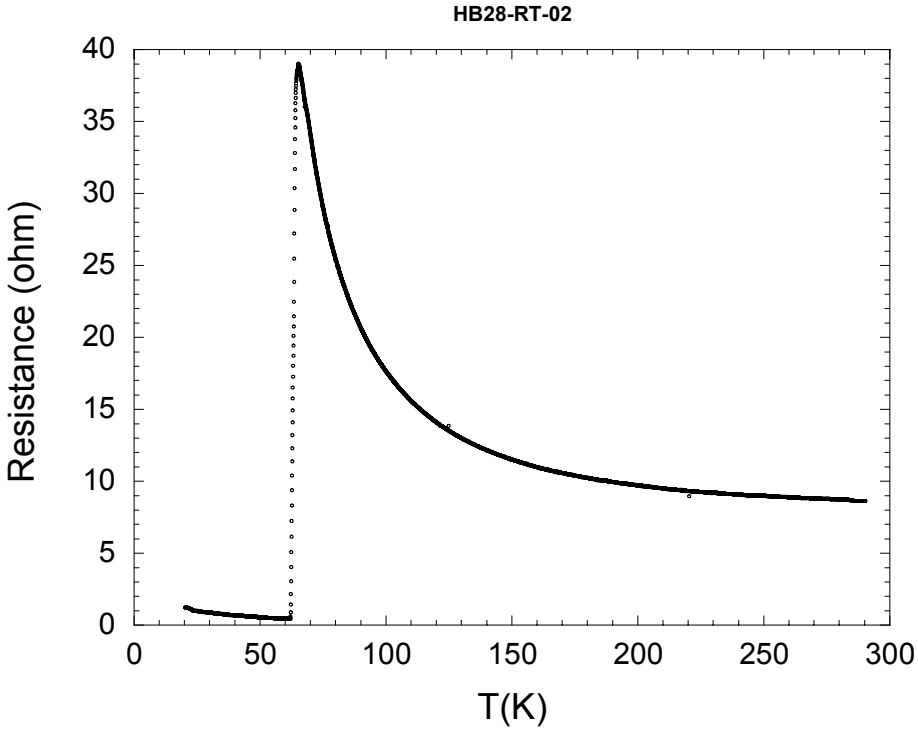

Figure 4.8. Variation of resistance versus temperature of HB28

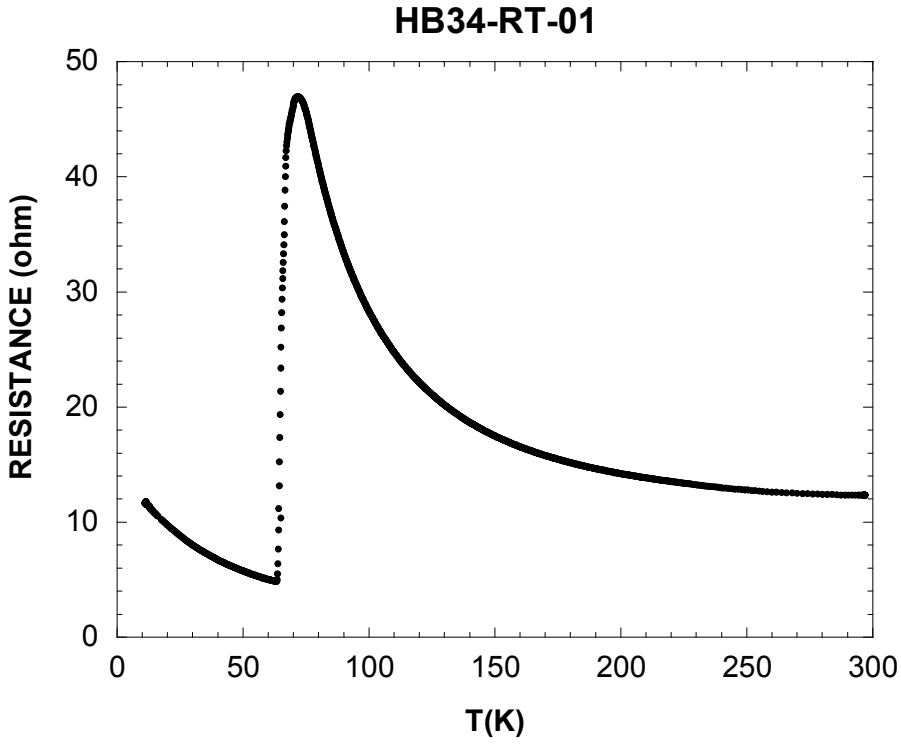

Figure 4.9. Variation of resistance versus temperature of HB34

4.2.2. Tunneling Characteristic of Bi2212 Single Crystal

In our I-V measurements of c-axis of Bi2212, the quasi-particle branches and large hysteretic behavior can be seen when temperature is below its T_c. They are characteristic c-axis tunneling behaviors of anisotropic superconducting material of Bi2212. The fabricated mesas include number of IJJs, so I-V measurements exhibit tunneling behaviors including the contributions of whole stacks of IJJs. The voltage jumps corresponding to quasi-particle branches are seen in these I-V graphs. While bias voltage increases these branches appear such a voltage jumps until all IJJs are completely in normal state. During the sweeping of bias voltage negatively and positively from zero voltage, each branch occurs when individual IJJ is switched from Josephson state to quasi-particle state by bias current exceeding its I_c. Therefore it is strongly expected that branches are observed as many as the number of IJJs (Yurgens 2000). Josephson and quasi-particle currents are demonstrated simultaneously in our detailed I-V graphs. Firstly Josephson current with hysteresis behavior is seen at zero bias and it only occurs from cooper pair tunneling while all IJJs are in superconducting state. The hysteretic behavior of Josephson current results from switching the current from cooper pair tunneling to quasi-particle tunneling (Ozyuzer, et al. 2000). After exceeding of Josephson current, I-V data traces on quasi-particle branches that are one by one corresponding IJJs. The voltage value on which all of IJJs start to pass into normal state is called as total conductance peak of IJJs. For example, if we want to find superconducting energy gap corresponding to an individual SIS Josephson junction, the voltage values in I-V data should be divided by the number of IJJs (Yurgens 2000). While decreasing bias voltage, I-V data does not trace these branches because there is a transition from normal state to superconducting state. Thus large hysteric I-V curve with many branches are obtained.

In order to obtain as much as more quasi-particle branches in I-V, the swept frequency should be low while ac bias current on mesa is swept negatively and positively by function generator. In our measurement, it was between 0.1 and 5 mHz to catch more branch and has triangle wave form. Especially, increasing bias voltage, ac current with low swept frequency were used because branches can be appears during increasing bias voltage negatively and positively. Also the output amplitude of function generator was gradually increased in order not to allow the heating in mesa due to high

bias current. Thus without encountering influence of joule heating, branches were obtained step by step increasing output amplitude of function generator. In order to learn maximum output amplitude for mesa before starting the experiment, oscilloscope was used. For the possibility of missing branch, I-V measurement was repeated many times at same amplitudes.

Normally if all IJJs are more identical with respect to critical current and junction area, distances between branches should have a same gradual current rise and the voltage jump. However, our fabricated mesas are about 1 μm, so we expect approximately 670 branches. Such more IJJs cause more heating in mesa and more heating makes not only catching of more branches difficult but also equidistance of voltage jumps become disarray (Yurgens 2000). The distance become more close each other at higher bias values (Kurter 2005). Also it is said calculation of energy gap heating from I-V graph is difficult because it decreases energy gap value of superconductor.

The influence of heating effect on our I-V measurement is seen in (Figure 4.10 and Figure 4.11). Less quasi-particle branches are seen in our measurements. Sometimes it may be due to measurement problem such high swept frequency and quick increasing in amplitude of function generator output but general aspect of our I-V measurement reveals heating effect. In (Figure 4.10.a) disorder and branching of total conductance peak in the nearby 1 V is an evidence of heating in mesa. Since our superconducting crystal has poor thermal conductivity, there are problem in distribution of heating during the applied bias current. Thus local heating occurs on crystal and if its temperature rises above critical temperature, superconducting state is destroyed at some regions. Moreover non-equilibrium quasi-particle tunneling due to thin insulating layer and joule heating cause back-bending (Tanabe, et al. 1996). In (Figure 4.11.a), back-bending is seen at high bias voltages.

I-V measurements of HB26 and HB28 have been done at same temperature and their mesa sizes same but mesa height of HB28 is greater than height of HB26 and the difference in mesa heights is about 200 nm. Therefore it is expected that total conductance peak of HB28 is more than HB26. However, if we compare two I-V graphs, it is seen not to be so that. The heating effect increasing with number of IJJs had caused to obtain less total conductance peak because of large number of IJJs in HB28 mesa. In the case, we did not analyzed variation in energy gap with respect to mesa height.

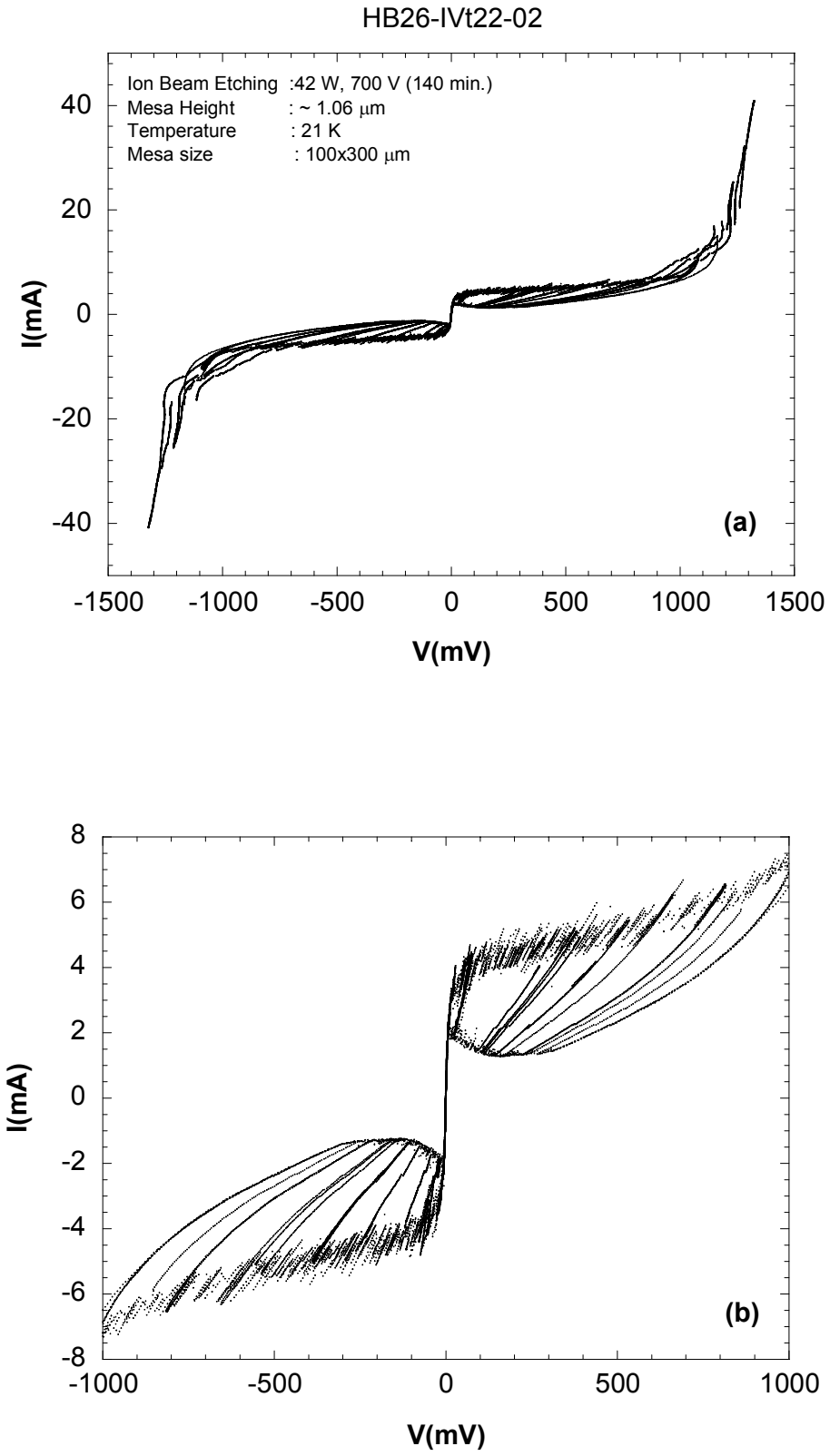

Figure 4.10. I-V measurement of HB26 (a) and its detailed graph (b)

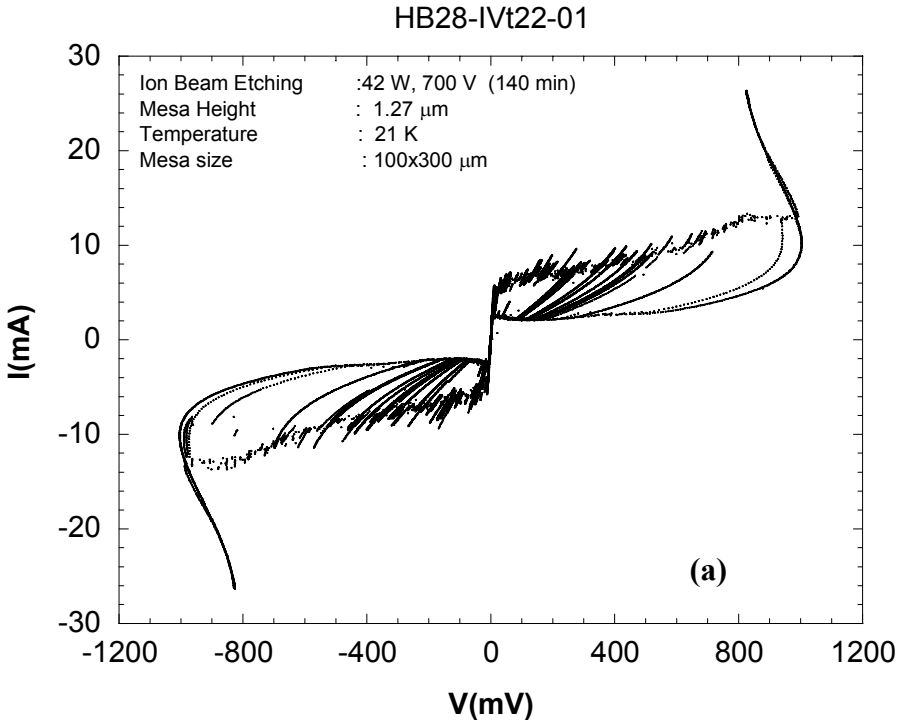

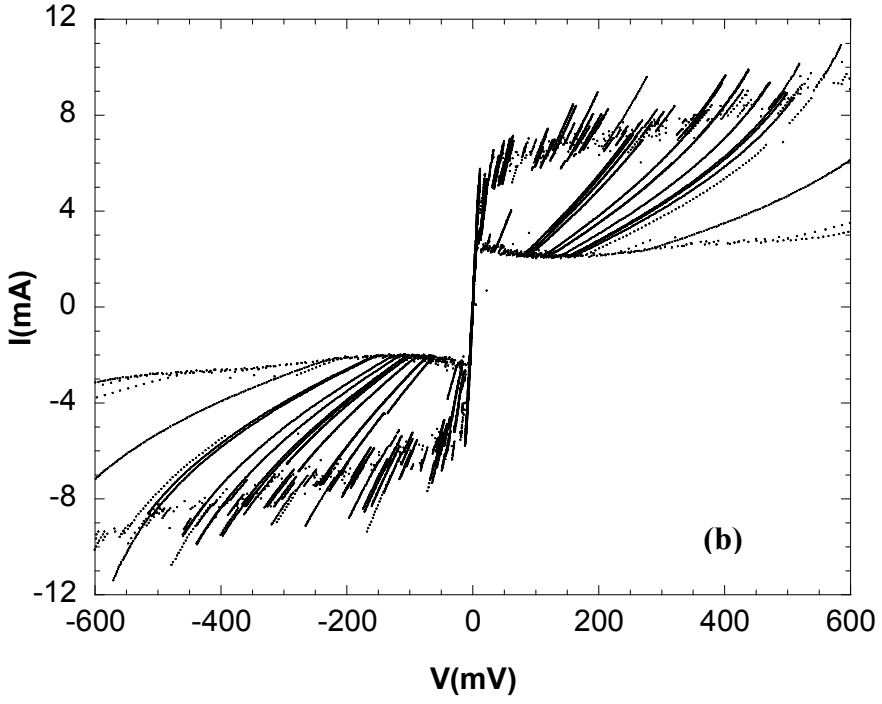

Figure 4.11. I-V measurement of HB28 (a) and its detail graph (b)

Detailed graphs of both HB26 and HB28, in (Figures 4.10.b and Figure 4.11.b) reveal Josephson current and clear quasi-particle branches. Their critical Josephson current values are between 3-4 mA. The order of critical current density J_{cc} is 10^1 A/cm^2. It shows under-doped behavior of Bi2212 single crystal (Inoue, et al. 1998). Small critical current value is required in our study because our objective is to generate THz emission from mesa and the influence of heating effect on emission destroys synchronization of all junctions at high currents. That is main reason of using the under-doped Bi2212 single crystal for THz radiation.

Temperature dependence of c-axis tunneling characteristic of Bi2212 single crystal was analyzed by I-V measurements done at some constant temperatures. The tunneling behaviors from superconducting state to normal state are seen in (Figure 4.12, Figure 4.13, Figure 4.14 and Figure 4.15) which are belong to iyte-mesa1, HB26, HB28 and HB34 respectively. In all of the superconducting I-V data, it is generally seen that total conductance peak value decreasing with increasing temperature. It is compatible with temperature dependence of energy gap of BCS theory mentioned in introduction part. For this reason, decreasing in individual energy gap reveals reducing in total conductance peak of IJJ stacks. That could be intrinsically observed in spite of the presence of Joule heating in large number of IJJs. Above T_c, the energy gap feature and other superconducting behavior such a Josephson current are disappeared but there is an interesting result seen in I-V measurements of same mesa at different high temperatures. It is nonlinearities in I-V that is corresponds to increasing c-axis resistance with decreasing temperature. It is presented such pseudo-gap behaviors that are precursor of superconductivity and defines unusual pre-formed of pairs above T_c (Yurgens 2000). It has been observed in under-doped and over-doped Bi2212 single crystals. While it is very hard to observe presence of pseudo-gap in heavily doped Bi2212, this gap feature is known as an under-doped behavior (Ozyuzer, et al. 2002).

Moreover while temperature increases toward their individual T_c, less quasi-particle branches were observed in these I-V measurements. Since decreasing in energy gap means reducing of distance between branches, it may prevent appearing of more quasi-particle branches clearly. Therefore it requires becoming more accurate in I-V measurements. As temperature increases toward T_c, hysterical behavior in I-V measurements decreases and above T_c it disappears in normal state.

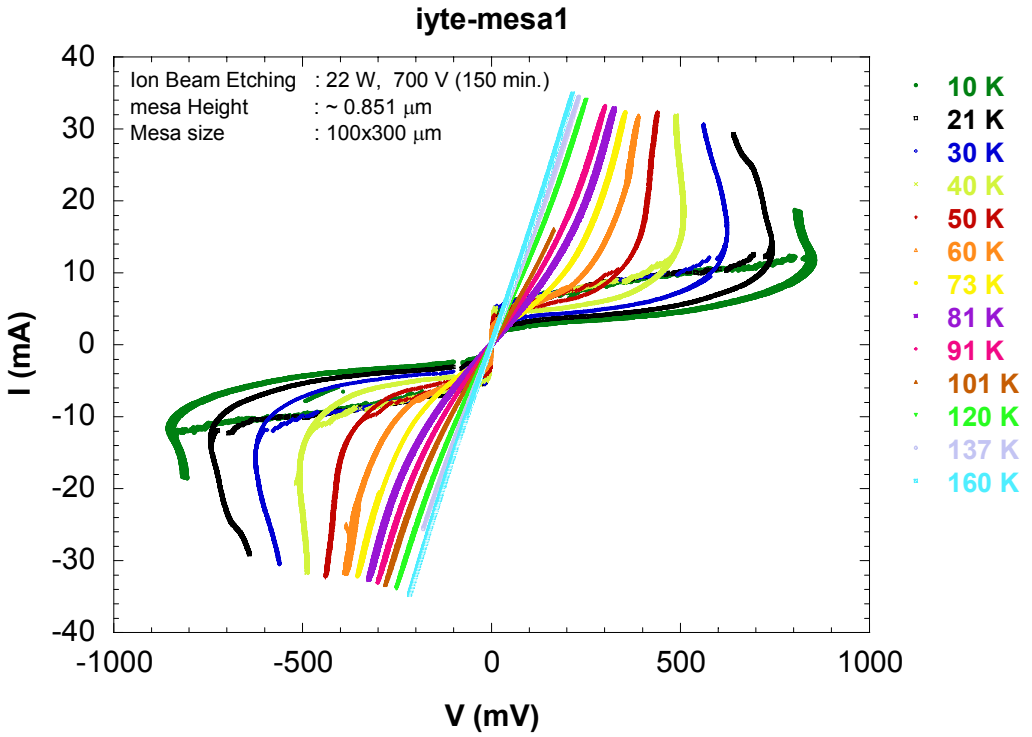

Figure 4.12. Temperature evolution of I-V characteristic of iyte-mesa1

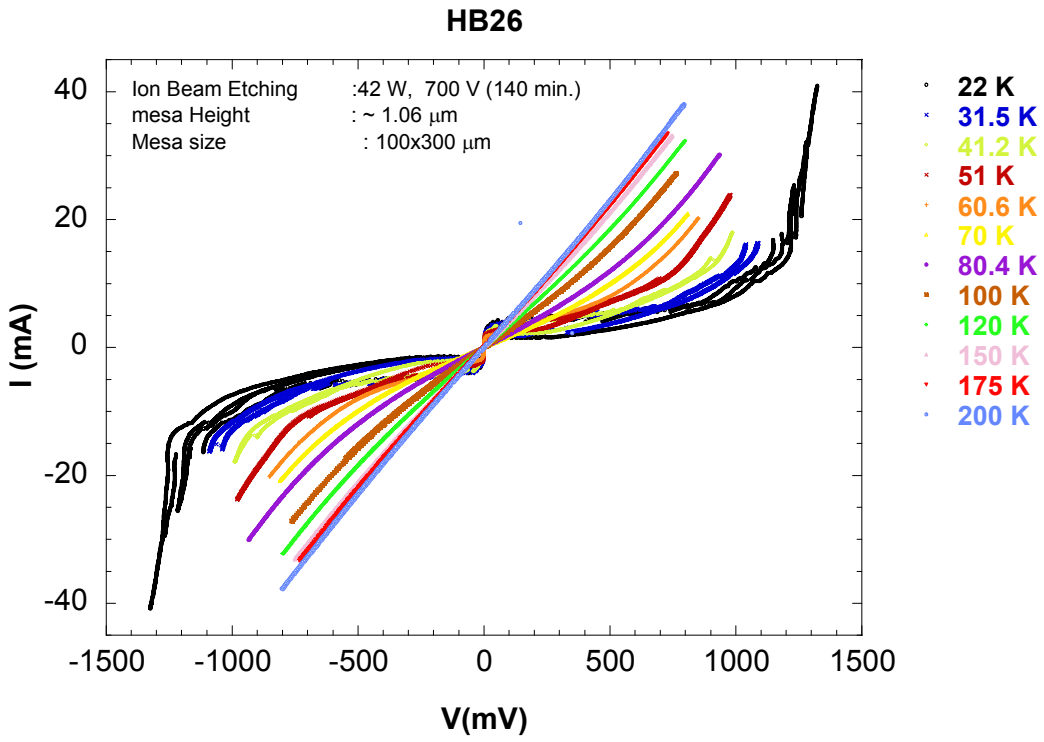

Figure 4.13. Temperature evolution of I-V characteristic of HB26

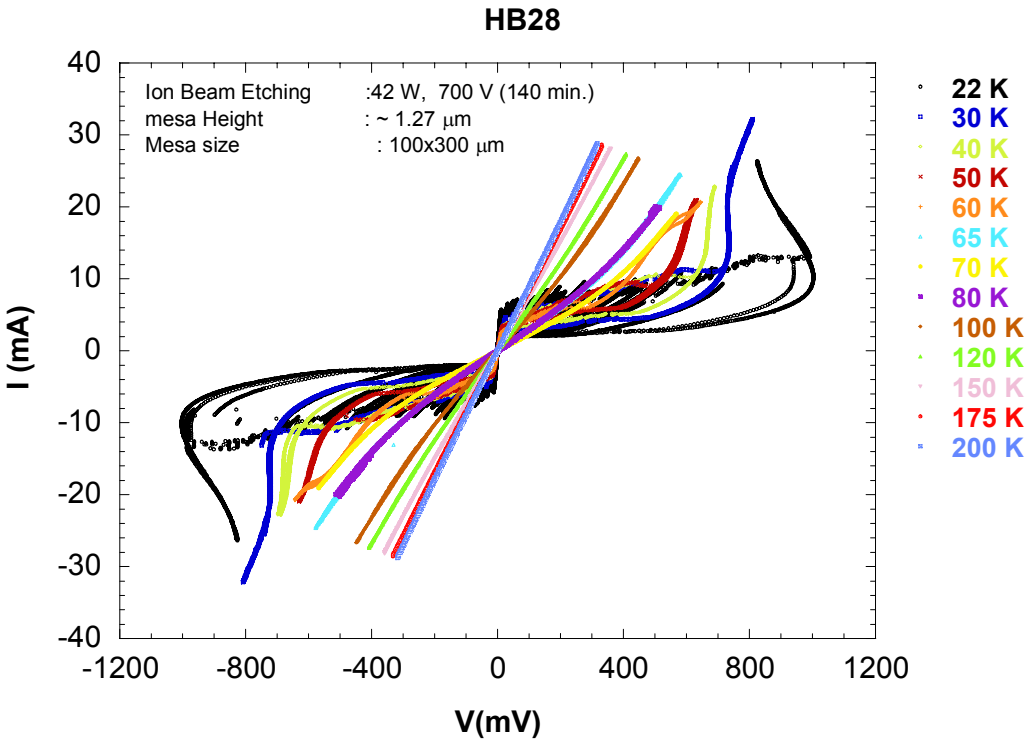

Figure 4.14. Temperature evolution of I-V characteristic of of HB28

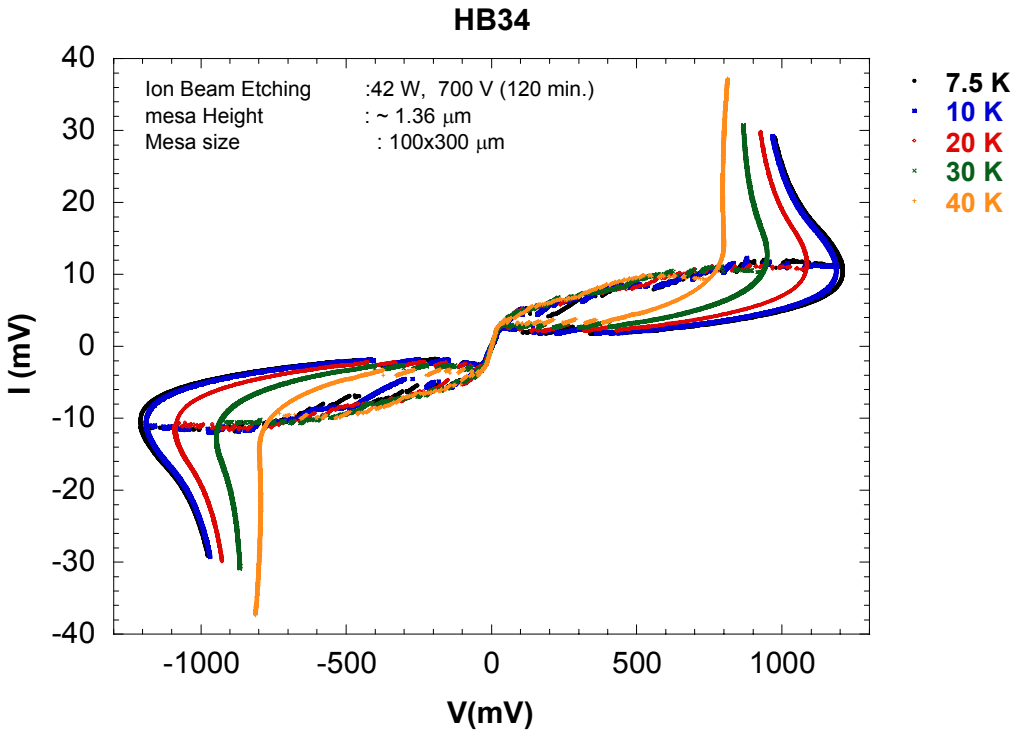

Figure 4.15. Temperature evolution of I-V characteristic of HB34

If temperature dependence of Josephson current (I_c) is investigated, it decreases with increasing temperature as shown in (Figure 4. 16). It is defined for one junction as zero resistive current at low temperature. We consider the temperature evolutions of critical current at near the zero bias voltage. However the influences of high temperature in mesa and contact resistance on I_c are seen as the extending of I_c in the neighborhood of zero bias negatively and positively, so it quite differs from zero resistive behavior of Josephson current. We have not investigated tunneling I-V characteristic of one Junction, so there are composed of whole IJJs stacks on I-V measurement. All of these junctions are in superconducting state when Josephson current is not exceeded. After it reaches I_c, first branch corresponding to quasi-particle state appears. While the bias current increases, other branches appear and the Josephson currents corresponding to each IJJ are seen from branch to next branch as a voltage jump. It is seen in I-V figures that jumping values of I_c gradually decrease along the high bias voltage and be sometimes suppressed in I-V.

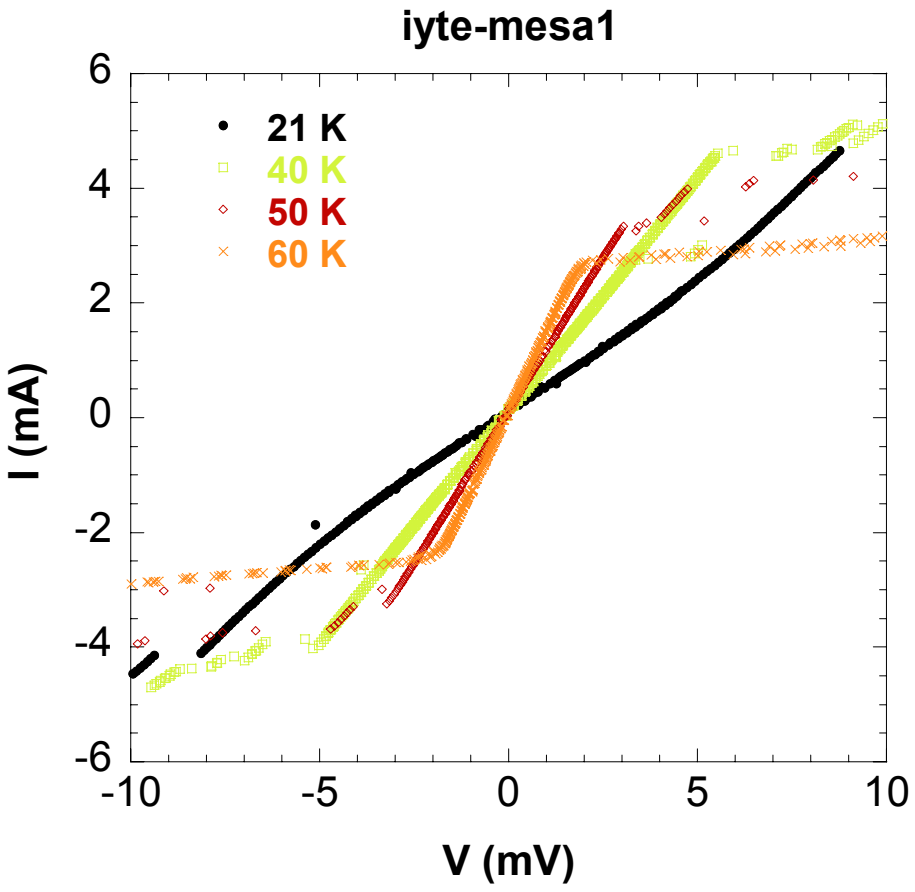

Figure 4.16. Temperature evolution of Josephson critical current of iyte-mesa1

According to our observation on temperature dependence of Josephson current nearby zero bias, generally it decreases with increasing temperature as shown clearly in (Figure 4.16). It is not properly seen in the other temperature evolution of I-V measurements as clear as sample of iyte-mesa1. However it can be said there is weak temperature dependence of I_c in our results. If critical currents at temperatures between low and nearly below T_c are compared, they tend to decreases with increasing temperature even if the differences between these values are small. It is seen that differences in I_c is smaller toward low temperatures. This behavior of temperature dependence of Josephson current differs from fundamental properties of conventional SIS junctions in BCS theory. According to the Ambegaokar Baratoff (A-B) theory describing temperature dependence of Josephson current for BCS theory, it rapidly increases as temperature decrease slowly down T_c and at low temperatures, variation with temperature is nearly constant (Ambegaokar and Baratoff 1963). On the other hand, in many studies on temperature dependence of I_c it has not be observed there was an almost well relation between experimental results and this theoretical values in unconventional SIS junctions. The theory is more available for temperature dependence of I_c in conventional (s-wave) superconductors than HTSs (Suzuki 1999).

In many studies, temperature evolution of I_c in HTSs was investigated and compatibility of these experimental results with A-B model were observed. In an interesting study published by (Suziki 1999), this behavior has been investigated with respect to doping level in Bi2212. In variation of doping level from over-doped to under-doped, differences in I_c with temperature get smaller and its variation tend to linear. In other words, critical currents from T_c to low temperatures are smaller than the values calculated from A-B theory. In our I-V results critical currents belong to under-doped Bi2212 single crystal are underestimated than fitting values of this theory. However in another study, it was found that products of I_c R_n of under-doped Bi2212 (where R_n is normal state resistance of Junction at that temperatures) increase with decreasing doping level. The approximated relation of A-B theory for T= 0 K is given by equation 2.5 in chapter 2. On the other hand this increasing in under-doped samples results from dominant increasing of normal state junction resistance in spite of quite decreasing in I_c. The temperature dependence of Josephson junction for d-wave superconductor was also investigated by (Kleiner and Muller 1999).

4.3. Bolometric Detection of Radiation from Mesa

All of electrical measurements of mesa were to characterize the superconducting material of Bi2212 single crystal for investigation of THz radiation. The experimental measurements on electrical behaviors of the superconducting material were not only instructive to understand the properties of HTSs, but also to investigate whether they satisfy our radiation considerations from Bi2212. The required mesa dimensions and experimental configurations for THz radiation from Bi2212 were mentioned in chapter 2 and their capabilities in THz emission have been demonstrated in a paper by (Ozyuzer, et al. 2007). A significant radiation at THz frequency range was obtained out of long edge of mesa on Bi2212 single crystal in zero magnetic field. It results from oscillating current due to voltage drop across the IJJs and it is based on ac Josephson effect. Because of the radiation frequency proportional to the voltage, Josephson junctions are used such a voltage-frequency converter (Josephson 1962). Thus a superconductor with large energy gap provides significant radiation at THz frequency range. In the study, tall mesas were fabricated, because larger number of IJJs provides more power radiation with better efficiency.

The synchronization of all IJJ stacks inside under-doped Bi2212 by a standing electromagnetic wave is very important to obtain THz radiation, so strong coupling between junctions should be inside mesa lateral dimensions and more identical Junctions are required. IJJs naturally stacked inside Bi2212 include more identical junction parameters than artificially fabricated junction stacks, so Bi2212 superconducting materials are a better candidate for THz radiation technology. However variation of junction parameters in IJJs may occur in spite of perfect junction structures. For example, if fabricated mesas have not such a smooth rectangular shape, they include junctions with different areas along the mesa height. Since synchronized oscillations are based on junction stacks with modulated Josephson critical current, they should be identical along the c-axis in the mesa. The other variations in junction parameter are caused by inhomogeneous heating inside mesas. It is well known the reasons of more heating in Bi2212 are their less thermal conductivity and larger number of IJJs. It was emphasized that the different parameters in junction destroy synchronization of whole IJJs or reduce emission capability. The influences of these junction parameters on radiation were theoretically investigated in a paper by (Koshelev and Bulaevski 2008).

According to our emission consideration, the frequency of emission in coherent phase modes is not tunable. The frequency range of emission is based on lateral and planar size of mesa (Ozyuzer, et al. 2007). Our first purpose is to detect emission peak by Si bolometer from long edge of mesa whose dimensions of 100x300 μm^2, while ac current with low swept frequency is applying along the c-axis of Bi2212 single crystal. Since the radiation emitted from Bi2212 results from recombination of pairs supremely, ac current with less swept frequency were applied during decreasing bias voltage. Two measurements which are I-V and bolometric detection from long edge of mesa were simultaneously recorded. In the paper, it was demonstrated that the generated emission was also detected until temperature of 50 K, so our measurements were done at different temperatures below T_c. Several bolometric detections with current voltage characteristics of fabricated mesas are shown in (Figures 4.17, Figure 4.18, Figure 4.19, Figure 4.20 and Figure 4.21). In bolometric measurements, y-axis corresponds to output signal from Si bolometer amplified by lock-in amplifier. It gives enough information on whether emission is obtained.

In these measurements, according to our emission consideration, since it is expected that the radiation from long edge of tall mesa is emitted and detected by bolometer while bias voltage decreases, swept frequency of ac current applied by function generator was reduced when it started to decrease. It provides not to skip the synchronization voltages of all junctions. Thus it was allowed to scan detection of radiation at each voltage. In order to ensure the emission from superconducting mesa structure, bolometric output peaks should be reproducible for each scanning of bias voltage decreasing toward to zero. Therefore I-V measurements were allowed to be repeated severally.

Against the influence of variation at ambient temperature on output signal of bolometer, the system was thermally isolated to reduce the background of spurious count. After background was subtracted by lock-in for sensitive detection, bolometric measurements were recorded together with I-V simultaneously. On the other hand variation in background is seen in (Figure 4.19). Our bolometer is sensitive to thermal radiation and joule heating occurring because of non-equilibrium quasi-particle tunneling in large and tall mesa is clearly seen at high bias voltages. The back-bending in I-V and thermal radiation in bolometric measurement at highest bias currents are good evidence of heating and they are clearly seen in (Figure 4.18).

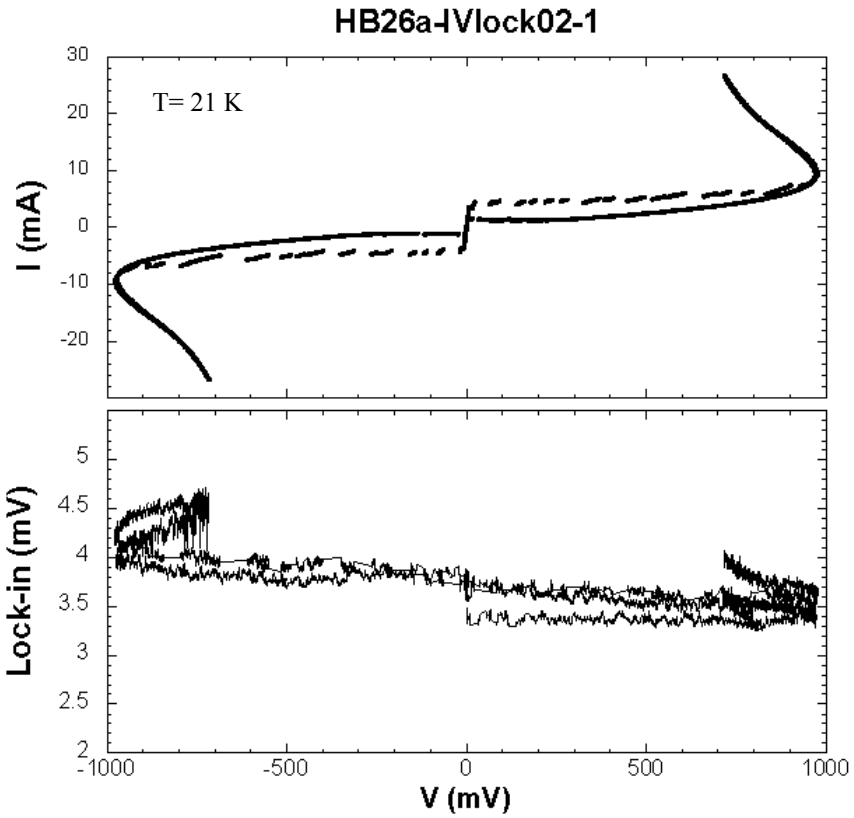

Figure 4.17. Bolometer (up) and I-V (down) measurements of HB26 at 21 K

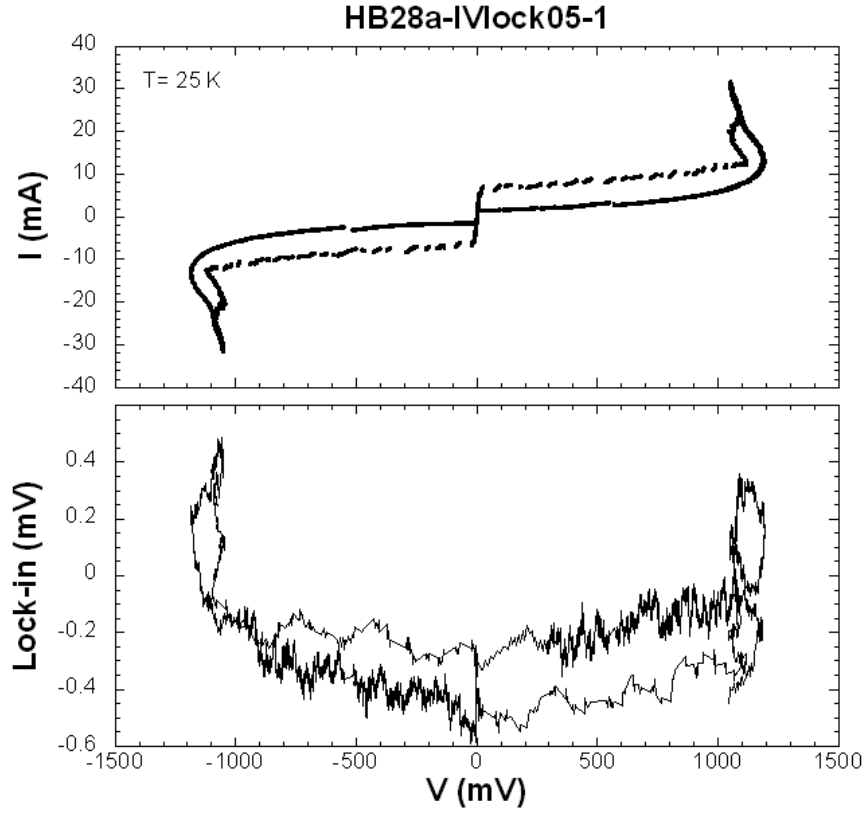

Figure 4.18. Bolometer (up) and I-V (down) measurements of HB28 at 25 K

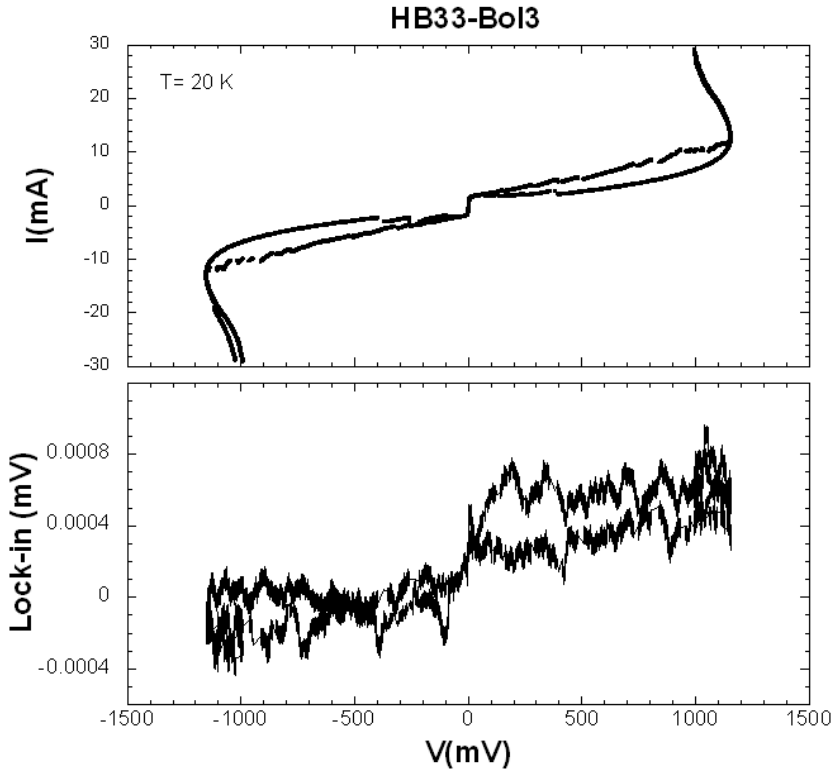

Figure 4.19. Bolometer (up) and I-V (down) measurements of HB33 at 20 K

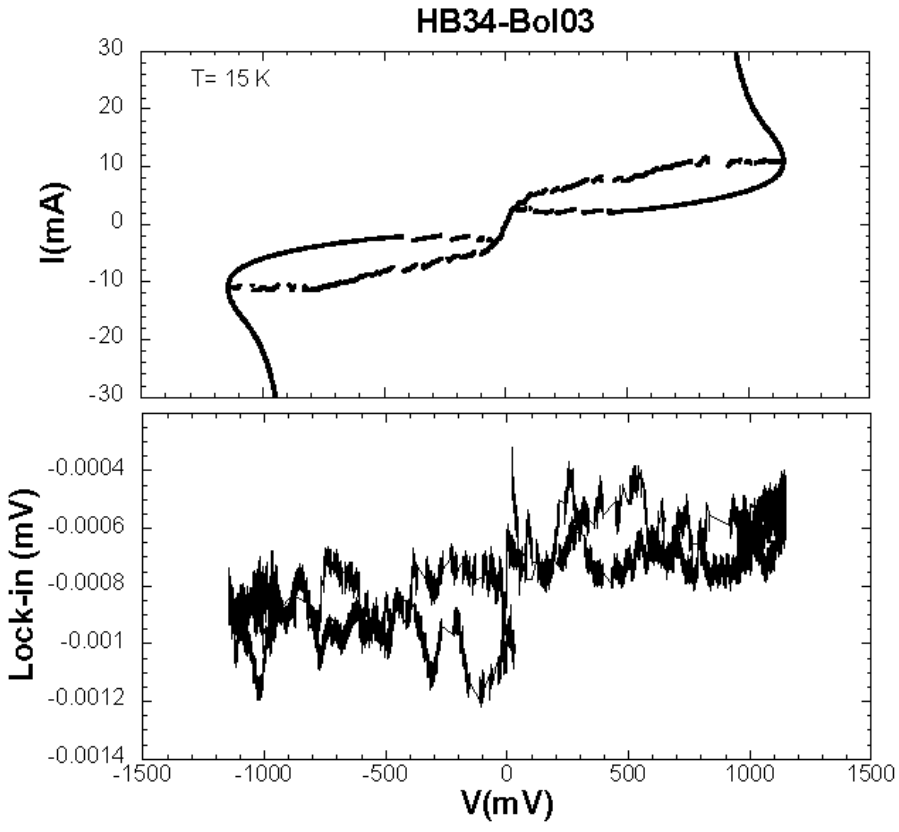

Figure 4.20. Bolometer (up) and I-V (down) measurements of HB34 at 15 K

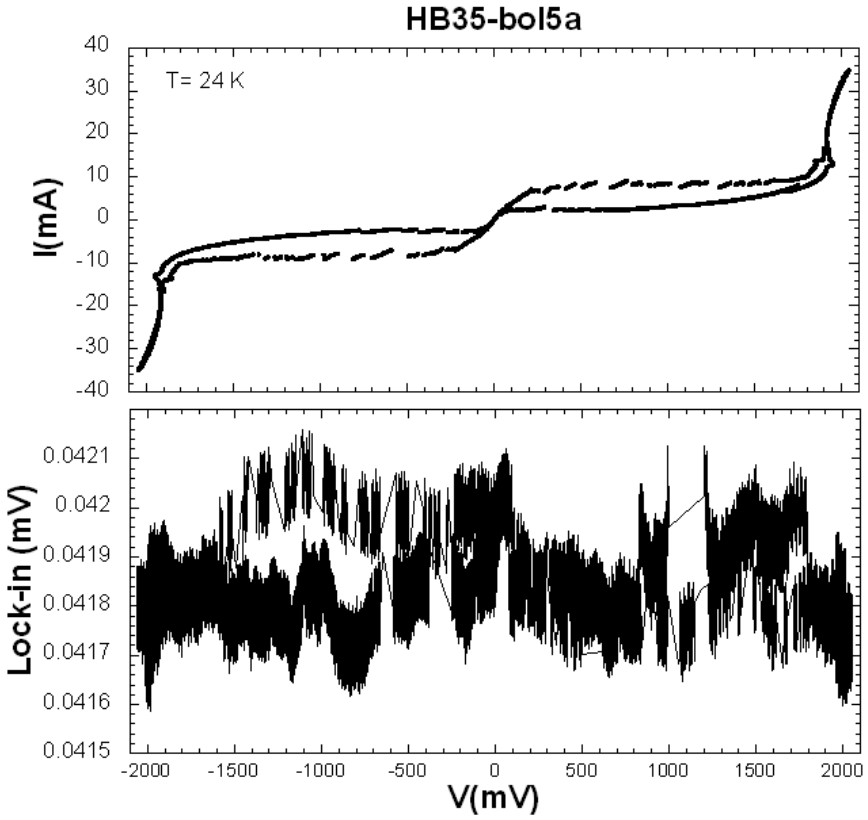

Figure 4.21. Bolometer (up) and I-V (down) measurements of HB35 at 24 K

As can be seen above figures, there are no emission peaks detected by bolometer. Some peaks in bolometric detections were not taken into account since they were both small and irreproducible. It was thought that main reason of non-emission is irregular mesa shapes. It is clearly seen in (Table 4.1) that not only lateral angles of mesas are low but also their distributions along the all lateral mesa dimensions are quite inhomogeneous. Low lateral angle shows to fabricate such a trapezoid mesa and because of non-rotational sample holder during etching different lateral angles at edges of mesa were obtained. It causes junctions with different areas along the mesa height because junction areas are extended from top of the mesa to crystal surface. Thus junctions have different critical current values. In order to synchronize junction stacks, they should have been identical with respect to junction parameters. However disorder of I_c along the mesa height destroy the synchronization of all IJJ stacks. Therefore fabrication processes are very important to obtain smooth rectangular mesas and many different fabrication processes have been experienced. Moreover in order not to change junction parameters without irregular mesa shape, it was avoided to use some fabrication techniques which cause the variations in crystal structures. For example

some annealing at high temperatures to reduce contact resistance was not preferable in fabrication processes because oxygen doping level may be changed or may lose their homogeneity in all junctions. Sometimes changing of surface modification and internal structure of Bi2212 single crystal by chemical processes may occur. In our study they were protected by deposited gold layer on the crystal. Heating of crystal during the etching were reduced by continuous flow water cooling at sample holder.

The other reason of de-synchronization in mesa is heating problem which is general problem for Bi2212. According to our emission consideration, tall and large mesas were fabricated on the contrary small mesa sizes are preferred in recent studies to avoid heating problem, so in our I-V measurements we encountered the effect of heating that is considered to destroy synchronization in IJJ stacks. However it was able to be manageable in large and tall mesas by using under-doped Bi2212 and coherent THz radiation were obtained (Ozyuzer, et al. 2007). Some fabrication design for improving thermal managements of the crystal was explained in a paper published by (Koshelev and Bulaevskii 2008).

CHAPTER 5

SUMMARY AND CONCLUSION

In the study, tall and large mesas on Ca-rich $Bi_2Sr_2CaCu_2O_{8+\delta}$ superconducting single crystal were fabricated by vacuum deposition, photolithography and ion beam etching techniques. After these processes, mesas whose planar dimensions and thickness are 100x300 μm^2 and about 1 μm respectively were obtained. The lateral angles and heights of mesas were analyzed by AFM measurement. After the tunneling behaviors of natural layered structure of SIS junctions inside Bi2212 were characterized by R-T and I-V measurements, bolometric detection of emission from long lateral size of mesas were done.

We used Ca-rich Bi2212 single crystals for the mesa fabrication. They were grown by floating zone method. These perfect IJJs in Bi2212 single crystal allowed measuring the tunneling behavior of HTSs clearly.

In long mesa fabrication processes, firstly the crystals having smooth alignment planes of SIS junction were glued onto a sapphire substrate by silver epoxy. In order to get a fresh surface, the crystal was cleaved for better mesa fabrication. Then a gold layer (~100 nm) was deposited using vacuum evaporation technique. Thus the crystal structures of Bi2212 HTS are protected by the gold layer during some chemical processes. To obtain natural IJJ stacks with various size and height, mesas on Bi2212 have been prepared by photolithography and argon ion beam etching techniques. We have obtained tall mesas with sizes are 100x300 μm^2.

Our fabrication parameters are shown in (Table 4.1). By using these parameters, mesas with thickness of about 1 μm were able to be fabricated. It was seen in the table the thicknesses measured on different edges of mesa are approximately similar. In spite of a good result in mesa height, low angles between their lateral planes and cleaved surface of the crystal are evidence that smooth rectangular mesas have not been fabricated. Whereas it was required their lateral angles approximate to vertical angles for better identical IJJs, they had been below 50 degrees. Moreover it was observed these lateral angles measured on all edges of mesa are quite different from each other because of un-rotated sample holder during the ion beam etching. Since ion beam with

incident angle of 45 degrees is accelerated through the sample holder, differences in lateral angles of mesa occur. Therefore sample holder should be rotated during ion beam etching. Furthermore in order not to change under-doped property of Bi2212 and lose photo-resist layer due to heating, better cooling on sample holder is required during etching. Thicker photoresist layers were patterned to obtain stronger protected area on mesa for long etch time but the thicker layer shades mesa lateral sizes at some regions and causes to fabricate mesas with lower lateral angles because while mesa height is becoming thicker by etching, lateral sizes extend from top of the mesa to crystal surface due to more shading of photoresist. Therefore beside better cooling and rotating the sample holder, photo-resist layers should be both thinner and stronger. In last studies, the new experimental designs improved with respect to above advices were used. The results will be presented in next studies of our group.

Since it is difficult to make a contact on mesa with small area, firstly CaF_2 insulating layer onto crystal and small area of the mesa and then a gold stripe onto mesa and CaF_2 were deposited by vacuum evaporation. After three points contacts were made, R-T and I-V measurements were performed. The experimental measurements were clearly defined in chapter 3.

In the R-T graphs, sharp phase transitions to superconducting state are seen and the transition temperatures of crystals are between 64 and 73 K. Besides these differences in T_c for crystals with same properties result from using different cooling system, oxygen doping level inside Bi2212 single crystals. On the other hand, the characteristic temperature dependent resistance behaviors of under-doped Bi2212 single crystal were seen in all of the R-T graphs. These behaviors in R-T measurements are exponential increasing of resistance at various temperatures from 300 K to T_c and lower T_c than Bi2212 crystals with optimally doped. Furthermore it should be considered the Bi2212 single crystals enriched with Ca. It was discussed in some study their critical temperatures are suppressed due to the excess of Ca content in Bi2212.

It is well known that Bi2212 single crystals have anisotropic electrical behaviors because of their layered SIS structures. Electrical measurements along the mesa height exhibit the characteristic tunneling behaviors including the contributions of whole stacks of IJJs. Large hysterical tunneling behavior of Bi2212 and many number of quasi-particle branches such a voltage jumps are seen I-V graphs. However less number of branches than calculated number of IJJs is seen because of joule heating. Also it causes back-bending at high bias current and causes to decrease total conductance peak

of all IJJs. While temperature increase toward T_c, decreases in both sum-gap voltages and hysterical behaviors are clearly seen in temperature evolution I-V graphs. It was found that the order of critical current density J_c is 10^1 A/cm^2. The magnitude is compatible with critical current densities of Bi2212 in under-doped region and lower than J_c of Bi2212 crystals with higher oxygen contents. It is thought to solve heating problems in Bi2212 markedly, because its low critical current does not allow being attained higher bias currents until sum-gap voltage of whole IJJ stacks. Thus less heating occurs in the crystal. Moreover, it is observed that the temperature evolutions of Josephson critical currents tend to decrease with temperature. However the order of temperature evolution of I_c is small at quite different temperatures and the differences get bigger with temperature differences.

In our bolometric measurements done to detect emission from Bi2212 superconductor, there is no emission peak. According to our emission consideration, we expected that the radiation from long edge of tall mesa is emitted while bias voltage along the c-axis in Bi2212 decreases. Therefore I-V and bolometer measurements were recorded simultaneously. After all bolometric measurements performed at different temperatures, the emission peaks have not been observed due to non-identical IJJ stacks with respect to junction area. It is known from AFM measurement on lateral dimensions of mesa that the lateral angles were too low, so junction areas along the mesa height are gradually changed. In order to synchronize all junction stacks in mesa, they should have identical planer areas and their other junction parameters should be same whereas different junction parameters destroy synchronization of whole IJJs or reduce emission capability. Therefore improvements in fabrication processes to obtain mesas with smooth and rectangular shapes are required.

In the future works, the experimental processes will be improved to fabricate better smooth rectangular mesas. After obtaining emission peaks, the radiation will be characterized to identify their power and frequency range. To generate THz radiation including more frequency and power, taller mesas will be fabricated and mesa width of mesa will be decreased.

REFERENCES

Ambegaokar, V. and A. Baratoff. 1963. High temperature superconductors: Processing and science. *Physical Review Letters* 10:486.

Akimitsu, J., A. Yamazaki, H. Sawa and H. Fujiki. 1987. Superconductivity in the Bi-Sr-Cu-O system. *Japanese Journal of Applied Physics* 26:2080.

Bae, M.H. and H.C. Lee. 2006. Progress in THz generation using Josephson fluxon dynamics in intrinsic junctions. *The Institute of Electronics, Information and Communication Engineers Transactions of Electronics* E89: 411.

Bae, M.H., H.C. Lee and J.H. Choi. 2007. Josephson vortex-flow terahertz emission in layered high-T_c superconducting single crystals. *Physical Review Letters* 98(4):27002.

Bardeen, J., L.N. Cooper and J.R Schrieffer. 1957. The Theory of Superconductivity *Physical Review Letters* 108:1175.

Batov, I.E., X.Y. Jin, S.V. Shitov, Y. Koval, P. Muller and A.V. Ustinov. 2006. Detection of 0.5 THz radiation from intrinsic $Bi_2Sr_2CaCu_2O_{8+x}$ Josephson junctions. *Applied Physics Letters* 88:262504.

Bednorz, J.G. and K.A Müller. 1986. Possible high-T_c superconductivity in the Ba-La-Cu-O system. *Zeitschrift Physics* B 64:189.

Bourdillon, A. and N.X. Tan Bourdillon, eds. 1994. *High temperature superconductor: Processing and Science*. New York: Academic Press INC.

Buckel, W. and R. Kleiner, eds. 2004. *Superconductivity Fundamentals and Application*. Tübingen: Wiley-VCH Verlag GmbH and Co. KGaA Weinheim.

Chu, C.W., J. Bechtold, L. Gao, P.H. Hor, Z.J. Huan, R.L. Meng, Y.Y. Sun, Y.Q. Wang

and Y.Y. Xue. 1998. Superconducting up to 114 K in the Bi-Al-Ca-Sr-Cu-O compound system without rare-earth elements, *Physical Review Letters* 60:941.

Duzer, T. V. and C.W. Turner, eds. 1999. *Principles of superconductive devices and circuits.* London: Prentice-Hall

Feigelson, R.S., D. Gazit, D.K. Fork and T.H. Geballe. 1988. Superconducting Bi-Ca-Sr-Cu-O fibers grown by the laser-heated pedestal growth methods. *Science* 249:1642.

Ferguson, B. and X.C. Zhang. 2002. Materials for terahertz science and technology. *Nature Materials* 1:26.

Giaver, I. 1960. Energy gap in superconductor measured by electron tunneling. *Physical Review Letters* 5:147.

Ginzburg, V.L. and L.D. Landau. 1950. On the theory of superconductivity. *Journal of Experimental and Theoretical Physics* 20:1064.

Gor'kov, L. P. 1959. Microscopic derivation of the Ginzburg--Landau equations in the theory of superconductivity. *Zh. Eksp. Teor. Fiz.* 36:1918.

Hazen, R.M., L.W. Finger, R.J. Angel, C.T. Prewitt, N.L. Ross, C.G. Hadidiacos, P.J. Heaney, D.R. Veblen, Z.Z. Shenh, A. El Ali and A.M. Hermann. 1988. 100 K superconducting phases in the Tl-Ca-Ba-Cu-O system. *Physical Review Letters* 60:1657.

Inoue, M., M. Yoshida, M. Tsuge, T. Senzaki, Y. Sugihara, J. Otsuka, K. Ohbayashi, A. Fujimaki and H. Hayakawa. 1998. A study on the control of the material properties of $Bi_2Sr_2CaCu_2O_{8+x}$ thin films for intrinsic Josephson junctions. *Physica C* 307:221.

Jin, S., T.H. Tiefel, R.C. Sherwood, R.B. Van Dover, M.E. Davis, G.W. Kammlott and

R.A. Fastnacht. 1988. Melt-textured growth of polycrystalline $YBa_2Cu_3O_{7-\delta}$ with high transport Jc at 77 K. *Physical Review B* 37:7850.

Josephson, B.D. 1962. Possible new effects in superconductive tunneling. *Physics Letter* 1: 251-253.

Kadowaki, K., I. Kakeya, T. Yamamoto, T. Yamazaki, M. Kohri and Y. Kubo, 2006. Dynamical properties of Josephson vortices in mesoscopic intrinsic Josephson junctions in single crystalline $Bi_2Sr_2CaCu_2O_{8+x}$. *Physica C* 437-438:111.

Kendziora, C., M.C. Martin, J. Hartge and L. Mihaly. 1993. Wide-range oxygen doping of $Bi_2Sr_2CaCu_2O_{8+x}$. *Physical Review Letters* 48:48.

Kleiner R., F. Steinmeyer, G. Kunkel, and P. Müller. 1992. Intrinsic Josephson effects in $Bi_2Sr_2CaCu_2O_8$ single crystals. *Physical Review Letters* 68:2394.

Kleiner, R. 2007. Filling the terahertz gap. *Science* 318:1254.

Köhler, R., A. Tredicucci and F. Beltram, H.E. Beere, E.H. Linfield, A.G. Davies, D.A. Ritchie, R.C. Iotti and F. Rossi. 2002. Terahertz semiconductor-hetero-structure laser. *Nature* 417:156.

Krasnov, V.M. 2006. Quantum cascade phenomenon in $Bi_2Sr_2CaCu_2O_{8+x}$ single crystal. *Physical Review Letters* 97:257003.

Kurter, C. 2005. Fabrication of mesa structures on superconducting $Bi_2Sr_2CaCu_2O_{8+\delta}$ single crystals. *Izmir Institute of Technology Thesis of M.S.*

Maeda, H., T. Tanaka, M. Fukutomi and T. Asano. 1988. A New high-T_c oxide superconductor without a rare earth element. *Japanese Journal of Applied Physics* 27:L209.

Martin, Y., C.C. Williams and H.K. Wickramasinghe. 1987. Atomic force microscope-

force mapping and profiling on a sub 100-Å scale. *Journal of Applied Physics* 61:4723.

Matsui, Y., H. Maeda, Y. Tanaka and S. Horiuchi. 1988. High-resolution electron microscopy of modulated structure in the new high-T_c superconductors of the Bi-Sr-Ca-Cu-O system. *Japanese Journal of Applied Physics* 27:L361.

Michishita, K., Y.H. Ikuhara and Y. Kubo. 1996. *Bi-based superconductor fabricated by floating-zone method*: *Bismuth-based high-temperature Superconductors*, Edited by Maeda, Hiroski. and Kazumasa Togano. New York: Marcer Dekker.

Miyakawa, N., P. Guptasarma, J.F. Zasadzinski, D.G. Hink and K.E. Gray. 1998. Strong dependence of the Superconducting gap on oxygen doping from tunneling measurements on $Bi_2Sr_2CaCu_2O_{8+x}$. *Physical Review Letters* 80:157.

Miyakawa, N., J.F. Zasadzinski, L. Ozyuzer, P. Guptasarma, D. G. Hink, C. Kendziora and K.E. Gray. 1999. Predominantly superconducting origin of large energy gaps in under-doped $Bi_2Sr_2CaCu_2O_{8+x}$ from tunneling spectroscopy. *Physical Review Letters* 83:1018.

Ozdemir M. 2006. Spin polarized tunneling spectroscopy of intercalated $Bi_2Sr_2CaCu_2O_{8+\delta}$. *Izmir Institute of Technology Thesis of M.S.*

Ohhassi, K., T. Horiuchi, S. Nasu and E. Sugimata. 2004. Synthesis and properties of HgI_2 intercalation of $Bi_2Sr_2CaCu_2O_y$ superconductor. J*ournal of Physics and Chemistry of solids* 65:603.

Ozyuzer, L., J.F. Zasadzinski, C. Kendziora and K.E. Gray. 2000. Quasiparticle and Josephson tunneling of overdoped $Bi_2Sr_2CaCu_2O_{8+x}$ single crystal. *Physical Review B* 61:3629.

Ozyuzer, L., J.F. Zasadzinski, K.E. Gray, C. Kendziora and N. Miyakawa. 2002. Absence of pseudo-gap in heavily over-doped $Bi_2Sr_2CaCu_2O_{8+x}$ from tunneling spectroscopy of break junction. *Europhysics Letters* 58:589.

Ozyuzer, L., J.F. Zasadzinski, K.E. Gray, D.G. Hinks and N. Miyakawa. 2003. Probing the phase diagram of $Bi_2Sr_2CaCu_2O_{8+x}$ with tunneling spectroscopy. *IEEE Transactions on Applied Superconductivity* 13:89.

Ozyuzer, L., C. Kurter, J.F. Zasadzinski, K.E. Gray, D.G. Hinks and N. Miyakawa. 2005. Comparison of intrinsic Josephson junction and SIS tunneling spectroscopy of $Bi_2Sr_2CaCu_2O_{8+x}$. *IEEE Transactions on Applied Superconductivity* 15:181-184.

Ozyuzer, L., A.E. Koshelev, C. Kurter, N. Gopalsami, Q. Li, M. Tachiki, K. Kadowaki, T. Tamamoto, H. Minami, H. Yamaguchi, T. Tachiki, K.E. Gray, W.K. Kwok and U. Welp. 2007. Emission of coherent THz radiation from superconductors. *Science* 318:1291.

Revcolevschi, A. and J. Jegoudez. 1997. Growth of large high-Tc single crystals by the floating zone method: A review. *Progress in Materials Science* 42:321.

Schilling, A., M. Cantoni, J.D. Guo and H.R. Ott. 1993. Superconductivity above 130 K in the Hg-Ba-Ca-Cu-O System *Nature* 363:15.

Schmidt, V.V. 1997. *The Physics of Superconductors*, Edited by P. Müller and A. V. Ustinov. Berlin: Springer- Verlag.

Silva, E., R. Fastampa, M. Giuru and S. Sarti. 2003. Normal state resistivity of BSCCO single crystal description with a two barrier models. *Physica C* 388-399:329.

Suziki, M., T. Watanabe and A. Matsuda. 1999. Short pulse tunneling measurements of intrinsic Josephson junction in Bi-Sr-Ca-O. *IEEE Transactions on Applied Superconductivity* 9:4507.

Suzuki, M. 1999. Characteristic temperature dependence of the maximum Josephson current in Bi-Si-Ca-Cu-O intrinsic junction. *IEEE Transactions on Applied Superconductivity* 9:4511.

Tachiki, M., T. Koyama and S. Takahashi. 1994. Electromagnetic Phenomena Related to a low frequency plasma in cuprate superconductors. *Physical Review B* 50:7065.

Tachiki, M., M. Lizuka, K. Minami, S. Tejima and H. Nakamura. 2005. Emission of continuous terahertz waves by high-T_c superconductors. *Physica C* 426-431:8.

Tanabe, K., Y. Hidaka, S. Karimoto and M. Suzuki. 1996. Observation of both pair and quasiparticle tunneling in intrinsic junction stacks fabricated on $Bi_2Sr_2CaCu_2O_{8+x}$ single crystals. *Physical Review B* 53:9348.

Ting-Wei L. 1995. Studies of crystal growth, oxygen diffusion, flux pinning and flux lattice melting on $Bi_2Sr_2CaCu_2O_x$ single crystals. *Leiden University Kammerlingh Onnes Laboratory and Van der Walls-Zeeman Laboratory Thesis of Phd.*

Tokita, H., H. Asano and H. Uwe. 2001. Magnetic susceptibility of the normal state in oxygen-controlled Ca-rich Bi-2212 cuprate. *Physica C* 357-360:166.

Yurgens, A., D. Winkler, N.V. Zavaritski and T. Claeson. 1996. Strong temperature dependence of the c-axis gap parameter of $Bi_2Sr_2CaCu_2O_{8+x}$ intrinsic Josephson junctions. *Physical Review B* 53:R8887.

Yurgens, A., D. Winkler N.V. Zavaritski and T. Claeson. 1997. The c-axis gap parameter and resistivity of an individual intrinsic tunnel junction in Bi-2212 single crystals. *Physica C* 293:181.

Yurgens, A. 2000. Intrinsic Josephson junctions: Recent developments. *Superconductor Science and Technology* 13:R85-100.

Wesche, Rainer. 1998. *High Temperature Superconductor Materials, Properties, and Application*. Boston: Academic Publishers.

Won, H. and H. Maki. 1994. *d*-wave Superconductor as a Model of High-T_c

Superconductors *Physical Review B* 49:1397.

Wu, M.K., J.R. Ashburn, C.J. Torng, P.H. Hor, R.L. Meng, L. Gao, , Z.J. Huang, Y.Q. Wang and C.W Chu. 1987. Superconductivity at 93 K in a new mixed-phase Y-B-C-O compound system at ambient pressure. *Physical Review Letters* 58:908.

Zasadzinski, J. 2002. *Tunneling spectroscopy of conventional and unconventional superconductors*: *The Physics of Superconductor,* Edited by Bennemann, K., H. and Ketterson, J. New York: Springer.